Physik Department

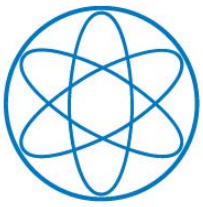

Model Systems of the Actin Cortex

a thesis
presented by

Oliver Lieleg

Technische Universität
München

Technische Universität München
Physik Department
Lehrstuhl für Zellbiophysik E27

Model Systems of the Actin Cortex

Oliver Lieleg

Vollständiger Abdruck der von der Fakultät für Physik der
Technischen Universität München
zur Erlangung des akademischen Grades eines
Doktors der Naturwissenschaften
genehmigten Dissertation.

Vorsitzender:		Univ.-Prof. Dr. Ralf Metzler
Prüfer der Dissertation:	1.	Univ.-Prof. Dr. Andreas Bausch
	2.	Univ.-Prof. Dr. Erwin Frey, Ludwig-Maximilians-Universität München

Die Dissertation wurde am 16.09.08 bei der Technischen Universität München eingereicht und durch die Fakultät für Physik am 05.11.08 angenommen.

Παντα χωρει κοι ουδεν μενει

—

Alles bewegt sich fort und nichts bleibt. (Platon)

Montes fluxerunt a facie Domini et Sinai a facie Domini Dei Israhel.

—

Und die Berge zerflossen vor dem Angesicht des Herrn, dem Gott Israels, und ebenso der Sinai. (Bibel, Richter 5,5)

Summary

Cross-linked or bundled actin networks are the key components in cell mechanics. By locally activating different actin binding proteins (ABPs) the cytoskeletal microstructure can be adjusted to meet the changing needs of the cell. Bundles of actin filaments are used for structural fortification during locomotion. Here, the cell relies on mechanical stability in order to endure the large forces created at the leading edge. Besides this mechanical stability the cytoskeleton has to allow for an ongoing remodeling of its microstructure to provide the cell with crucially needed adaptibility. To shed light on the microscopic principles in cell mechanics, reconstituted actin networks have been proven of utmost importance. Only in such reconstituted systems physical and biochemical parameters can be controlled independently.

In this thesis the microstructure and viscoelastic properties of reconstituted actin networks are correlated. The first part of this thesis focuses on the structural organization of actin filaments by different actin cross-linking and/or bundling proteins. A remarkable polymorphism of network microstructures is observed; the detailed network configuration is set by both the type and concentration of the ABP used. Furthermore, it is demonstrated that the different structural phases of reconstituted actin networks are directly correlated with distinct regimes in the macromechanical network response. It is shown that the transitions between these structural and mechanical phases can be induced by varying the effective concentration of a given cross-linking protein. This can be achieved by either varying the total amount of cross-linking molecules or by adjusting their binding affinity towards actin by temperature. The resulting network structures can be either homogeneous or heterogeneous. In the latter case the local viscoelastic properties are observed to drastically differ from the macroscopic network mechanics. As an outstanding example of structural heterogeneities the formation of bundle clusters is described. These clusters exhibit a fractal dimension which also extends to larger mesoscopic length scales of the cluster network.
Local heterogeneities are also observed in weakly cross-linked networks and seem to be a generic prerequesite for the transition into a homogeneous phase which is dominated by cross-links rather than by entanglements between filaments. This cross-link transition is parameterized and the microscopic origin of this transi-

tion is identified. Similarly, the transition from a weakly cross-linked phase into a purely bundled network is investigated. In contrast to the so far commonly accepted belief, in stiff bundle networks the microscopic origin of the network elasticity is completely different from that of isotropically cross-linked networks: non-affine bending deformations have to be considered instead of affine stretching deformations. By comparing theoretical predictions of affine stretching models and non-affine bending models with the elastic response of different actin networks it is shown that the network microstructure sets the local deformation mode and with that the static viscoelastic response of actin networks.

In a second part the dynamic properties of cross-linked actin networks are adressed. The transient character of the cross-links and its impact on the viscoelastic frequency spectrum of cross-linked actin networks is analyzed. Thermally activated cross-linker unbinding dominates the viscoelastic response at low frequencies. Consistently, the cross-linker off-rate is identified as the pivotal time scale that sets the frequency regime at which transient binding effects dictate the viscoelastic spectrum. Based on this finding a simple semi-phenomenological model is introduced which is predicated on single cross-link unbinding events and successfully reproduces the frequency spectrum of transiently cross-linked actin networks. Further experiments show that not only the cross-linker off-rate but the whole microscopic interaction potential of an actin/ABP bond dictates the frequency dependent viscoelastic response of transiently cross-linked actin networks. Such an interaction potential is expected to be sensitive towards forces which act on the actin/ABP bond. Therefore, the elastic behavior of transiently cross-linked actin networks under mechanical load is investigated. A highly complex and tunable non-linear response is observed that is in sharp contrast to existing theoretical predictions. It is demonstrated that forced cross-linker unbinding limits the stability of cross-linked actin networks. Surprisingly, even in complex actin bundle networks the loading rate dependence of the rupture forces of actin/ABP bonds follows the Bell prediction for a single molecular bond. This suggests that collective phenomena can be neglected. Furthermore, the non-linear behavior of actin bundle networks reveals an equivalence of cross-linker density and force loading rate. This observation is employed to establish a novel superposition principle of cross-linker density and time which is then used to describe the self-similar actin/fascin system with a master curve. Interestingly, such actin/fascin bundle networks as well as bundle networks formed by α-actinin can be trapped in a meta-stable state. Yet, the transient nature of cross-linking molecules allows for an (at least partially) retarded equilibration of these kinetically arrested network configurations which gives rise to very slow dynamics in these networks.

The physical principles and effects described in this thesis establish a microscopic understanding of the structural organization and viscoelastic properties of

reconstituted actin networks. These reconstituted networks constitute valuable model systems of the actin cortex of living cells. Thus, the conclusions drawn in this thesis may also help to gain a better understanding of complex cytoskeletal networks *in vivo*.

Contents

1 Introduction

The cytoskeleton of eucaryotic cells consists of three major classes of filamentous biopolymers: microtubules, actin filaments and intermediate filaments. The role of intermediate filaments is only poorly understood; microtubules, however, are known to serve as "tracks" for molecular motors that transport vesicles or small organelles through the cell and play an important role during cell division. The mechanical properties of cells are mainly attributable to a meshwork of actin filaments (light blue fibres in Fig. 1.1).

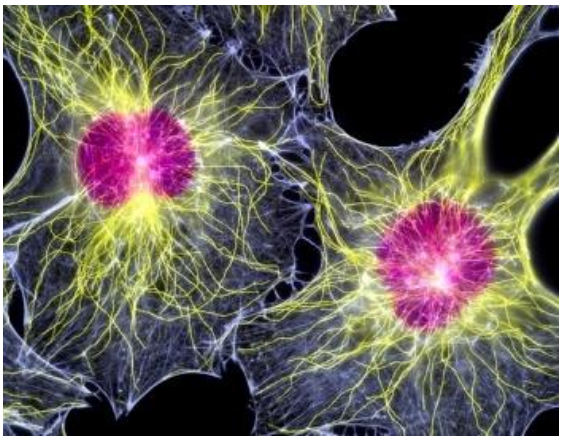

Figure 1.1: Fluorescence micrograph of fibroblast cells, showing their nuclei (pink) and the cytoskeleton. Microtubules are labelled in yellow, actin filaments in light blue.

The viscoelastic properties of the actin cortex are the key to a microscopic understanding of the complex mechanical function of the cytoskeleton. The role of the actin cytoskeleton in cell mechanics includes:

1. exerting forces e.g. for cell motility
2. withstanding deformations and mechanical load
3. allowing for changes in cell morphology, e.g. during cytokinesis
4. potentially providing means for mechanosensing.

Already this relatively short list directly implies that distinct network microstructures are required to meet all these different challenges: For motility stiff and mechanically stable structures are crucial and conctractility is of high importance during cytokinesis. In this context, a rich structural polymorphism of actin networks is indispensable. The easier cells can switch between different

microstructures the faster cells are able to adapt to their actual needs – which drastically change during the cell cycle.

Moreover, these different network morphologies do not only have to offer a wide range of mechanical properties but must also be easily built up *and* destroyed. This requirement seems to present a conflict regarding the likewise needed mechanical toughness. The apparent dilemma is solved by using transiently cross-linked networks instead of covalently cross-linked structures. It remains to be shown if transiently cross-linked networks also exhibit favorable mechanical properties in contrast to permanently cross-linked networks – besides the obvious advantage of facile destructibility.

The biological complexity of the cytoskeleton is overwhelming: nature offers a myriade of actin binding proteins (ABPs) that can be locally produced and disintegrated, de- and reactivated on demand by e.g. phosphorylation. In combination with forces that are internally created by molecular motors or in response to external stress cells can not only adjust their morphology but also their protein expression, a phenomenon which is known as mechanotransduction. Mere changes in the substrate stiffness can evoke a completely different differentiation of naive stem cells [Engler et al. 2006]. Obviously, a coupling of extracellular and intracellular (bio)chemical signalling pathways is not sufficient to rationalize the highly adaptive behavior of cells. Transiently cross-linked actin networks which are mechanically coupled to the cell membrane may also contribute to mechanosensing tasks, i.e. in converting mechanical forces into biochemical signals.

To shed light on the underlying physical principles governing the mechanical properties of the cytoskeleton simple *in vitro* reconstitutions of cytoskeletal elements have been proven essential [Bausch and Kroy 2006]. Here, the type and concentration of the involved ABPs are tuned independently from the actin filament density which allows for studying selected parts or paths in the possible actin/ABP phase diagram. By specifically choosing ABPs with distinct biochemical properties and/or molecular structures, the influence of chemical and physical parameters on the biophysical properties of cytoskeletal networks can be disentangled. As demonstrated in this thesis, an integrated approach combining micro- and macromechanical techniques with optical microscopy, theoretical modelling and simulations provides detailed insight into the structural organization and mechanical properties of complex actin networks *in vitro*. Finally, this approach may also set the basis for a microscopic understanding of cytoskeletal mechanics *in vivo*.

2 Materials and Methods

The actin cortex and actin bundles are the main structural and mechanical elements of the cytoskeleton. Actin binding proteins (ABPs) have various effects on the strutural organization of filamentous actin solutions as well as on the polymerization/depolymerization kinetics of the filament. For instance, actin binding proteins can sever, cap, cross-link or bundle actin filaments. By the local activation of such ABPs cells can not only manipulate their microstucture but also their micromechanical properties. This provides the cell an enormous dynamic adaptibility which outmaches technical polymers by far.

2.1 Actin and actin binding proteins

2.1.1 Actin

Monomeric G-actin is a globular protein (Fig. 2.1, top line) with a molecular weight of 42 kDa. In presence of ATP and divalent ions as present in the polymerization buffer ("F-buffer"), actin monomers polymerize and form helical filaments (see Fig. 2.1, middle line) with a period of 72 nm corresponding to 26 monomer subunits. G-actin is obtained from rabbit skeletal muscle and stored in lyophilized form at -21 °C [Spudich and Watt 1971]. For measurements the lyophilized actin is dissolved in deionized water and dialyzed against G-Buffer (2 mM Tris, 0.2 mM ATP, 0.2 mM $CaCl_2$, 0.2 mM DTT and 0.005 % NaN_3, pH 8) at 4 °C. The G-actin solutions are kept at 4 °C and used within seven days of preparation. Polymerization is initiated by adding 1/10 volume of 10x F-buffer (20 mM Tris, 20 mM $MgCl_2$, 2 mM $CaCl_2$, 1 M KCl and 2 mM DTT, pH 7.5) and gently mixing for 10 s. Following this protocol, *in vitro* actin filaments can grow up to lengths of 100 μm. Actin filaments are dynamic polymers that grow and shrink at the same time; after short times the filaments reach a steady state called "treadmilling" where the average filament length does not change anymore [Howard 2001].

2.1.2 Gelsolin

Gelsolin belongs to a family of actin cutting/capping proteins. By nucleation, filament capping and severing gelsolin regulates the length distribution of actin

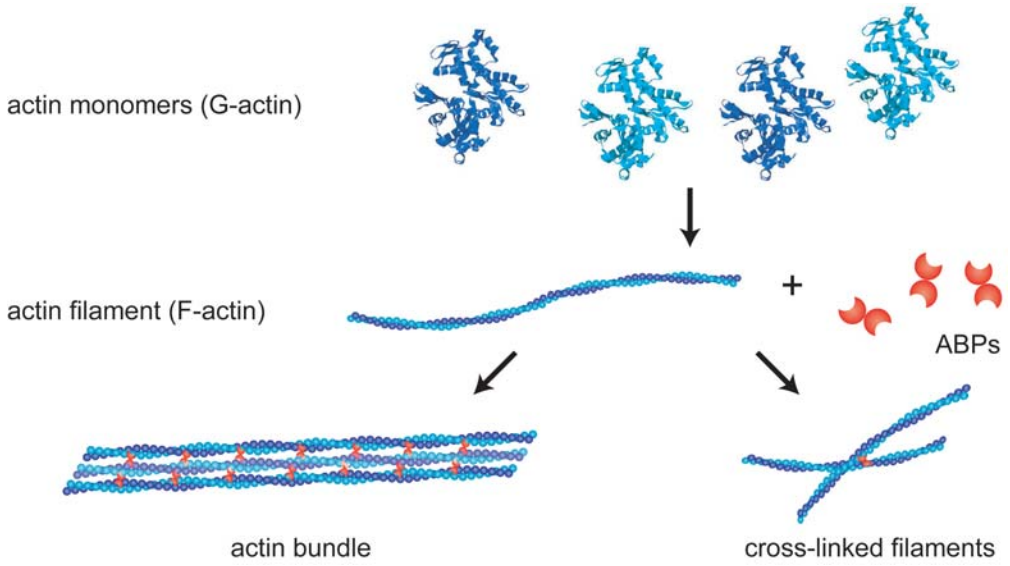

Figure 2.1: Monomeric G-actin (top) polymerizes to filamentous F-actin (middle). These actin filaments can be interconnected or bundled by actin binding proteins (bottom).

filaments [Janmey et al. 1986]. Gelsolin is prepared from bovine plasma serum following [Kurokawa et al. 1990]. For the experiments shown in this thesis, the average actin filament length was adjusted to 21 μm, i.e. the actin filaments have to be regarded semi-flexible (compare section 2.2).

2.1.3 Phalloidin

Phalloidin is an F-actin stabilizing molecule which binds between two neighboring actin monomers und suppresses the treadmilling process. Phalloidin is isolated from the poisonous mushroom amanita phalloides (death cap). It is a cyclic peptide with a molecular weight of 789 Da and can be used to attach a fluorophor to the actin filament. For the fluorescence micrographs shown in this thesis tetramethylrhodamine labelled phalloidin (TRITC-phalloidin) was used.

2.1.4 Heavy meromyosin (HMM)

The molecular motor myosin II can be enzymatically cleaved by chymotrypsine. The larger of the two resulting fragments, heavy meromyosin (HMM), has a molecular weight of 350 kDa [Lowey et al. 1969] and retains the two actin binding domains of myosin II as well as the ATP binding site; however, it has lost its cargo binding tail (see Fig. 2.2). In the ATP-depleted rigor state, HMM can be used as

an ideal actin cross-linking protein [Tharmann et al. 2007]. In actin/HMM networks the transition from active ATP-HMM to rigor ADP-HMM can be recorded rheologically as described in [Tharmann 2007].

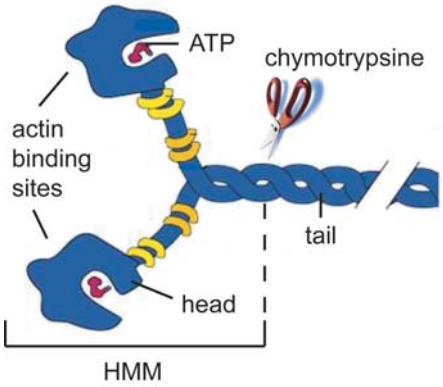

Figure 2.2: Schematic view of the molecular structure of HMM. After enzymatic cleavage of myosin II by chymotrypsine, HMM still possesses the two actin binding domains. Thus, in the ADP rigor-state it can be used as an actin cross-linking molecule.

2.1.5 Fascin

Human fascin is a relatively small ABP with a molecular weight of 55 kDa [Yamashiro-Matsumura and Matsumura 1985]. It is most prominently found in the filopodia of cells where it organizes actin filaments into thick bundles [Vignjevic et al. 2006]. Recombinant fascin was prepared by a modification of the method of [Ono et al. 1997] as described by [Vignjevic et al. 2002].

2.1.6 α-actinin

α-actinin is a large dimeric protein with a molecular weight of 215 kDa [Craig et al. 1982]. α-actinin is isolated from turkey gizzard smooth muscle following [Craig et al. 1982], dialyzed against G-buffer and stored at 4 °C for several weeks. α-actinin belongs to a highly conserved family of ABPs; its different isoforms are ubiquitous in muscle as well as in non-muscle cells [Sjöblom et al. 2008]. In the latter, α-actinin is predominantly found to form stiff contractile bundles – so called "stress-fibers" [Yamashiro-Matsumura and Matsumura 1986].

2.2 Viscoelasticity of semi-flexible polymers

2.2.1 Classification of polymers

The physical description of polymers relies on parameters that are independent of the chemical substructure of the polymer. The most important physical parameters for the classification of polymers are the persistence length l_p and the end-to-end distance R_e. While R_e characterizes the size of a polymer chain, $l_\mathrm{p} = \frac{\kappa}{k_\mathrm{B}T}$ is defined as the direct ratio of the polymer bending stiffness κ and thermal energy $k_\mathrm{B}T$. It represents the typical length scale over which thermal fluctuations dominate the shape of the polymer. The persistence length and the end-to-end distance are coupled via the polymer contour length L_c as described by the following relation [Landau and Lifschitz 1979]:

$$R_\mathrm{e} = l_\mathrm{p}^2 \left(\frac{L_\mathrm{c}}{l_\mathrm{p}} - 1 + \exp\left(-\frac{L_\mathrm{c}}{l_\mathrm{p}} \right) \right) \tag{2.1}$$

Depending on the magnitude of l_p and R_e with respect to the contour length L_c three classes of polymers can be distinguished (see table 2.1).

flexible polymers	semi-flexible polymers	stiff polymers
$l_\mathrm{p} \ll L_\mathrm{c}$	$l_\mathrm{p} \approx L_\mathrm{c}$	$l_\mathrm{p} \gg L_\mathrm{c}$
$R_\mathrm{e} \ll L_\mathrm{c}$	$R_\mathrm{e} < L_\mathrm{c}$	$R_\mathrm{e} \approx L_\mathrm{c}$

Table 2.1: Classification of polymers according to their flexibility

Technical polymers usually belong to the class of flexible polymers. Yet, actin filaments with a contour length of $L_\mathrm{c} = 21\,\mu$m and a persistence length of $17\,\mu$m [LeGoff et al. 2002a] are semi-flexible which complicates the theoretical description of actin networks. Due to the mechanical coupling of several filaments in actin bundles, l_p is much larger in actin/fascin or actin/α-actinin bundles and can reach values up to several mm. Moreover, l_p depends sensitively on the bundle length and the spacing of cross-linking molecules within the bundle [Claessens et al. 2006, Bathe et al. 2008]. Thus, actin bundles can span a broad regime ranging from semi-flexibility to the stiff limit. While solutions and networks of flexible polymers can be well described by means of statistical physics accounting for purely entropic effects, matters are complicated for semi-flexible polymers where enthalpic effects cannot be neglected. Finally, in the limit of stiff polymers entropic effects are negligible which again simplifies theoretical descriptions. In that sense, semi-flexible polymers constitute the most complex class of polymers.

2.2.2 Rheometric principles

In general, all polymer solutions and networks show characteristics of both elastic solids and viscous fluids. This is described by the Boltzmann principle of superposition which relates the temporal evolution of the sample stress $\sigma(t)$ to the exerted deformation γ:

$$\sigma(t) = \int_{-\infty}^{t} \mathrm{d}t' \, G(t-t') \, \frac{\partial \gamma(t')}{\partial t'} \tag{2.2}$$

Herein, $G(t)$ denotes the relaxation modulus, which can be interpreted as a memory function – according to the Boltzmann principle of superposition the impact of subsequent deformations can be added up [I]. This relaxation modulus characterizes the material properties of the investigated sample.

Experimentally, the viscoelastic properties of soft matter are studied best by rheological techniques (see section 2.3.1 and 2.3.2). In principle, transient and oscillatory techniques report the same viscoelastic response. In the first case the relaxation modulus $G(t)$ is obtained while the latter reports the complex modulus $G^*(f)$; both moduli are related by a fourier transformation. The complex modulus $G^*(f)$ can be split into its real part $G'(f)$ and its imaginary part $G''(f)$. The storage modulus $G'(f)$ represents the frequency dependent elasticity, the loss modulus $G''(f)$ describes the viscous dissipation:

$$G'(f) = \frac{\sigma_0}{\gamma_0} \cdot \cos(\delta) \tag{2.3}$$

$$G''(f) = \frac{\sigma_0}{\gamma_0} \cdot \sin(\delta) \tag{2.4}$$

For the derivation of these relation a linear response is assumed [II], i.e. the oscillating deformation $\gamma(t) = \gamma_0 \cdot \sin(2\pi f t)$ is assumed to be small enough [III] to evoke an oscillating stress with the same frequency f, as $\sigma(t) = \sigma_0 \cdot \sin(2\pi f t + \delta)$. The phase shift δ sets the ratio of elastic and viscous properties: For a purely elastic sample $\delta = 0$, for a purely viscous sample $\delta = \pi/2$ is valid. In this context it is often helpful to plot the loss factor $\tan(\delta) = G''(f)/G'(f)$ in addition to the usual frequency spectra which removes the absolute values of the moduli and thus emphasizes the qualitative dominance of either elastic or viscous effects.

[I] for a detailed derivation of this relation see [Landau and Lifschitz 1975]

[II] for a detailed comparison see [Lieleg 2005] and [Landau and Lifschitz 1975]

[III] For large deformations this assumption breaks down and the viscoelastic moduli $G'(f)$ and $G''(f)$ are not well-defined anymore. In this case the differential modulus K can be used to characterize non-linear effects (compare section 4.1.4).

2.2.3 Viscoelastic frequency spectrum of entangled actin solutions

For solutions and networks of semi-flexible polymers the viscoelastic moduli $G'(f)$ and $G''(f)$ are strongly dependent on the probed frequency regime. In the following the frequency spectrum of an entangled actin solution is exemplarily discussed. Beyond the overlap concentration actin filaments cannot fluctuate freely but are confined by other actin filaments. The reptation model [De Gennes 1979, Doi and Edwards 1986] accounts for this confinement effect by considering a virtual tube representing the surrounding filament solution (Fig. 2.3).

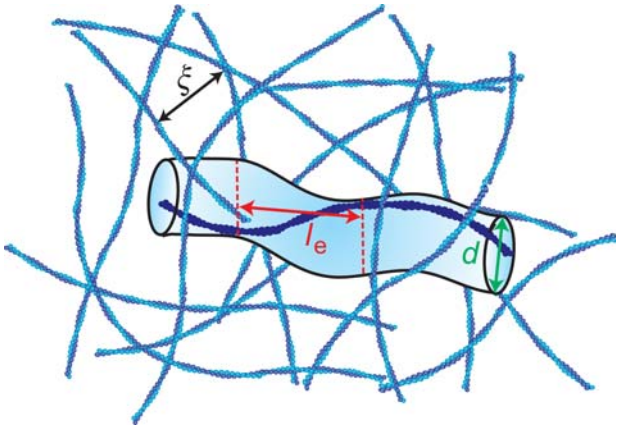

Figure 2.3: In the reptation model each filament is considered to be confined to a virtual tube which represents the surrounding polymers. The density of polymers is described by the mesh size ξ; the entanglement length l_e and the tube diameter d represent the strength of the confinement effect.

The density of filaments sets the mesh size of the solution:

$$\xi = 0.3\,\mu\text{m} \cdot \left(\frac{c_a}{\text{mg/ml}}\right)^{-1/2} \tag{2.5}$$

where c_a denotes the actin monomer concentration in mg/ml [MacKintosh et al. 1995, Tharmann et al. 2007]; for 9.5 μM actin $\xi \approx 0.5\,\mu$m is obtained. The entanglement length l_e describes the typical distance between two touching points between a given actin filament and its tube and the tube diameter d represents the maximum fluctuation amplitude of the actin filament. Obviously, l_e and d also depend on the actin filament density [Frey 2001]. Qualitatively, the frequency spectra of entangled actin solutions beyond the overlap concentration resemble each other. A typical spectrum is schematically shown in Fig. 2.4.

Two characteristic time scales separate the frequency response of entangled actin solutions into three distinct regimes: the terminal relaxation time τ_d and the entanglement time τ_e. In these three frequency regimes different microscopic mechanisms dictate the viscoelastic response of the filament solution:

- (I): $f < \frac{1}{\tau_d}$:
  At very low frequencies the viscous properties of the solution dominate the

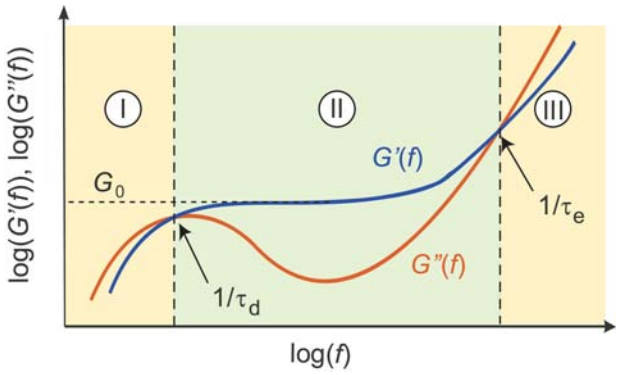

Figure 2.4: Typical frequency spectrum of an entangled actin solution. Three distinct regimes emerge: The asymptotic regimes (yellow) are dominated by viscous properties, only the intermediate frequency regime (green) is dominated by elasticity.

response. τ_d denotes the time which a given actin filament needs to perform a diffusive motion along its whole contour, i.e. after this time scale the filament has completely left its tube. This diffusive motion ("reptation") exhibits a strongly dissipative character ("viscous flow") and is accompanied by a drastic drop in the elasticity towards zero frequency.

- (II): $\frac{1}{\tau_\mathrm{d}} < f < \frac{1}{\tau_\mathrm{e}}$:
  In an intermediate frequency regime (typically between a few mHz and several Hz) the elastic properties of the solution dominate the frequency response. The loss modulus $G''(f)$ exhibits a minimum while the storage modulus shows a weak plateau. In this regime, collective phenomena have to be accounted for which arise from the entanglements between distinct filaments. As a consequence, the dominating length scale is the entanglement length l_e which also sets the plateau elasticity G_0. In detail, a scaling relation $G_0 \sim c_\mathrm{a}^{7/5}$ is predicted by the tube model [Hinner et al. 1998, Frey 2001].

- (III): $f > \frac{1}{\tau_\mathrm{e}}$:
  At high frequencies only relaxation modes at length scales smaller than l_e are fast enough to relax an external stress. As a consequence, this high frequency regime is dominated by single filament properties again. The fast fluctuation of a single actin filament is strongly dissipative similar to regime (I) and depends sensitively on the solvent viscosity. In this regime, typically at frequencies larger than 1 kHz, both viscoelastic moduli are reported to scale with a common power law of $G'(f) \sim G''(f) \sim f^{0.75}$ [Morse 1998, Gisler and Weitz 1999].

For cross-linked actin networks two qualitative differences in this frequency response are expected:

1. The elastic plateau at intermediate frequencies should become more pronounced with increasing degree of cross-linking.

2. The cross-links should suppress the reptation process at low frequencies.

While the first expectation is fulfilled for both chemically [IV] and physically [V] cross-linked actin networks, the latter is only strictly valid in the case of covalent cross-links (compare section 4.1.1).

[IV] i.e. permanently or covalently cross-linked networks
[V] i.e. transiently or noncovalently cross-linked networks

2.3 Experimental techniques

The viscoelastic moduli $G'(f)$ and $G''(f)$ introduced in section 2.2 characterize the mechanical response of actin solutions and networks. Yet, a detailed understanding of the macroscopic network properties requires both macroscopic and microscopic information. Such information can be obtained by rheological and optical techniques, each of them possessing their own intrinsic advantages and limitations. Macrorheology (section 2.3.1) allows for the detailed quantification of the macroscopic network elasticity – however, information about the network microstructure is lacking. A direct observation of labelled actin networks is ideal to investigate this network structure (section 2.3.3) but inappropriate for determining filament dynamics in densely cross-linked networks. This is due to contrast limitations that arise from labelling techniques and cannot fully be suppressed even in confocal microscopy. Local information about actin networks can also be obtained by microrheological techniques. For instance, active magnetic tweezer microrheology (section 2.3.2) can be used to map the local viscoelastic properties of an actin network; yet this technique is limited to soft networks. This limitation does not apply to dynamic light scattering (DLS), which is a label-free technique that offers a very broad accessible frequency range. However, the correlation data obtained from DLS is rather difficult to analyze. Only a combination of these different techniques provides sufficient information for a detailed characterization of complex actin networks.

2.3.1 Macrorheology

The macroscopic viscoelastic response of actin networks is determined by measuring the frequency-dependent viscoelastic moduli $G'(f)$ and $G''(f)$ with the stress-controlled rheometer Physica MCR 301 (Anton Paar, Graz, Austria) within a frequency range of typically three decades. Approximately 500 μl sample volume is loaded into the rheometer using a 50 mm plate-plate geometry with 160 mm plate separation (see Fig. 2.5). This plate separation is the smallest dimension of the sample volume but still exceeds the typical length of actin filaments or bundles which legitimates the "macroscopic" character of the measurement. To ensure linear response only small torques ($\approx 0.5\,\mu$Nm) are applied. Actin polymerization is carried out *in situ*; measurements are taken 60 min after the polymerization is initiated. To avoid drying, millipore water is added to the reservoir around the sample plate and the measuring geometry is covered with two metal half-shells. For longtime measurements a thin film of polydimethylsiloxane (ABCR, Karlsruhe, Germany) is used to cover the spacing between the measuring head and the bottom plate of the rheometer.

For actin networks the viscoelastic properties can vary over more than 3 orders

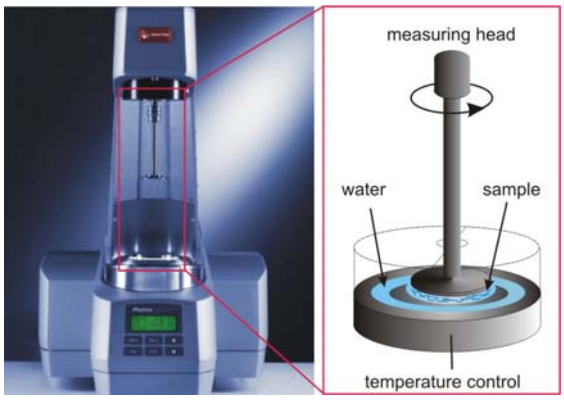

Figure 2.5: Measuring setup of the macrorheometer Physica MCR 301. A measuring head with a plate-plate geometry and 160 mm plate separation is used for all measurements shown in this thesis.

of magnitude which requires an adjustment of the measuring parameters in dependence of the sample stiffness. The following measuring protocol has been proven ideal:

1. After loading of the sample into the rheometer the polymerization is followed over time by recording $G'(0.5\,\mathrm{Hz})$ at a given but tiny torque of $0.5\,\mu$Nm. This protects the sample from mechanical overstraining during polymerization [VI].

2. As soon as a steady state is reached (typically after $t_{ss} = 40 - 60\,\mathrm{min}$) the current strain $\gamma^* = \gamma(t_{ss})$ used by the rheometer is read out.

3. A frequency spectrum in a typical range of $10\,\mathrm{mHz} - 10\,\mathrm{Hz}$ is taken with constant strain γ^*. Since γ^* was determined in the steady state with a very low torque this protocol guarantees linear response during the frequency sweep. Interestingly, this type of frequency sweep reports the frequency spectrum with much higher accuracy than a corresponding measurement with constant stress [VII].

4. After the frequency spectrum (or a series of frequency spectra) is finished, an experiment with constant shear rate is performed to probe the non-linear network properties (compare section 4.1.4). It is important to note that during such a shear rate experiment the sample is usually subjugated to plastic deformations.

Deviations from this protocol are only used for:

- *Glutaraldehyde fixation:* Glutaraldehyde is added together with HMM to prepolymerized actin filaments. The solution is gently mixed with a cut pipette

[VI] The minimum torque this rheometer can apply is approximately $0.1\,\mu$Nm.
[VII] This is somewhat counterintuitive for a stress-controlled rheometer but is due to the detailed feedback mechanism implemented in the measuring software.

tip to avoid breaking of filaments and then loaded into the rheometer for equilibration according to step 1, i.e. until a comparable elastic modulus is reached as observed for the corresponding network without glutaraldehyde. Steps 3 and 4 are followed as described above.

- *Prestress measurements:* To determine the force dependence of the viscoelastic response increasing amounts of constant prestress σ_0 are applied. Only densely cross-linked networks are investigated under prestress to avoid plastic deformation during the measurement. Full relaxation of the network is ensured in between two prestress measurements. The frequency dependence of $G'(f)$ and $G''(f)$ is determined with an oscillating measuring stress $\sigma_{\mathrm{m}}(t) = \sigma_{\mathrm{m}}^0 \cdot \sin(2\pi f t)$ whereas $\sigma_{\mathrm{m}}^0 = 0.2 \cdot \sigma_0$.

- *Ageing measurements:* Step 1 and 2 are conducted as described before. The full ageing process is recorded with constant strain γ^* which is acceptable since the changes in the viscoelastic moduli during sample ageing are usually less than 1 order of magnitude and γ^* is still small enough to ensure a linear response.

2.3.2 Microrheology

A magnetic tweezer microrheometer equipped with phase contrast microscopy is used to obtain local information on the viscoelastic moduli [Ziemann et al. 1994]. Approximately 20 μl sample volume is loaded into a cuvette, covered with a glass slide, and sealed with vacuum grease. Monodisperse paramagnetic beads (4.5 μm in diameter, Dynal M-450; Invitrogen, Karlsruhe, Germany) are added before polymerization and used as probing particles (see Fig. 2.6). An oscillating magnetic field is employed to apply forces to these paramagnetic beads [VIII].

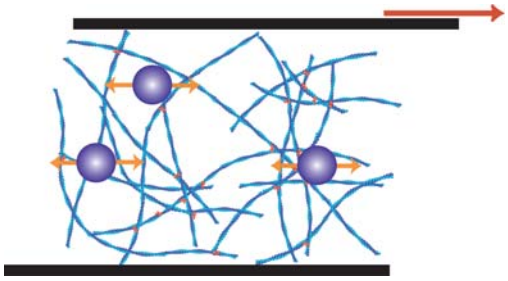

Figure 2.6: The viscoelastic response of an actin network can be probed macrorheologically by shearing the whole network (red arrow) or microrheologically by displacing embedded magnetic beads (orange arrows).

Although the position of the magnetic coils is fixed with respect to the objective, the cuvette holder can be displaced. This ensures that all observed particles are

[VIII] for a schematic representation of the magnetic tweezer setup see [Lieleg 2005]

placed in the center of the magnetic coils. This facilitates the microrheometer calibration, which is conducted in glycerol saturated with CsCl. The bead oscillation is recorded with a CCD camera and analyzed by a tracking algorithm which is implemented in the image acquisition software OpenBox [SCHILLING et al. 2004]. The maximum force applicable with this setup is 5 pN, limiting the use of this technique to materials softer than about 10 Pa.

2.3.3 Optical microscopy

For fluorescence microscopy actin is labelled with TRITC-phalloidin (Sigma). To avoid photobleaching 0.6 μM glucoseoxidase, 0.03 μM catalase and 0.01 M glucose are added. Confocal images are acquired with a confocal microscope (TCS SP5, Leica, Wetzlar, Germany). The samples for transmission electron microscopy (Philips EM 400T) are adsorbed to glow-discharged carbon-coated formvar films on copper grids. The samples are washed in a drop of distilled water and negatively stained with 0.8 % uranyl acetate; excess liquid is drained with filter paper.

2.3.4 Dynamic light scattering

Samples are loaded into a glass cuvette, sealed with parafilm and kept at room temperature for 60 min to allow for polymerization and structural equilibration. For measurements the samples are illuminated for several hours with a laser using light of wave length $\lambda = 532.5\,\text{nm}$. Scattered light from a sample area of 250 μm x 1000 μm is detected with a CCD camera at 90 °. At this scattering angle a correlation in the sample dynamics is probed at a length scale of 50 nm. A characteristic speckle pattern is observed as depicted in Fig. 2.7.

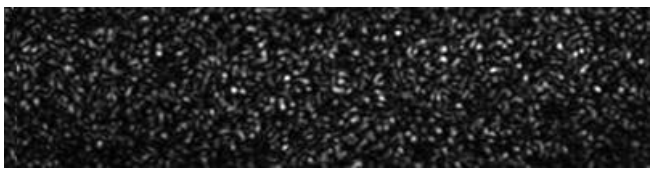

Figure 2.7: Typical speckle pattern as obtained from DLS. The shown sector corresponds to a sample area of 250 μm x 1000 μm.

This speckle pattern is not static but varies over time which is due to the internal dynamics of the probed sample. To quantify this dynamics the correlation function of the speckle pattern $c_\text{I}(t,\tau)$ is calculated at different delay times τ

$$c_\text{I}(t,\tau) = \frac{\langle I_\text{P}(t) I_\text{P}(t+\tau)\rangle_\text{P}}{\langle I_\text{P}(t)\rangle_\text{P}\,\langle I_\text{P}(t+\tau)\rangle_\text{P}} - 1 \tag{2.6}$$

where I_P is the intensity of a given pixel P and t denotes the sample age (compare [DURI et al. 2005]). Note, that due to the rather uncommon normalization $c_\text{I}(t,0)$

is somewhat smaller than 1.

For the data shown in this thesis the full area of $250\,\mu\text{m} \times 1000\,\mu\text{m}$ is analyzed as a whole; yet, the use of a CCD camera instead of a photomultiplier in principle also allows for a separate analysis of different regions of interest and thus for a spatial comparison of local dynamics.

3 Static network properties: Correlating the microstructure to the macroscopic network response

Cells make use of semi-flexible polymers to form networks that provide structural integrity and can withstand mechanical load. The mechanical properties of cells are mainly attributed to the cytoplasmic biopolymer actin which is organized in filamentous networks and bundles. These actin bundles are e. g. located in the filopodia where cells create large forces that are required for motion processes. Actin bundles are also present in the cell body where "stress-fibers" span throughout the whole cell (compare Fig. 3.1). Besides these prominent bundle structures, actin filaments are organized into cross-linked networks that are the main component of the actin cortex; if bundles are embedded in these networks, composite phases are created.

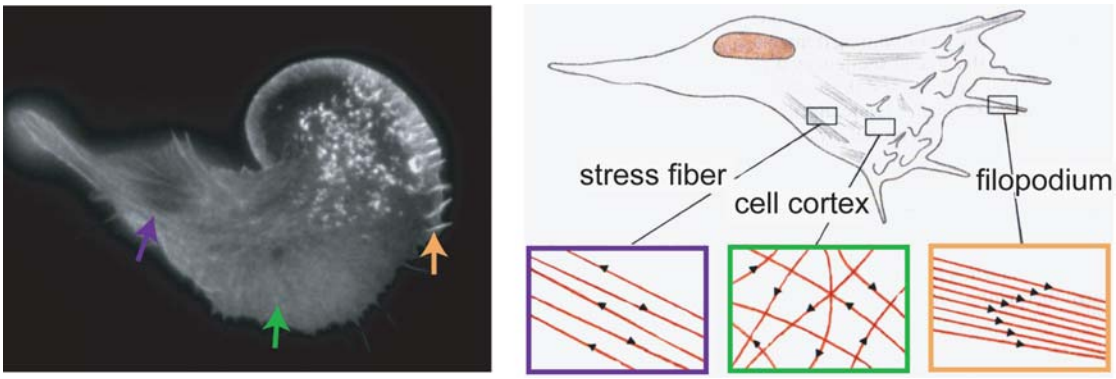

Figure 3.1: Different morphologies of actin networks *in vivo*. Stiff actin bundles are observed in the filopodia (orange) and in stress-fibers (purple). Cross-linked networks, however, are the main component of the actin cortex (green).

Cells combine various actin binding proteins (ABPs) to locally control the formation of the different microstructures. Usually, one specific cross-linking or bundling protein is predominant in one of these local cytoskeletal structures. As a consequence this ABP is usually exclusively associated with exactly this particular

region of the cytoskeleton, e. g. α-actinin and fascin are often regarded to be solely actin bundling proteins.

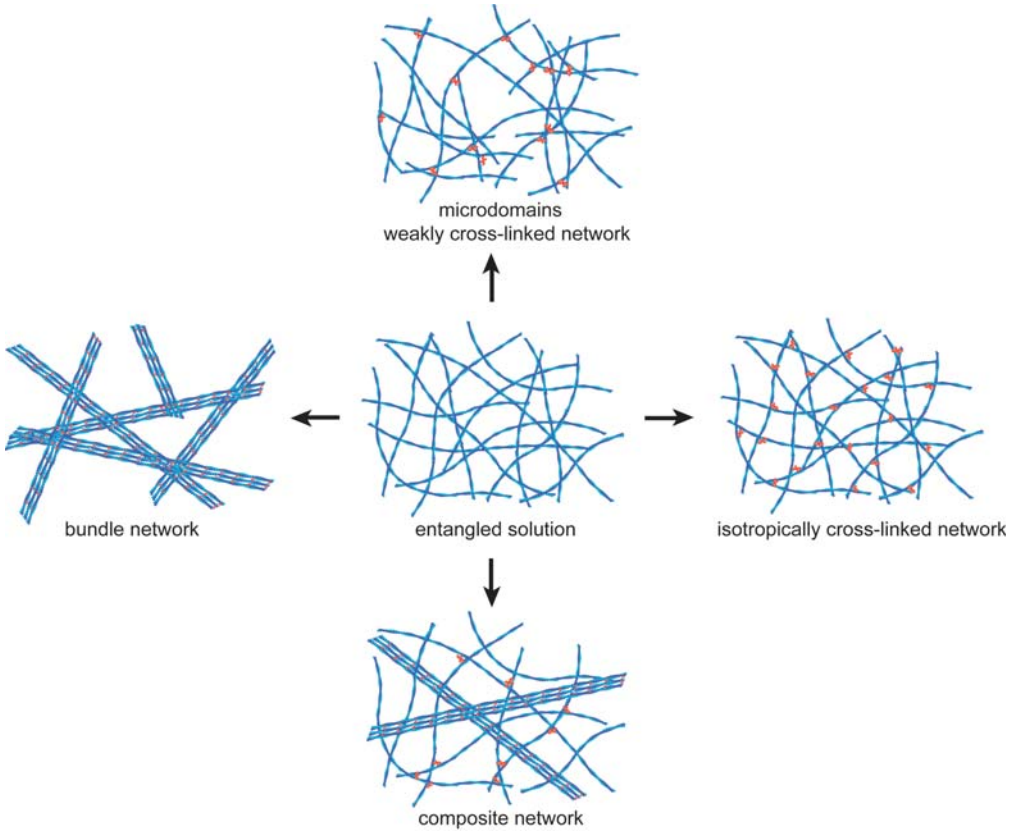

Figure 3.2: Structural phase diagram for *in vitro* reconstituted actin networks. Depending on the type of ABP used, an entangled solution (center) can be rearranged into a weakly cross-linked network (top), an isotropically cross-linked network (right), a bundle network (left) or a composite network (bottom).

Simple *in vitro* reconstitutions of cytoskeletal network elements [I] can result in the formation of similar structures as observed *in vivo* [Bausch and Kroy 2006] – if the "correct" ABP is chosen (Fig. 3.2). In a classical cell-biological view, an actin bundling protein such as α-actinin or fascin should exclusively be able to create bundle networks. However, from a physical point of view it is reasonable to assume that a given ABP is able to organize actin filaments into different network configurations – depending on the concentration of the ABP relative to the filament density [Tempel et al. 1996]. Such a complex phase behavior was theoretically predicted by [Borukhov et al. 2005]. A systematic investigation of actin/cross-linker phase diagrams is crucial to identify the physical principles

[I] i.e. a combination of actin filaments with only one type of ABP

governing the formation of different network structures that are observed for distinct ABPs. The phase behavior of actin networks formed by the ABPs fascin, α-actinin and rigor-HMM is discussed in section 3.1. Section 3.2 addresses the influence of local heterogeneities on the network elasticity and the actin/α-actinin system is exemplarily discussed. It is a challenging task to relate the different observed microstructures to the macroscopic network elastictiy as e. g. determined from rheological experiments. In section 3.3 a detailed microscopic description of the elasticity of actin/fascin bundle networks is compared to the microscopic model that can be used to describe isotropically cross-linked networks as they are formed by rigor-HMM and implications for composite networks are discussed.

3.1 Structural and mechanical transitions in actin networks

Entangled solutions of the biopolymer actin are mechanically weak – at least in the regime of linear viscoelasticity. The macroscopic elastic response of entangled actin solutions can be significantly enhanced by the addition of cross-linking or bundling proteins. To quantify the dependence of the network elasticity on the ABP concentration, the plateau modulus $G_0 = G'(10\text{ mHz})$ is a suitable parameter that can be analyzed as a function of the cross-linker concentration c_{ABP} relative to the actin monomer concentration c_{a}. The experimental control parameter is the relative cross-linker concentration $R = \frac{c_{\text{ABP}}}{c_{\text{a}}}$ (compare Fig. 3.3). Depending on the type and the concentration of the ABP, different mechanical regimes are observed which manifest themselves in different scaling relations $G_0 \sim R^x$. The scaling exponent x describes the sensitivity of the network elasticity on the ABP concentration. It is the result of various microscopic network parameters. Besides the micromechanical properties of the network constituents such as the bending stiffness of individual actin bundles [Claessens et al. 2006] or the persistence length of single actin filaments, the network microstructure determines the deformation mode (compare section 3.3) and with that mainly dictates the static elasticity of cross-linked and bundled actin networks. Therefore, the existence of distinct mechanical scaling regimes directly implies that different network structures are present.

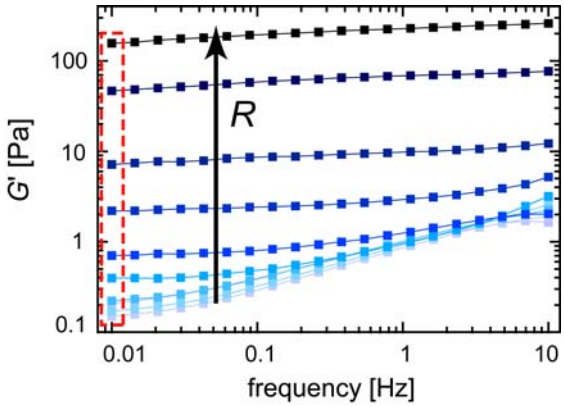

Figure 3.3: The quantification of the static network elasticity with respect to the relative ABP concentration, R, is exemplarily shown for actin/fascin networks ($c_{\text{a}} = 0.4\,\text{mg/ml}$, $R = 0$ up to $R = 0.5$). The frequency spectrum of the storage modulus $G'(f)$ is employed to define a plateau modulus $G_0 = G'(10\,\text{mHz})$.

In the following sections the elasticity of actin networks that are cross-linked and/or bundled by the three ABPs α-actinin, fascin and HMM are compared and the phase behavior of the networks is discussed. For homogeneous bundle networks and isotropically cross-linked networks the phase boundary is parameterized and a simple relation is obtained which gives a constraint for the phase transition.

3.1.1 Structural polymorphism in actin/α-actinin networks: temperature dependent transitions

By increasing the relative α-actinin concentration from $R = 0$ up to $R = 0.5$, the macroscopic elastic response of actin/α-actinin networks at 18 °C can be enhanced by more than 3 orders of magnitude. However, this enhancement is not monotonic throughout the whole concentration regime; with respect to R, the plateau modulus $G_0 = G'(10\,\mathrm{mHz})$ reveals 3 distinct regimes (Fig. 3.4) which for simplicity are approximated best by power laws: At low α-actinin concentrations, the network elasticity depends only weakly on R, $G_0 \sim R^{0.5}$. Above a critical concentration of $R^* \approx 0.01$, a strong increase in the plateau modulus is observed, $G_0 \sim R^{2.3}$. This scaling regime at intermediate α-actinin concentrations crosses over to a third regime at $R^\# \approx 0.1$. Here, the plateau modulus still increases with respect to R; however, the observed enhancement of the network elasticity is weaker than before, $G_0 \sim R^{0.6}$.

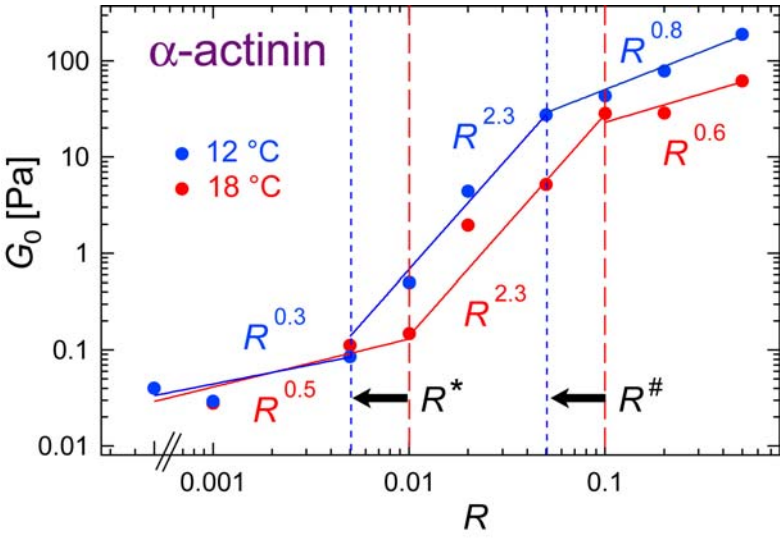

Figure 3.4: Mechanical regimes for α-actinin networks ($c_a = 9.5\,\mu$M). The plateau modulus G_0 is depicted as a function of the relative α-actinin concentration, R. Three distinct mechanical regimes are observed, the transition points between these regimes (R^* and $R^\#$) can be shifted by temperature as indicated by the dashed lines (red symbols and lines: 18 °C, blue symbols and lines: 12 °C) while the scaling relations in these regimes remain basically unaffected.

The elastic response of actin/α-actinin networks depends sensitively on temperature [Tempel et al. 1996]. This can be rationalized since the binding affinity of ABPs towards actin is temperature dependent. The data discussed so far was obtained at 18 °C where the binding affinity of α-actinin is low; at lower temper-

ature the effective amount of bound α-actinin molecules should be increased. As a consequence, the mechanical transition points discussed before are expected to shift to lower nominal R-values. Indeed, exactly such a behavior is observed: Both mechanical transitions, R^* and $R^\#$, occur at lower α-actinin concentrations if the network is probed at 12 °C. However, although the bounderies of the 3 mechanical regimes are shifted, the observed scaling relations $G_0 \sim R^x$ are almost unaffected by the temperature change (Fig. 3.4).

The weak dependence of the plateau modulus on the α-actinin concentration that is observed in the first regime below R^* is generic for other cross-linking or bundling ABPs (e. g. hisactophilin-constructs [Wagner et al. 2006], rigor-HMM or fascin (see section 3.1.2) and even low levels of depletion forces [Tharmann et al. 2006] [II]). In this first mechanical regime the networks appear homogeneous and isotropic and show no signs of bundles or composite phases. Furthermore, the plateau modulus G_0 scales with the actin concentration as $G_0 \sim c_a^{1.3}$ suggesting that entanglements dominate the elastic response [Hinner et al. 1998]. This is in contrast to networks at higher cross-linker densities where the elasticity is dominated by the cross-linker distance (see section 3.1.2 and 3.3).

Concomitant with this first mechanical transition at $R = R^*$, the formation of bundles can be observed in confocal microscopy images (Fig. 3.5B) in agreement with former observations [Bendix et al. 2008]. This onset of bundling occurs in a very similar concentration regime as also reported for scruin [Shin et al. 2004a] and fascin (compare Fig. 3.8B), which underlines the comparable binding affinities of these actin bundling proteins. In contrast to the purely bundled network formed by fascin, α-actinin creates a heterogeneous, composite phase above the bundling transition: Distinct bundles of various thickness are embedded in a network that still contains single actin filaments (Fig. 3.5A).

This composite phase resembles the actin/scruin networks reported in [Shin et al. 2004a]. Indeed, the observed scaling behavior of the plateau modulus in this composite regime is comparable to the scaling relation obtained by Shin *et al.* for scruin networks in the composite phase. As the confocal image depicted in Fig. 3.5A shows, thick actin/α-actinin bundles are only sparsely present at intermediate α-actinin concentrations. The degree of bundling can be tuned: increasing the nominal [III] α-actinin concentration [Bendix et al. 2008] at a given temperature leads to the formation of thicker bundles and increases the bundle density. Increasing the effective α-actinin concentration by lowering the temperature has the same effect (Fig. 3.5B). In either case, the resulting network structure retains

[II] Note, that for actin/PEG networks pseudo-cross-links are formed in this first regime. This makes a microscopic comparison with networks cross-linked by ABPs difficult.

[III] In the context of this thesis the *nominal* ABP concentration represents the total amount of ABPs present in the sample while the *effective* ABP concentration refers to the amount of ABPs that are bound to actin.

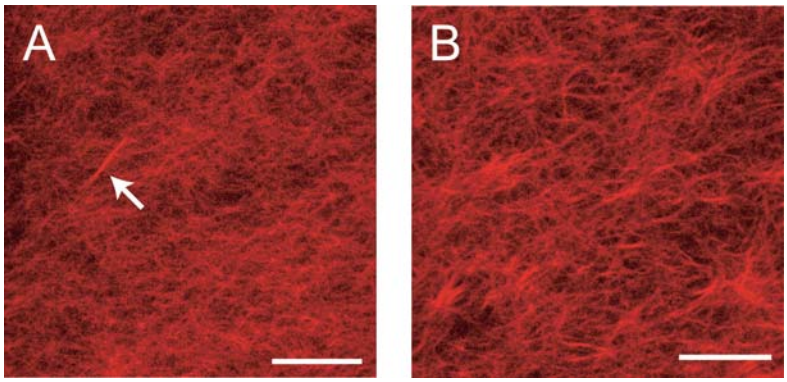

Figure 3.5: Confocal micrographs of composite actin/α-actinin networks ($c_a = 4.75\,\mu$M, $R = 0.05$); bundles are locally embedded in the network, the degree of bundling can be adjusted by temperature. (A): At 27 °C bundles are very rare (arrow); (B): At 7 °C the degree of bundling is increased, but the network structure is still highly heterogeneous. Scale bars denote 10 μm.

its heterogeneous character.

The heterogeneities described so far are still quite modest; on the mesoscopic length scale accessible with classical phase contrast microscopy or epifluorescence, individual bundles as detected by confocal microscopy are hardly visible – the bundle diameters are still too small to distinguish the bundles from single filaments in such a composite network. However, very thick bundles and even stronger heterogeneities in the local network structure should be detectable. Such structural rearrangements occur at higher α-actinin concentrations, i. e. in the third regime $R > R^{\#}$, and can be observed by light microscopy techniques as depicted in Fig. 3.6: Star-shaped clusters are observed both in epifluorescence (Fig. 3.6A) and phase contrast micrographs (Fig. 3.6B). The star-shaped regions resemble actin/α-actinin foci that are found in living cells [Yamashiro-Matsumura and Matsumura 1986]. These regions of clustered bundles are not detectable at α-actinin concentrations $R < R^{\#}$.

Confocal images reveal, that in theses clusters many bundles are concentrated in localized spots that have a size of $\approx 5 - 10\,\mu$m. The spatial distribution of the star-shaped bundle clusters shown in Fig. 3.6 can be visualized by a projection of a confocal z-stack at low magnification as depicted in Fig. 3.7A [IV]. In order to determine the fractal (or Hausdorff) dimension d of such bundle clusters, the cluster mass M_{cluster} has to be related to the cluster size R_{cluster} similar to the analysis of colloidal aggregates [Weitz and Oliveria 1984]: $M_{\text{cluster}} \sim R^d_{\text{cluster}}$. The integrated fluorescence intensity of a bundle cluster is proportional to the amount of actin filaments in the cluster and can thus be used to represent M_{cluster}. Using

[IV] This picture was binarized to enhance visibility.

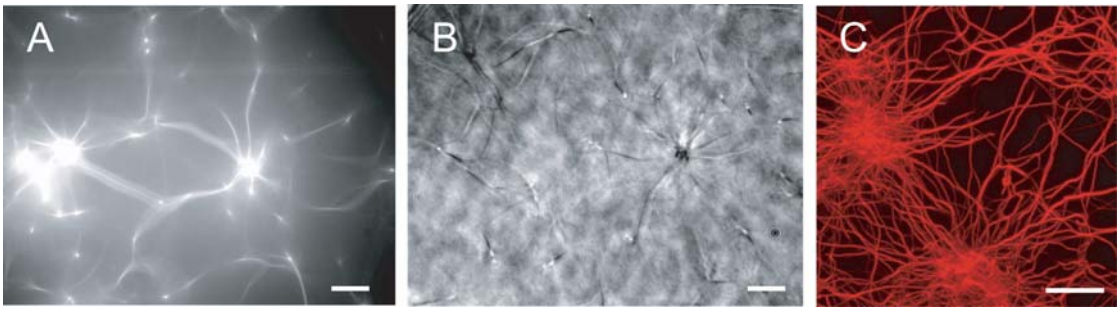

Figure 3.6: Epifluorescence (A) and phase contrast (B) micrograph of actin/α-actinin networks ($R = 0.5$, $c_a = 2.4\ \mu$M) showing bundle clusters. (C) Z-projection (20 μm) of a confocal micrograph of bundle clusters ($R = 0.5$, $c_a = 4.75\ \mu$M). Scale bars denote 10 μm.

this method a power law behavior $M_{\text{cluster}} \sim R_{\text{cluster}}^{1.8\pm0.2}$ is observed (Fig. 3.7B), which corresponds to a fractal cluster dimension of $d \approx 1.8$. Interestingly, an evaluation of relatively large sample volumes with $R_{\text{cluster}} = 150\,\mu$m suggests that the network organisation follows this fractal dimension also on larger length scales creating a self-similar material (compare section 4.2).

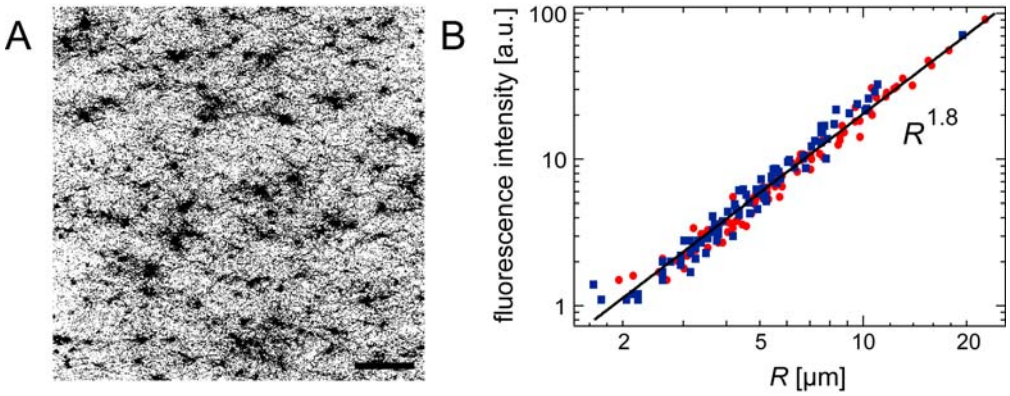

Figure 3.7: (A) Confocal micrograph of a bundle cluster network ($c_{\text{a}} = 4.75\,\mu$M, $R = 0.5$) at low magnification (the scale bar represents 50 μm). The picture shows a projection of a z-stack of $\Delta z = 150\,\mu$m height which was binarized to enhance visibility. (B) The integrated fluorescence intensity of the bundle clusters depicted in (A) is plotted as a function of cluster size, R_{cluster}. Circles denote data points that were obtained by assuming spherical clusters, squares denote a polygon approximation. A power law behavior $M_{\text{cluster}} \sim R_{\text{cluster}}^{1.8}$ is observed for both methods.

The occurrence of bundle clusters is not limited to the ABP α-actinin, qualitatively similar heterogeneities can be observed for filamin bundle networks, but not for bundle networks formed by scruin [Shin et al. 2004a], fascin (section 3.1.2.2)

or espin [Purdy et al. 2007]. A possible explanation for this observation could be, that the size of the ABP is the crucial parameter for cluster formation and long and flexible ABPs like α-actinin or filamin might be required to perform cross-linking and clustering besides bundling. Interestingly, in this bundle cluster regime of actin/α-actinin networks the enhancement of the macroscopic plateau elasticity is significantly weaker than in the composite phase. While a microscopic description of the macroscopic network elasticity is extremely difficult for such heterogeneous networks, microrheological techniques and simulations can be employed to investigate the influence of structural heterogeneities on the macroscopic network response. This is described in section 3.2. However, it is clear that the different scaling regimes observed in the plateau elasticity of actin/α-actinin networks are directly related to changes in the network microstructure.

3.1.2 Structural and mechanical transitions in homogeneous networks: describing the phase boundary

For a detailed physical understanding of structural and mechanical phase transitions well-defined model systems are necessary. Two rather simple model actin networks are given by the actin/HMM and actin/fascin system. In contrast to the highly complex actin/α-actinin system, actin/fascin networks exhibit only two different mechanical phases (Fig. 3.8B); the same holds true for actin/HMM networks (Fig. 3.8A and [Tharmann et al. 2007]). The structural polymorphism observed for actin/α-actinin networks does not occur in actin/HMM and actin/fascin networks.

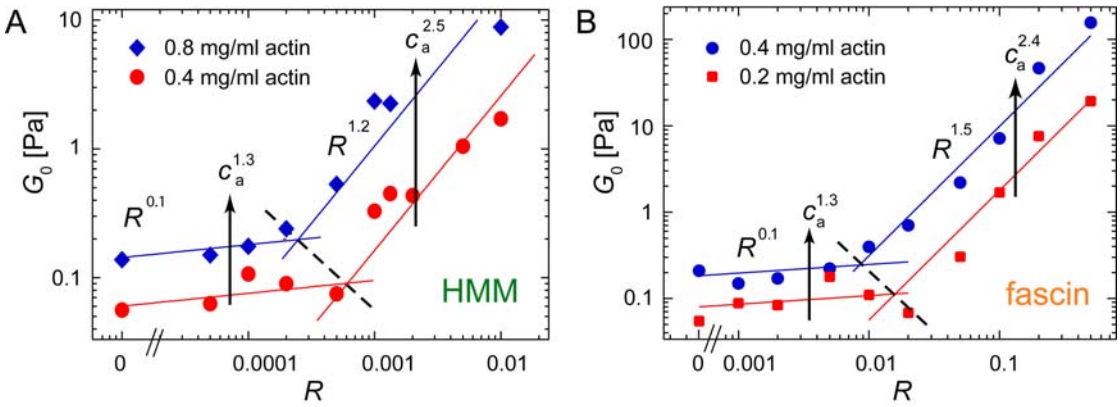

Figure 3.8: Mechanical regimes for (A) actin/HMM and (B) actin/fascin networks: The plateau modulus G_0 is depicted as a function of the relative ABP concentration R. As indicated by the colors, two different actin concentrations are investigated. The dependence of G_0 on c_a is obtained by scaling the fits for the low-c_a data upon the high-c_a data points. The dashed line shows the boundary separating the two scaling regimes.

3.1.2.1 Isotropically cross-linked networks

If rigor-HMM is employed to create cross-links in actin solutions, the overall filament organization of the actin solution is not significantly altered - the HMM molecules solely create cross-links between distinct actin filaments thereby decreasing the cross-linker distance l_c with increasing R [THARMANN et al. 2007]. For actin/HMM networks, the plateau modulus $G_0 = G'(10\,\mathrm{mHz})$ at low R is only slightly dependent on R, $G_0 \sim R^{0.1}$, while above a critical value $R^{\#}$, G_0 increases with $G_0 \sim R^{1.2}$ (Fig. 3.8A). These exponents fit the data for both actin concentrations probed; furthermore the second scaling regime also extends to higher R-values [THARMANN et al. 2007]. The transition point $R^{\#}$ depends slightly on the actin concentration ($R^{\#}(0.8\,\mathrm{mg/ml}) \approx 0.002$, $R^{\#}(0.4\,\mathrm{mg/ml}) \approx 0.004$).

In the first regime ($R < R^{\#}$), the observed dependence of the plateau elasticity on the polymer density, $G_0 \sim c_a^{1.3}$, is in good agreement with predictions for entangled actin solutions [HINNER et al. 1998] [V]. Thus, at very low HMM densities a theoretical description based on the tube model holds suggesting that the network elasticity in this first regime is still dominated by entanglements rather than cross-links. In the second regime, the dependence on the actin concentration as predicted by an affine stretching model [MACKINTOSH et al. 1995] is reasonably reproduced, $G_0 \sim c_a^{2.5}$ [VI]. This suggests that in this second regime the actin/HMM cross-links dominate over the remaining entanglement points.

In order to pin down the microscopic length scale that sets the transition from the entanglement dominated regime to the cross-link dominated regime an mathematical description of the mechanical transition in actin/HMM networks (as indicated by the dashed lines in Fig.3.8A) would be of avail. It would have to relate the two competing length scales, i. e. the cross-linker distance l_c and the entanglement length l_e to give a quantitative criterion for the cross-link transition. As already mentioned, the exact position of the cross-link transition $R^{\#}$ depends on the actin concentration. With the observed scaling behavior $G_0(R, c_a)$ the plateau modulus is parameterized in both cross-linker concentration regimes, i e. before ($i = \mathrm{I}$) and after the cross-link transition at $R^{\#}$ ($i = \mathrm{II}$):

$$G_0(R, c_a) = G_0(R^t, c_a^t) \cdot f_i\left(\frac{c_a}{c_a^t}\right) \cdot g_i\left(\frac{R}{R^t}\right) \tag{3.1}$$

where $G_0(R^t, c_a^t)$ denotes an arbitrary but fixed transition point and the functions f_i and g_i can be read from the scaling relations depicted in Fig. 3.8A. At the cross-over concentration $R = R^{\#}$ these two parameterizations have to be equal. This uniquely determines the scaling of $R^{\#}$ with the actin concentration, $R^{\#} \sim c_a^{-6/5}$,

[V] The tube model predicts a scaling $G_0 \sim c_a^{7/5}$ (compare section 2.2.3).
[VI] The affine stretching model predicts a scaling $G_0 \sim c_a^{11/5}$.

which results in a constraint describing the phase boundary: $c_{\mathrm{HMM}} \cdot c_{\mathrm{a}}^{1/5} = \mathrm{const.}$ Using the entanglement length $l_{\mathrm{e}} \sim c_{\mathrm{a}}^{-2/5}$, the latter can be approximated to

$$c_{\mathrm{HMM}} \cdot l_{\mathrm{e}}^{-1/2} = \mathrm{const.} \tag{3.2}$$

This suggests that with increasing actin concentrations (corresponding to decreasing l_{e}) smaller absolute concentrations of HMM molecules are sufficient to induce the crossing-over to the second scaling regime. Thus, the critical parameter which is held constant along the "phase boundary" is the average cross-linker distance l_{c} – no overall rearrangement in the network structure occurs. This is consistent with the experimental finding that the cross-linker distance at the transition points is roughly constant [Luan et al. 2008] and comparable to the persistence length of an actin filament. $l_{\mathrm{c}} \approx 14 - 17\,\mu$m refers to the percolation threshold at which the cross-link density is high enough to evoke an overall network response that is not dominated by entanglements any more. The entanglement length in turn is set by the persistence length – determining the length scale for tube confinement effects. The overall network structure of actin/HMM networks will not be changed when crossing $R^{\#}$; no extra free energy or enthalpy compensation is needed for structural rearrangements. Thus, less HMM molecules are required to induce the mechanical transition at higher filament densities.

While the viscoelastic response of weakly cross-linked actin networks is still dominated by entanglements, low cross-linker concentrations have a small but significant influence on the plateau elasticity. Obviously, the HMM molecules are able to slightly change the network properties even at very low concentrations. To elucidate the impact of cross-linking molecules *before* the cross-link transition $R^{\#}$, an investigation of the microscopic network elasticity might be of avail. The local viscoelastic moduli are determined at $\approx$ 100 positions per sample for an intermediate frequency of 0.1 Hz. From the distribution data of $G'(0.1\,\mathrm{Hz})$ cumulative probabilities are calculated for different R, i.e. below and above $R^{\#}$ (Fig. 3.9A). Based on the shape of the resulting distributions two regimes can be distinguished: below $R^{\#}$ the distribution curves show pronounced heterogeneities of G_0 whereas above the critical concentration $R^{\#}$ homogeneous distributions are obtained. In the latter, the mean values and the absolute widths of the distributions increase with increasing cross-linker concentration R. Thus, normalizing the cumulative probabilities by their respective average elastic modulus (Fig. 3.9B) results in a collapse of all probability distributions onto a single curve. Interestingly, this normalized distribution curve is identical to the distribution curve obtained for an entangled actin solution, confirming the cross-linking of actin filaments into homogeneous and isotropic networks by rigor-HMM [Tharmann et al. 2007].

The relative distribution width is given by the normalized standard deviation $\sigma_{\mathrm{rel}} = \frac{\sigma}{<G'(0.1\ \mathrm{Hz})>}$. A relative width of $\sigma_{\mathrm{rel}} = 20\%$ is obtained for an entangled actin

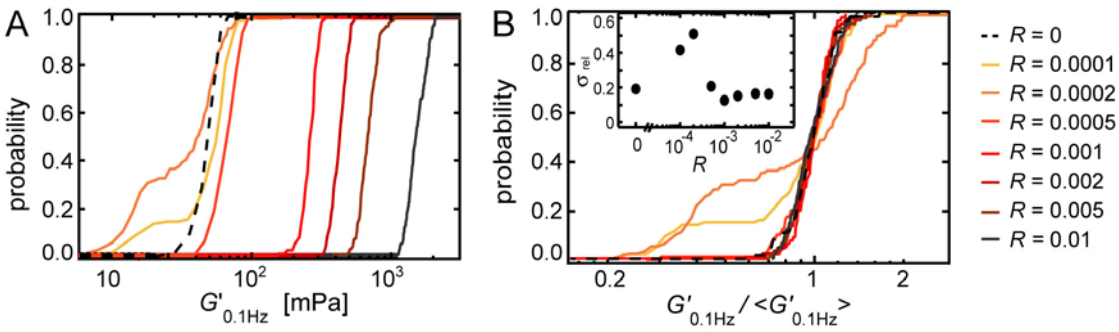

Figure 3.9: (A) Cumulative probabilities of the network elasticity are obtained from the local distribution data of $G'(0.1\,\mathrm{Hz})$ for different R. (B) Normalization by the respective average value $< G'(0.1\,\mathrm{Hz}) >$ allows an overlay of curves for $R > R^{\#}$. This is not possible for samples $R < R^{\#}$ as their relative distribution width $\sigma_{\mathrm{rel}} = \frac{\sigma}{<G'(0.1\ \mathrm{Hz})>}$ is almost twice as large as for the other samples as depicted in the inset.

solution as well as for cross-linked networks ($R > R^{\#}$) as depicted in the inset of Fig. 3.9B. At low HMM concentrations ($R < R^{\#}$), $\sigma_{\mathrm{rel}} = 40 - 50\,\%$ is more than twice as large corresponding to the broad shape of the distribution curves: the degree of heterogeneity is increased by the addition of a few cross-linking molecules, until at the transition point $R^{\#}$ a homogenous microstructure is reached again. The occurrence of heterogeneities at low cross-linker concentrations was also reported by [Tempel et al. 1996] for actin/α-actinin networks and referred to as "microgelation". There, this hypothesis was mainly based on electron microscopy pictures which are prone to artifacts. However, the microrheological characterization of the weakly cross-linked regime discussed here provides strong and direct experimental evidence which unambiguosly demonstrates the local heterogeneity of the elastic network properties.

Interestingly, the distributions obtained for the two lowest ratios ($R = 1/5,000$ and $R = 1/10,000$) contain values even lower than the elastic modulus of an entangled actin solution; the corresponding histogram exhibits a second peak at $G'(0.1\,\mathrm{Hz}) \approx 20\,\mathrm{mPa}$. At the same time, only very few values exceed the elastic modulus obtained for $R = 0$. To elucidate the network microstructure responsible for this peculiar broadening, full frequency spectra are determined at different sample positions. All obtained spectra have comparable shapes, none of them exhibits a minimum in $G''(f)$ within the frequency range probed. As discussed in detail in section 4.1.1 of this thesis, a minimum in $G''(f)$ would be a clear signature of a transiently cross-linked network. However, the locally obtained frequency spectra are merely shifted lack this feature and are merely shifted with respect to their absolute values. This finding might suggest that in this first cross-linker concentration regime ($R < R^{\#}$) the observed heterogeneity in the

local viscoelastic response is caused by local filament density fluctuations induced by the few HMM molecules present rather than by a formation of cross-linked microdomains. In either case, the observed formation of local heterogeneities may be a more generic phenomenon and a prerequisite for the structural transition into a network dominated by percolating cross-links.

3.1.2.2 Purely bundled networks

In contrast to the cross-link transition in actin/HMM networks, the mechanical transition in actin/fascin networks is accompanied with a major structural rearrangement. In the presence of high concentrations of fascin, actin filaments organize into a network of bundles (Fig. 3.10A) while below a critical value $R^* \approx 0.01$ no bundles can be observed. Both fluorescence and transmission electron microscopy do not show any sign of a composite phase as reported for other ABPs like scruin [Shin et al. 2004a] or hisactophilin-constructs [Wagner et al. 2006]. Moreover, the existence of a purely bundled phase can be demonstrated by a cosedimentation assay (see appendix).

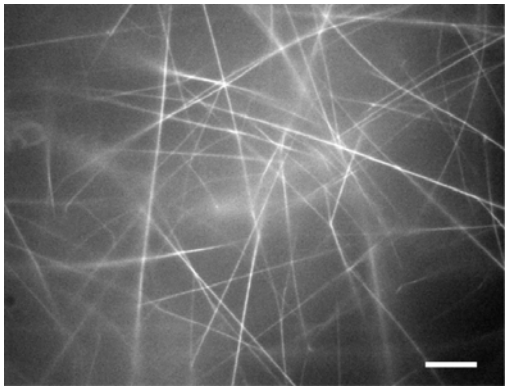

Figure 3.10: Fluorescence micrograph of an actin/fascin network (0.1 mg/ml actin): at high fascin concentrations a purely bundled network is formed (the scale bar represents 10 μm).

For actin/fascin networks, the mechanical transition point occurs at a significantly larger ABP concentration than for actin/HMM networks. Here, $R^* \approx 0.01$ is determined from the rheological data at $c_a = 0.4\,\mathrm{mg/ml}$ which agrees well with the structural transition observed in microscopy. Below R^* the plateau modulus scales with the actin concentration as $G_0 \sim c_a^{1.3}$ suggesting that entanglements dominate the elastic response – comparable to the low-R regime of actin/HMM networks. Interestingly, the transition into a regime dominated by the cross-linking ABP occurs at much higher R-values compared to actin/HMM networks. This suggests that fascin might not be an equally effective cross-linking molecule as rigor-HMM which could be due to the small size of fascin. Accordingly, the transition observed for actin/fascin networks is a bundling transition rather than a cross-link transition. Above R^* a different scaling regime occurs with $G_0 \sim c_a^{2.4}$.

So far no theoretical predictions for this scaling relation existed for networks of stiff actin bundles; it is by coincidence a similar scaling relation as obtained for isotropically cross-linked networks, however the microscopic origin of the network elasticity is fundamentally different for a network of stiff bundles. The detailed properties of actin/fascin bundle networks as well as an appropriate modeling of the network elasticity are addressed in section 3.3.

Combining the different R-dependencies before and after the transition, a constraint for the transition line can be calculated following the same formalism as in 3.1.2.1. A surprisingly simple criterion is also obtained for this bundling transition

$$c_{\text{fascin}} \cdot l_{\text{e}}^{+1/2} = \text{const.} \tag{3.3}$$

which is qualitatively different from equation (3.2): higher actin concentrations (corresponding to smaller l_{e}) require larger fascin concentrations to induce the mechanical (and structural) transition in actin/fascin networks. In contrast to the simple cross-link/percolation transition of actin/HMM networks, the relation obtained for actin/fascin networks defies an obvious explanation and a detailed theoretical model is still lacking. Such a model would need to account for the subtle interplay between the confinement free energy of polymers in both the bundle and the network as well as the binding enthalpy of the cross-linking proteins.

In direct correlation with the mechanical (and in case of actin/fascin networks also structural) transition, the microscopic origin of the network elasticity changes. While the confinement of filament fluctuations to length scales smaller than the entanglement length is responsible for the elastic response of an entangled solution or a weakly cross-linked networks, stretching and bending of filaments or bundles is expected to dominate at high cross-linker densities. The exact type of the deformation mode as well as the respective degree of (non-)affinity is still under debate and no unified theoretical description exists so far. This problem is further addressed in section 3.3 of this thesis where the microscopic origin of bundled actin/fascin networks is compared to isotropically cross-linked and composite networks.

3.1.3 Accessible paths in the phase diagram

As described in section 3.1.1 and 3.1.2, *in vitro* reconstitutions of actin/ABP networks can result in several structural and mechanical phases. Actin/HMM networks exhibit only one single transition from a weakly cross-linked phase to an isotropically (= strongly) cross-linked regime. Actin/fascin networks also show only one transition: at low R weakly cross-linked networks are observed while a purely bundled phase is formed above a critical fascin concentration (Fig. 3.11). For actin/α-actinin networks a highly complex structural polymorphism is observed: three different regimes are identified – both in the mechanical response and the network organization.

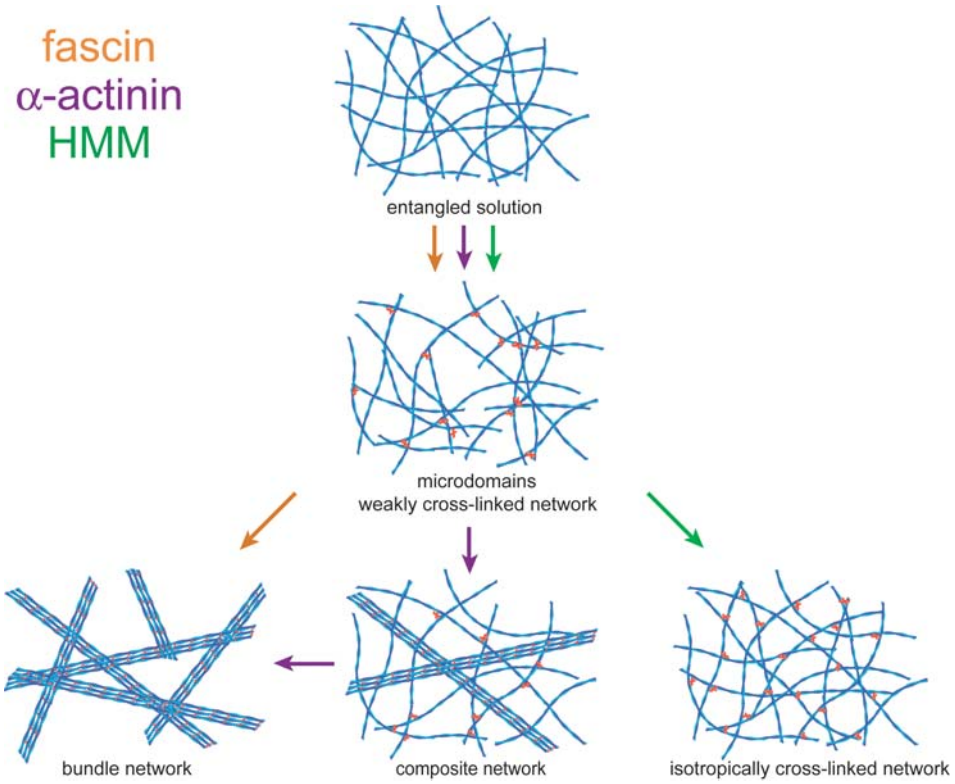

Figure 3.11: Accessible paths in the phase diagram for actin/α-actinin, actin/fascin and actin/HMM networks. For each ABP the path through the phase diagram starts with the generic weakly cross-linked phase.

Theoretical predictions for charged stiff rods cross-linked by molecules of different affinity [Borukhov et al. 2005] suggest that the interaction energy between actin and the cross-linking molecule is the key parameter which can be used to classify a given ABP as either "cross-linking" or "bundling". While this simple picture is appealing, many ABPs do not follow this rigorous classification. The direct comparison of the three actin/ABP systems mentioned above shows that a variation of the relative cross-linker concentration allows for the creation of at least two different structural and/or mechanical phases in cross-linked actin networks. However, the exact concentration regimes for these phases as well as the accessible parts of the phase space drastically vary for different types of actin binding proteins.

Besides the relative cross-linker concentration, the inherent microscopic characteristics such as the size, shape, flexibility and binding affinity of a given ABP determine the microstructure of the resulting cross-linked and/or bundled actin network. In [Wagner et al. 2006] it was shown, that the spacer distance between actin binding domains is an important parameter that influences the microstruc-

ture of actin/ABP networks. For engineered hisactophilin constructs where the actin binding site and thus the binding energy is conserved, the "bundling propensity" increases with decreasing spacer distance of the ABP. Qualitatively, this result can also be confirmed for the ABPs studied here; a comparison with other ABPs is given in table 3.1:

ABP	molecular weight	prominent structural phases
espin	30 kDa	bundle network/composite network
fascin	55 kDa	bundle network
scruin	120 kDa	composite network
α-actinin	215 kDa	structural polymorphism
HMM	350 kDa	isotropically cross-linked network
filamin	560 kDa	bundle network

Table 3.1: Different ABPs of increasing molecular weights are compared regarding the most prominent structural phases that they form in reconstituted actin networks. The generic weakly cross-linked regime at low ABP concentrations is not explicitely mentioned for all those ABPs.

Fascin is a very small ABP and creates a purely bundled phase. Similar results can be obtained for espin, which has an even lower molecular weight (30 kDa [Bartles et al. 1998]) but is proposed to form a composite phase at intermediate concentrations [Purdy et al. 2007]. Such a composite phase is definitely present for the much larger ABP α-actinin (section 3.1.1) and the ABP scruin [Shin et al. 2004a] (molecular weight 120 kDa [Way et al. 1995]) – although the binding mode of scruin is fundamentally different. Finally rigor-HMM is an ideal cross-linking molecule which does not form bundles at all. This comparison seems to suggest that at least a common trend might be present with respect to the size of the cross-linking molecule. The huge human ABP filamin (560 kDa [Wang et al. 1975]) serves as a prominent exception from this rule of thumb as actin/filamin networks – in contrast to what can be read in many text books – show a purely bundled phase at sufficently high filamin concentrations [Schmoller et al. 2008b].

This demonstrates that a simple categorization of ABPs into cross-linking or bundling molecules is futile. Any theoretical model which takes into account ei-

ther merely strutural or biochemical information [VII] on the ABP can obviously not be sufficient to predict the complex phase behavior of reconstituted actin/ABP networks. Therefore, such theoretical approaches are – at this point of research – bound to fail in rationalizing the even more complicated structural organization of living cells. As a consequence, a clean and systematic experimental investigation of the phase behavior of *in vitro* reconstitutions of cytoskeletal networks is indispensable to shed light on the underlying physical principles that lead to the formation of different structural and therefore mechanical phases as well as the transitions between them.

Recall that both the isotropically cross-linked networks formed by rigor-HMM and the bundle networks formed by fascin are very homogeneous. However, in the generic weakly cross-linked regime at low cross-linker concentrations the formation of local heterogeneities is observed right before the transition to a homogeneous phase (compare section 3.9). Heterogeneous network structures are also observable for actin/α-actinin networks. There, a composite phase at intermediate R and bundle clusters at high R were identified (compare section 3.1.1). The influence of such mesoscopic heterogeneities on the macroscopic network elastictiy is addressed in the next section of this thesis.

[VII] such as binding affinity

3.2 Influence of heterogeneities on the static network elasticity

In living cells, stiff actin bundles are embedded into softer networks constituted of single filaments. In this way a highly heterogeneous material is created. Because of its complexity, a physical understanding of composite cytoskeletal networks calls for well-defined *in vitro* model systems. So far, a quantitative physical description of the viscoelastic properties of cross-linked or bundled actin networks relies on a homogeneous microstructure. A theoretical description of composite networks is very difficult: the heterogeneous character of composite networks questions the convential approach of assuming a dominating deformation mode (compare section 3.3.3). Thus, a systematic identification of relevant network heterogeneities as well as a characterization of their impact on the viscoelastic network properties is crucial. Only an integrated approach combining micro- and macrorheological techniques with optical microscopy and simulations can provide the basis for a detailed understanding of the mechanical properties of heterogeneous cytoskeletal networks.

In section 3.1.1 it was demonstrated that *in vitro* reconstituted actin/α-actinin networks show pronounced structural polymorphism. Three distinct mechanical regimes were identified and it was shown that these regimes can directly be related to major rearrangements in the network microstructure. This is summarized in Fig. 3.12.

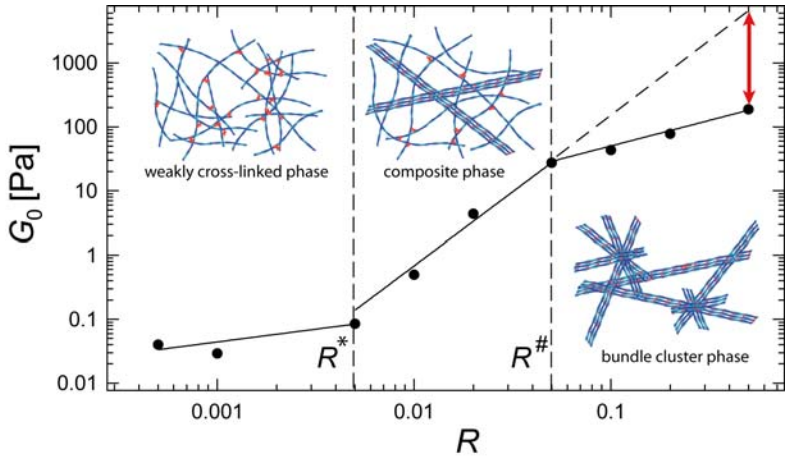

Figure 3.12: The mechanical transitions in actin/α-actinin networks are induced by major rearrangements in the network microstructure. Two types of structural heterogeneities are identified: At intermediate α-actinin concentrations a composite network is formed while at high R a bundle cluster phase occurs.

It remains to be investigated how these structural heterogeneities manifest themselves in the elastic network response. Two imminent questions are addressed in the following section of this thesis: First, despite the well-defined macromechanical response of such heterogeneous networks, the viscoelastic properties could be drastically different on a local length scale. This problem is addressed for composite networks in section 3.2.1. Second, it is a priori unclear how the occurrence of pronounced heterogeneities such as bundle clusters affect the macroscopic elastic response of bundle networks. Finite element simulations are employed in section 3.2.2 to elucidate this aspect.

3.2.1 Composite bundle phase

Already the semi-flexible nature of actin filaments themselves results in a separation of length scales. At length scales that are much smaller than the persistence length the actin filament behaves as a stiff rod rather than as a flexible chain (compare section 2.2.1). Furthermore, the elastic properties of an entangled actin solution depends critically on the density of entanglement points which in turn is set by the filament density. A microscopic measurement cannot fully report collective properties of actin solutions if the probed length scale is smaller than this entanglement length. As a consequence, the local viscoelastic properties of an entangled actin solution can significantly differ from the macrorheological response [Liu et al. 2006]. In isotropically cross-linked actin/HMM networks the viscoelastic response is determined by the average distance between cross-linking points. It has been shown that the elasticity of actin/HMM networks is systematically underestimated if the network response is probed at a length scale that is smaller than the cross-linker distance l_c [Luan et al. 2008]. Similar effects might have to be considered for heterogeneous composite networks – albeit here the critical length scales would be expected to be set by the dimension of the occuring heterogeneities.

In order to test composite actin/α-actinin networks regarding a putative difference between the local and bulk mechanical properties, a microrheological characterization of such composite networks would be of avail. The microscopic storage modulus at a given frequency, $G'(0.1\,\mathrm{Hz})$, is determined and compared to the macrorheological value. Distributions of this local modulus are obtained by analyzing 80 different bead positions in a given sample for a composite network, i.e. at an intermediate α-actinin concentration of $R = 0.02$ (Fig. 3.13A). The obtained moduli are approximately one order of magnitude lower than the macroscopic result (Fig. 3.13B); however, in either case the network elasticity can be enhanced by increasing the binding affinity upon decreasing the temperature. Moreover, the locally obtained frequency spectrum of such a network (Fig. 3.13C) resembles the spectrum of a weakly cross-linked network below the cross-link transition [Luan

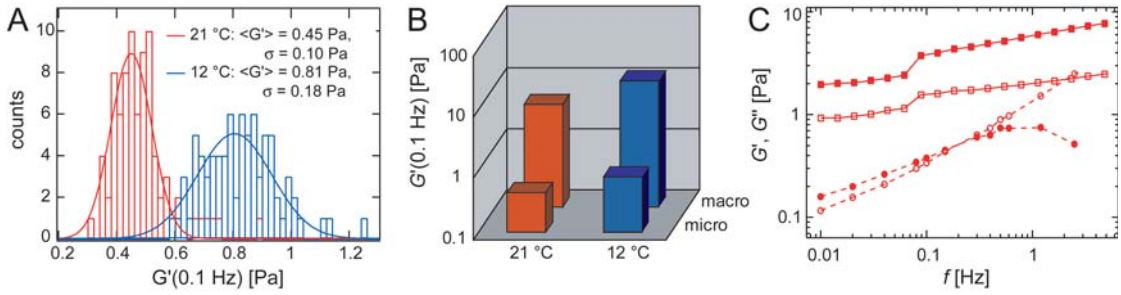

Figure 3.13: A composite actin/α-actinin network ($c_a = 9.5\,\mu$M and $R = 0.02$) is investigated by micro- and macrorheology. (A) The distribution of the microscopic storage modulus at a given frequency, $G'(0.1\,\text{Hz})$, is shown for 21 °C (red) as well as 12 °C (blue). A Gaussian is fitted to the distribution data to determine the average value $< G' >$ and the distribution width σ. (B): Local (front line) and macroscopic (rear line) elasticity of a composite network ($c_a = 9.5\mu$M, $R = 0.02$) at 21°C (red) and 12°C (blue). (C) Macroscopic (squares) and microscopic (circles) frequency response. Closed symbols denote $G'(f)$, open symbols denote $G''(f)$.

et al. 2008]. In this context it is crucial to recall that microrheology probes the mechanical properties of the network on a length scale comparable to the size of the probing particle – in this case 4.5 μm representing the diameter of the beads used. In the intermediate α-actinin concentration regime the bundle density is still quite low, thus the strong macromechanical fortification caused by the embedded bundles is not detectable on this local scale.

An appropriate parameter to quantify the degree of micromechanical heterogeneity is the relative distribution width $\sigma_{rel} = \sigma / < G'(0.1\,\text{Hz}) >$ of the local storage moduli, where $< G'(0.1\,\text{Hz}) >$ denotes the average value of the distribution as depicted in Fig. 3.13A and σ represents the absolute distribution width. For composite α-actinin networks ($R = 0.02$), this relative distribution width is very low, $\sigma_{rel} \approx 0.22$ for both temperatures investigated and corresponds to values obtained for isotropic networks (compare Fig. 3.9 in section 3.1.2.1). This further underlines that the observed heterogeneities affect the mechanical properties of the network only on length scales larger than 4.5 μm.

3.2.2 Bundle cluster phase

As already discussed in section 3.1.1, actin/α-actinin bundles can also form large aggregates; the occurrence of bundle clusters coincides with the second mechanical transition point $R^{\#}$ (Fig. 3.12). This suggests that the lower effectiveness of elasticity enhancement observed for high α-actinin concentrations is attributable to this type of structural heterogeneity. In order to analyze the effect of local bundle clustering on the mechanical response of bundle networks, 3-dimensional finite

element simulations similar to [Huisman et al. 2007] are employed in cooperation with Christian Cyron [VIII].

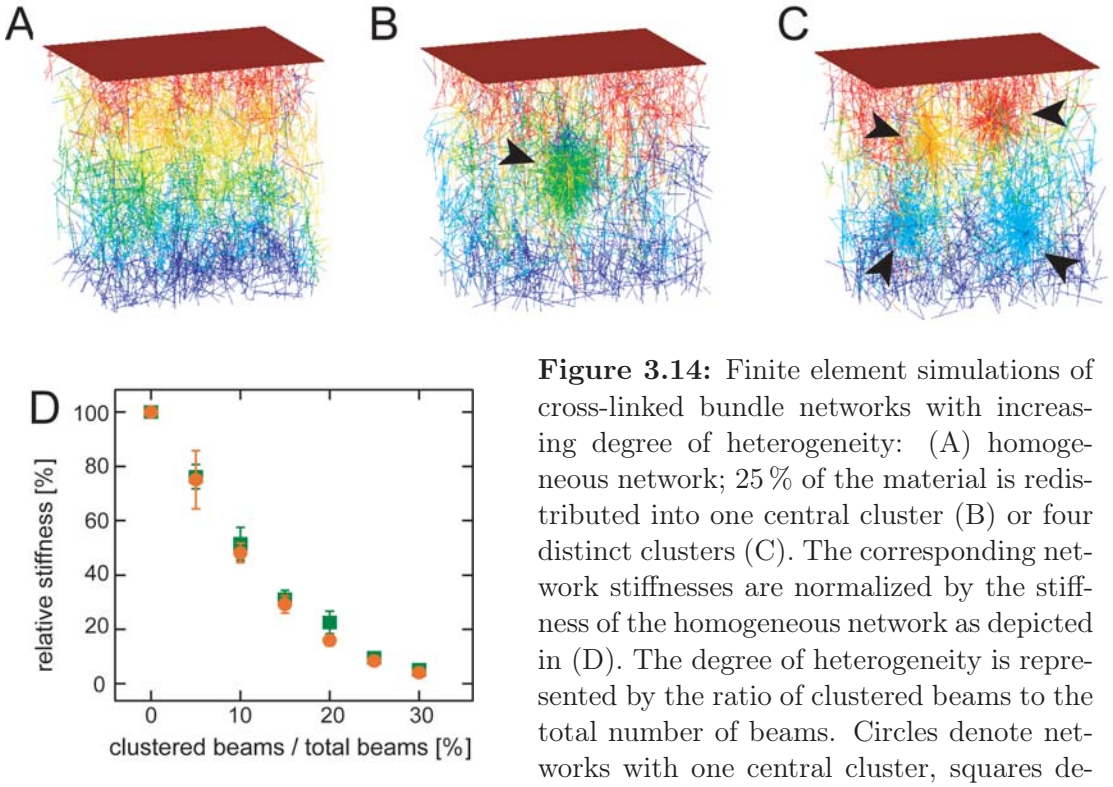

Figure 3.14: Finite element simulations of cross-linked bundle networks with increasing degree of heterogeneity: (A) homogeneous network; 25 % of the material is redistributed into one central cluster (B) or four distinct clusters (C). The corresponding network stiffnesses are normalized by the stiffness of the homogeneous network as depicted in (D). The degree of heterogeneity is represented by the ratio of clustered beams to the total number of beams. Circles denote networks with one central cluster, squares denote networks containing four clusters.

A cross-linked network composed of stiff beams ("bundles", each beam is discretized by 11 nodes) with random beam position and orientation (Fig. 3.14A) is compared to networks with increasing degree of heterogeneity. Networks with one centered cluster of increasing size (Fig. 3.14B) and networks containing four distinct clusters (Fig. 3.14C) are investigated. For cluster creation, the beams are merely rearranged to create increasingly heterogeneous network structures. In all cases, the total amount of material is preserved. For simplicity, we assume full degree of cross-linking; i.e. a cross-link is introduced between each pair of nodes that are closer than 500 nm [IX]. As depicted in Fig. 3.14D, the stiffness of such a network of cross-linked stiff beams decreases roughly exponentially with increasing degree of clustering. The key parameter is the amount of material that is localized in isolated spots; the simulation result is largely insensitive to the number of clusters formed. Note, that clustering drastically affects the network elasticity.

[VIII] Arbeitsgruppe Wall, Lehrstuhl für Numerische Mechanik, TU München

[IX] The qualitative result of our simulation is largely insensitive towards the detailed assumptions made on the microstructure.

Already a degree of heterogeneity of 20 % leads to an 80 % decrease in the network stiffness.

Despite the occurrence of bundle clusters, an increase of the network elasticity is observable in the macrorheological experiments at high α-actinin concentrations – albeit weaker than at intermediate R (compare Fig. 3.12). It is important to note, that this result is based on increasing R-values. Increasing α-actinin concentrations induce two types of structural rearrangements, that have competing effects on the network elasticity. First, clustering of bundles weakens the network elasticity by concentrating material in localized and isolated spots that are too sparse to allow for a percolation of these stiff regions. Second, the bundle density, thickness and stiffness further increase, which counteracts the increase in average meshsize – similar to what was observed for purely bundled networks as discussed in section 3.3.2. Still, the drastic effect of bundle clustering on the network elasticity observed in the simulations is consistent with the relatively low plateau moduli observed for high α-actinin concentrations ($R > R^{\#}$). If the strong R-dependence valid for intermediate α-actinin concentrations would also extend into the high-R regime, a 30 times higher elasticity would occur for a $R = 0.5$ network (red arrow in Fig. 3.12). From confocal micrographs (see Fig. 3.7) a degree of heterogeneity of $\approx$ 10 % can be estimated for such a $R = 0.5$ bundle cluster network. This indicates that the simplified simulation approach discussed here is able to capture the qualitative impact of bundle clustering on the elastic response of bundle networks. However, more detailed modeling approaches will be needed to achieve quantitative agreement with the relatively low network elasticity that is observed experimentally.

In conclusion, two types of structural heterogeneities dictate the macromechanical response of bundle networks formed by α-actinin. On the one hand, the formation of a composite phase where bundles are locally embedded into the network strengthens the macroscopic network response while the local elasticity remains low. On the other hand, the rearrangement of bundles into star-like clusters drastically concentrates material in localized spots, which weakens the network elasticity. These findings demonstrate that a detailed knowledge of the network microstructure is crucial to rationalize macromechanical behavior of complex actin networks. So far, the transitions between different structural and mechanical phases and their correlation with the macromechanical network response were addressed. It remains to be shown how the microscopic origin of the network elasticity is determined by the network microstructures. This is addressed in the next section of this thesis.

3.3 The network microstructure determines the local deformation mode

In the absence of cross-linking molecules, the elasticity of entangled actin solutions is successfully described by the spatial confinement of thermal bending undulations upon affine tube deformations [Hinner et al. 1998]. The viscoelastic response of cross-linked semi-flexible polymer networks, on the other hand, is in general dominated by an interplay between polymer stretching and bending modes. The precise form of the local deformation mode, as well as the degree of non-affinity, strongly depends on the network microstructure [Heussinger and Frey 2006b]. So far the mechanical response of cross-linked actin networks in the linear viscoelastic regime has mainly been described assuming purely affine entropic stretching deformations [Gardel et al. 2004a, Shin et al. 2004a, Tharmann et al. 2006] – also in the presence of bundles and composite phases. An alternative model was lacking. The affine stretching model developed by [MacKintosh et al. 1995] is especially successful in describing the static elasticity of isotropically cross-linked actin/HMM networks [Tharmann et al. 2007]. However, an applied tension can stretch a thermally undulating polymer only as far as there is excess contour length[X] available (Fig. 3.15).

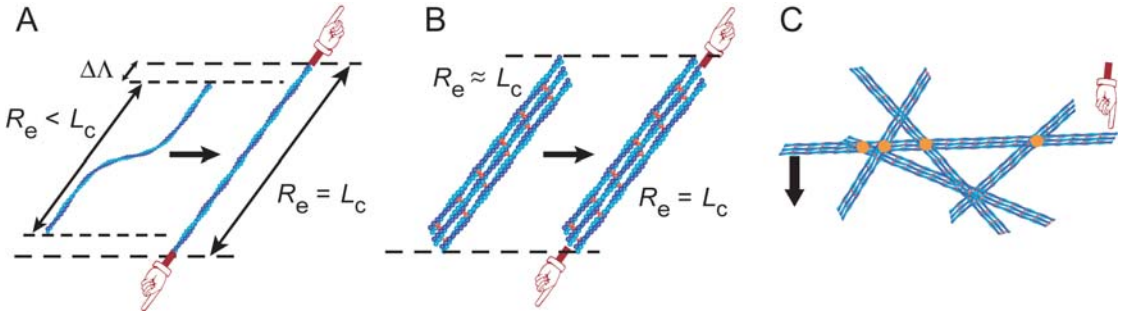

Figure 3.15: (A) Due to thermal undulations, the end-to-end distance R_e of an actin filament is considerably shorter than its contour length L_c. If a force is applied to the filament, this thermal contraction can be reversed by "pulling out" the thermal excess length $\Delta\Lambda$. This gives rise to an elastic response. (B) For stiff polymers like actin bundles thermal undulations are suppressed. As a consequence, forces acting on such a stiff polymer can hardly evoke a considerable mechanical stretching deformation. (C) A bending deformation can be transduced along the contour of a stiff polymer – even over length scales larger than the typical distance between two neighboring cross-linking points (orange circles). This bending induces non-affinities in contrast to the affine stretching deformations.

[X] also called "thermal excess length" $\Delta\Lambda$

As the maximal amount of stored length is inversely proportional to the persistence length of a polymer, entropic stretching is suppressed in networks of stiff polymers. Moreover, the highly non-linear nature of the force-extension relation of semi-flexible polymers implies that linear elasticity theories are only valid as long as only a fraction of the total excess length is pulled out. The recently introduced concept of the "floppy modes" may be better suited to describe the polymer elasticity in situations where entropic effects are suppressed [Heussinger and Frey 2006a]. These floppy modes constitute bending excitations which, unlike the affine stretching deformations, retain a highly non-affine character (see the sketch in Fig. 3.15C). Section 3.3.1 describes the experimental characterization of actin/fascin bundle networks. These experimental findings indicate that a description of the macroscopic elasticity of actin/fascin bundle networks should be based on bending deformations rather than stretching deformations. In section 3.3.2 this microscopic modeling approach is described in detail. Finally, in section 3.3.3 implications for composite networks are discussed.

3.3.1 Experimental results for actin/fascin networks

As described in section 3.1.2.2, actin/fascin networks exhibit a structural transition from a weakly cross-linked network into a purely bundled phase at a relative fascin concentration of $R^* \approx 0.01$. The bundles formed are very long ($> 100\ \mu$m) and straight over large length scales which is consistent with the high measured bending rigidity κ [Claessens et al. 2006] and suggests that stretching deformations are not suitable to describe the elastic response of actin/fascin bundle networks. TEM micrographs reveal that above R^* the actin/fascin bundle thickness D and therefore the number of actin filaments per bundle, N, increases weakly with R (Fig. 3.16A). The bundle thicknesses are extracted from the TEM-micrographs by fitting a Gaussian to the intensity profiles, obtaining a scaling of $D \sim N^{1/2} \sim R^x$ with $x = 0.27$.

Concomitant with the structural alterations the macroscopic viscoelastic properties of the network change: with increasing R both the storage modulus $G'(f)$ and the loss modulus $G''(f)$ increase over the whole frequency range probed (Fig. 3.16B). The storage modulus $G'(f)$ exhibits a plateau at low frequencies, while the loss modulus $G''(f)$ reveals a well-defined minimum which shifts to higher frequencies with increasing fascin concentrations [XI]. In the bundle phase, the plateau modulus G_0 follows the scaling relation $G_0(R, c_\mathrm{a}) \sim R^{1.5} \cdot c_\mathrm{a}^{2.4}$ (Fig. 3.16C). A theoretical description of the elastic response of actin/fascin bundle networks

[XI] This is attributable to increasing impact of thermal cross-linker unbinding events and is explained in detail in section 4.1.1. Further experimental evidence for the existence of cross-links between distinct bundles can be obtained by observing the correlated thermal fluctuation of putatively connected neighboring bundles [Schmoller 2008].

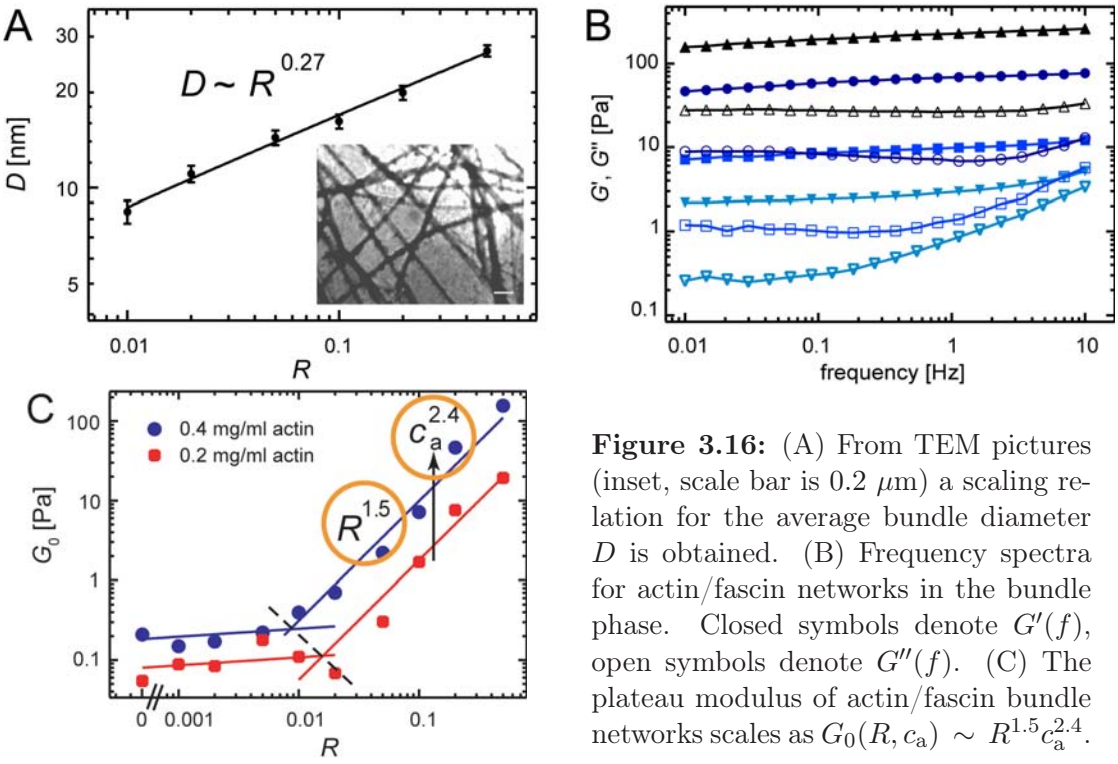

Figure 3.16: (A) From TEM pictures (inset, scale bar is 0.2 μm) a scaling relation for the average bundle diameter D is obtained. (B) Frequency spectra for actin/fascin networks in the bundle phase. Closed symbols denote $G'(f)$, open symbols denote $G''(f)$. (C) The plateau modulus of actin/fascin bundle networks scales as $G_0(R, c_\mathrm{a}) \sim R^{1.5} c_\mathrm{a}^{2.4}$.

would have to reproduce this macroscopic scaling behavior on the basis of the microscopic findings considering the high stiffness of actin/fascin bundles.

3.3.2 Non-affine bending deformations in actin/fascin bundle networks

As motivated in section 3.3.1, the mechanical properties of actin/fascin bundle networks may be understood in terms of a non-affine bending model which is based on a floppy mode description developed for athermal networks of stiff rods [Heussinger and Frey 2006a]. In such a model the network elasticity is attributed to bending modes of wavelengths comparable to the average distance between two cross-links, l_c, and with stiffness $k_\perp \sim \kappa / l_\mathrm{c}^3$. In this picture typical deformations of the network do not follow the macroscopic strain affinely but scale as $\delta_\mathrm{na} \sim \gamma L_\mathrm{B}$, where L_B is a constant length over which an individual bundle within the network can be assumed to be straight (compare the sketch in Fig. 3.15C). Fluorescence and TEM pictures indicate that this length can expected to be comparable to the bundle length. As a consequence the linear elastic modulus of the bundle network reads

$$G_0 \sim \nu k_\perp \delta_\mathrm{na}^2 \tag{3.4}$$

with the polymer density $\nu \sim 1/\xi^2 l_c$. This model can be tested by relating the structural parameters of the actin/fascin bundle network, the mesh size ξ and the cross-linker distance l_c, and the bending elasticity κ of the bundle segment to the concentration of actin and fascin monomers (c_a, c_f).

The structural information obtained by EM and fluorescence microscopy justifies the assumption that the bundles form an isotropic network similar to an entangled structure of single filaments. With increasing fascin concentration R, filaments and smaller bundles reorganize to form larger bundles that are spaced further apart. The mesh size ξ of such a self-similar bundle network therefore depends on R as $\xi \sim \xi_0 N^{1/2}$, where $\xi_0 \sim c_a^{-1/2}$ is the mesh size of the filamentous network. Cross-linking of the bundles will typically occur on the scale of the entanglement length l_e, which describes the distance between bundle-bundle intersections (entanglement points). Since on average only a fraction of those entanglement points will be occupied by a cross-linking molecule, it can be assumed that distances between cross-links along the same bundle are given by $l_c \sim R^{-y} l_e$ [Tharmann et al. 2007, Shin et al. 2004a]. Doubling the cross-linker concentration R should halve the distance between them, suggesting an exponent $y \approx 1$.

For a description of the elastic properties of the bundles it is necessary to realize that fascin only leads to loosely coupled bundles, where bending is dominated by the shear stiffness of the cross-linking proteins [Claessens et al. 2006, Bathe et al. 2008]. The key quantity in this context is the bundle coupling parameter $\alpha(l_c) = (l_c/b)^2$, where the length-scale $b \sim d_c^{1/2}$ encodes the properties of the ABPs inside the bundle, in particular via the average distance d_c between cross-links. In general, d_c will depend on the concentrations c_f and c_a; however, the precise relationship is not known.

From fluorescence images the mesh size of the bundled network at $R = 0.5$ can be approximated which allows to calculate l_e and thus l_c. From this one can estimate the coupling parameter to be $\alpha > 1$ for the whole bundle regime, implying that the effective bundle bending stiffness κ acquires a wavelength dependence [Bathe et al. 2008], leading to $\kappa(\lambda) \sim N\kappa_f\alpha(\lambda)$, where λ is the wavelength of the deformation mode. This stands in marked contrast to what is known for single filaments or scruin-bound bundles where fully coupled bundles, $\kappa \sim N^2\kappa_f$, have been assumed [Shin et al. 2004b].

The wavelength dependence of the bundle stiffness has far reaching consequences for the static as well as dynamic properties of semi-flexible polymer bundles [Heussinger et al. 2007]. In particular, it implies that the entanglement length l_e has to be reevaluated. The correct expression of l_e is derived from the suppression of long wavelength fluctuations by confining a polymer into a tube [Odijk 1983], l_e is highly sensitive to a wavelength dependent $\kappa(\lambda)$. Assuming this wavelength dependence results in $l_e^3 \sim (Nl_p)\xi^4/b^2$, which is different

from the usual expression $l_e^5 \sim l_p \xi^4$ valid for single filaments, where in both cases $l_p = 17\,\mu$m [LeGoff et al. 2002a] denotes the persistence length of a single actin filament.

Combining the above results and setting the deformation mode length λ equal to l_c one arrives at the following prediction for the scaling of the plateau modulus [XII]

$$G_0 \sim R^z c_a^w \cdot d_c^{-1/3}, \tag{3.5}$$

where the exponents are given by $z = 2y - 4x$ and $w = 7/3$. Thus the scaling exponent of the plateau modulus can be related to parameters describing the microstructure such as the scaling of the mesh size as well as the dependence of the bundle thickness and elasticity on R. From our measurements of $x = 0.27$ and $z = 1.5$, and by assuming d_c to be constant, a value of $y = 1.29$ is obtained, which is in reasonable agreement with the expected $y \approx 1$. This result is largely insensitive to the assumption of constant d_c, since by assuming d_c to change according to simple Langmuir kinetics an exponent $y \approx 1.21$ is obtained.

To further characterize the elastic properties in the bundled regime, the non-linear elasticity of the network is investigated. For samples with $R > R^*$ a constant shear rate is applied and the resulting stress is reported. From the smoothed $\sigma(\gamma)$ relation the numerical derivative yielding the differential modulus $K = \partial\sigma/\partial\gamma$ is calculated (Fig. 3.17, compare section 4.1.4). For small strains of $\gamma = 1 - 10$ % linear response is observed, where the differential modulus follows $K \sim R^{1.5}$ in agreement with our oscillatory measurements. A non-linear response is observed above γ_c, which is determined as the strain at which K deviates by 5 % from its value in the linear regime. Up to $R = 0.1$ strain hardening occurs while for very high values of R the linear regime is directly followed by strain weakening. The disappearance of the strain hardening at high concentrations of fascin is the result of the rupturing of fascin-actin bonds as discussed in section 4.1.4.

The floppy mode description also has implications on the onset of the non-linear behavior. As has been argued in [Heussinger and Frey 2006a] large strains necessarily lead to mechanical stretching of the bundle even if the deformations were only of bending character. This amount of bundle stretching Δ is related to the transverse displacement δ_{na} by simple geometric considerations as $l_c^2 + \delta_{na}^2 = (l_c + \Delta)^2$. The floppy mode description thus applies as long as this stretching is small compared to the available thermal excess length $\Delta\Lambda \sim l_c b/N l_p$ [Heussinger et al. 2007]. This defines a critical strain $\gamma_c \sim l_c (b/N)^{1/2} \sim R^{-y+x} b^{-1/6} \sim R^{-1.0} d_c^{-1/12}$ for the onset of non-linear effects. The scaling with R is in excellent agreement with our measurements (see inset of Fig. 3.17). The weak dependence on the cross-linker spacing $\gamma_c \sim d_c^{-1/12}$ also implies that this result is insensitive towards any putative dependence on the fascin

[XII] A step-by-step derivation of this equation is given in the appendix.

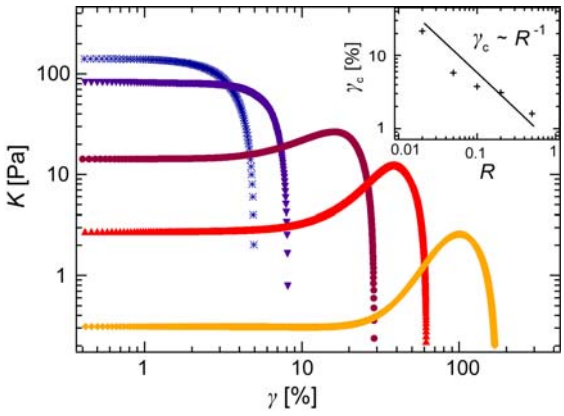

Figure 3.17: Differential modulus $K = d\sigma/d\gamma$ plotted versus the deformation γ for fascin networks in the bundle phase ($c_a = 0.4$ mg/ml and increasing R: diamonds $R = 0.02$, upright triangles: $R = 0.05$, circles: $R = 0.1$, downright triangles: $R = 0.2$, stars: $R = 0.5$). The inset shows the critical strain γ_c in dependence on R.

concentration via $d_c = d_c(c_f)$.

In conclusion, the elasticity of actin/fascin networks in the bundled phase is well explained in terms of a recently developed floppy mode picture [Heussinger and Frey 2006a]. In the absence of a significant amount of stored length in the bundles, non-affine bending is the dominant low energy excitation. This approach explains both the linear elasticity and the onset of non-linear behavior. Despite the absence of significant amounts of thermal excess length in stiff bundles, it could be argued that an affine stretching model [MacKintosh et al. 1995] would also be able to correctly describe the elastic response of actin/fascin networks in the bundle phase. However, to obtain a reasonable data fit with the affine stretching description a different picture emerges, where $d_c(c_f)$ has to be tuned. In such a model one would assume the plateau modulus of a bundle network to be given by $G_{aff} \sim \nu k_{\|} \delta_{aff}$, where $k_{\|} \sim \alpha^{3/2}(N\kappa_f)^2/l_c^4$ is the stretching stiffness of a single bundle [Heussinger et al. 2007]. The deformations are assumed to be affine, implying $\delta_{aff} \sim \gamma l_c$. The modulus thus reads as $G_{aff} \sim R^{2x} c_a \cdot d_c^{-3/2}$ while the critical strain $\gamma_c \sim d_c^{1/2} R^{-2x}$ is obtained by equating $\Delta\Lambda$ with the affine deformation $\delta_{aff} \sim \gamma l_c$. This model can only partially fit the data by assuming $d_c \sim c_f^{-\beta}$ with an exponent in the range of $\beta = 0.6 - 0.9$. For $\beta = 0.6$ the R-dependence of the modulus and for $\beta = 0.9$ the c_a-dependence of the modulus is reproduced. To finally decide whether or not the application of an refined affine stretching model can be equally successful as the floppy mode approach, $d_c(c_f)$ would have to be determined independently, e. g. by scattering experiments – which is very difficult.

3.3.3 Coexistence of bending and stretching deformations in composite networks

The occurrence of stiff bundles is not limited to the actin/fascin system. In the composite networks formed by α-actinin or scruin at intermediate concentrations bundles are embedded into isotropically cross-linked filament networks. So far, affine stretching deformations were thought to be the dominating deformation mode in such composite networks [Shin et al. 2004a]. In the following, the floppy mode-based non-affine bending approach is applied to describe composite networks formed by scruin on the basis of experimental data as published in [Shin et al. 2004a][XIII].

By again assuming non-affine bending deformations and – this time – considering strong filament coupling $\kappa \sim N^2\kappa_\mathrm{f}$, the plateau modulus of composite actin/scruin networks would be predicted to scale as

$$G_0 \sim R^{4y-22x/5} c_\mathrm{a}^{13/5} \tag{3.6}$$

which reproduces the dependence on the actin concentration equally well as the affine stretching model as presented in [Shin et al. 2004a]. Considering the experimental result for the R-dependence of the plateau modulus of actin/scruin networks, $G_0 \sim R^2$, and the increasing thickness of actin/scruin bundles with respect to the relative scruin concentration, $D \sim R^{0.3}$ [Shin et al. 2004a], the prediction of the non-affine bending model can be cross-checked. Since in the fully coupled bundle case, the stored length in a bundle is given by $\Delta\Lambda \sim l_\mathrm{c}^2/N^2 l_p$, the non-affine bending model predicts the onset of non-linear behavior to scale as $\gamma_c \sim R^{1.1}$. This prediction – by coincidence – is the same as for the affine stretching model and therefore matches the observed scaling $\gamma_c \sim R^{0.6}$ reported by Shin *et al.* equally well – or equally bad, depending on the point of view.

The validity of both models discussed here seems to depend strongly on the network microstructure: While the elasticity of isotropic networks is predominantly determined by the entropic stretching of single filaments between two neighboring cross-linking points, networks that are composed of stiff bundles can only be described by non-affine bending deformations. Furthermore, a re-evaluation of actin/scruin data as discussed here indicates that the elastic response of composite networks might be determined by a combination of affine stretching and non-affine bending deformations. Such a combination of the two different approaches would require highly detailed microscopic information about the composite network. Yet, the exemplary discussion of purely bundled actin/fascin networks and composite

[XIII] The actin/scruin system is a more appropriate candidate for a thorough test than the actin/α-actinin system. This is due to the fact that in actin/scruin networks the composite phase spans a much broader concentration range than in the actin/α-actinin system.

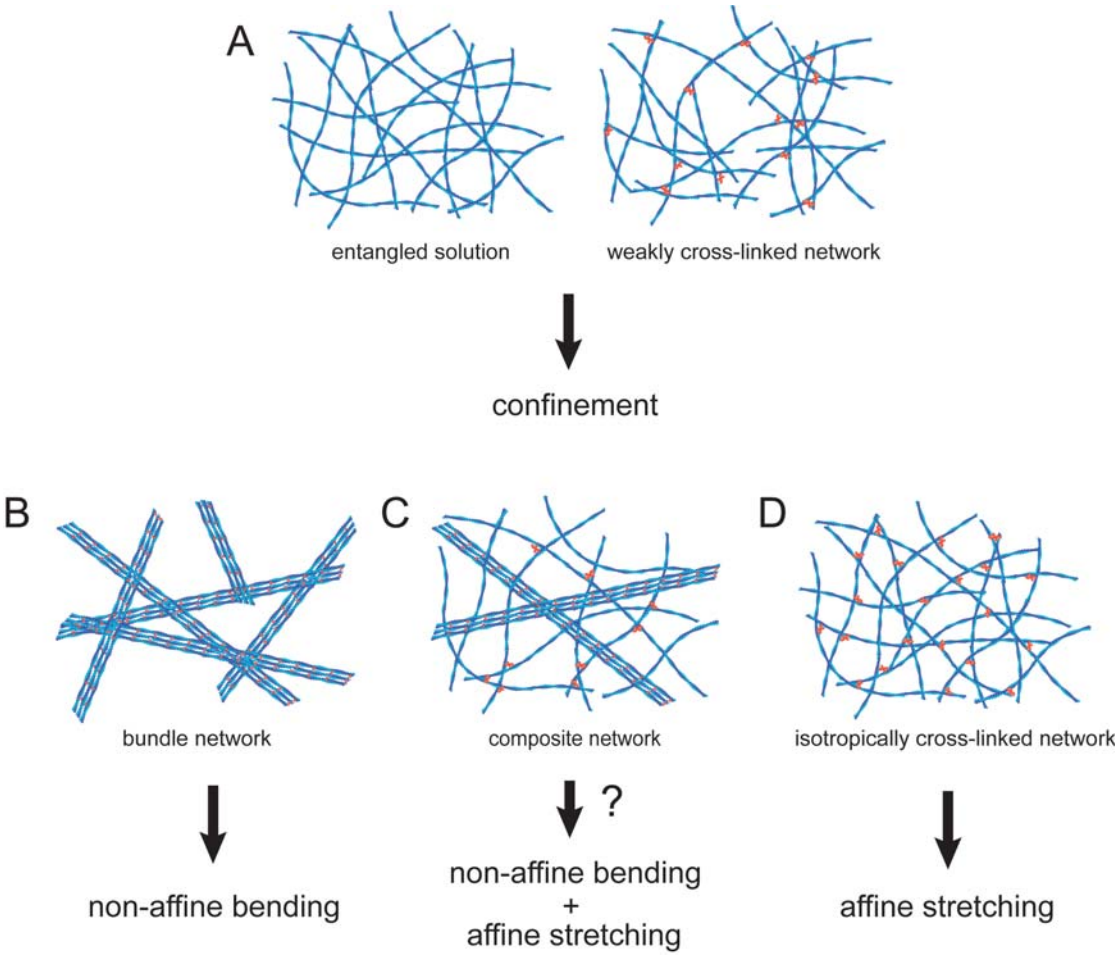

Figure 3.18: The network microstructure determines the microscopic deformation mode: (A) Entangled actin solutions and weakly cross-linked networks below the cross-link transition can be described by confinement effects. (B) In stiff bundle networks non-affine bending is the dominating deformation mode while in (C) composite networks affine stretching might have to be considered, too. The latter is the dominating deformation mode in (D) isotropically cross-linked networks.

actin/scruin networks nicely demonstrates that the network microstructure dictates the microscopic deformation mode (Fig. 3.18).

4 Dynamic network properties: Transient binding of cross-linking molecules

For living cells it is of utmost importance not only to withstand mechanical strains but also to allow for an ongoing remodeling of the cytoskeletal microstructure. The cytoskeletal biopolymer actin itself is dynamically growing by the polymerization of monomers at the ATP-end of the filament. At the same time monomers detach at the ADP-end of the filament, the polarity of the filament is controlled by ATP hydrolysis. This treadmilling can be controlled by polymerization accelerators such as profilin or depolymerization agents such as cofilin. The dynamic growth and shrinkage of actin filaments is a major strategy for the remodeling of the cytoskeletal microstructure. Additionally, restructuring of cytoskeletal networks is facilitated by employing transiently cross-linking proteins instead of covalent linkages. Despite this dynamic remodeling of the cytoskeletal microstructure, quantitative research on cytoskeletal networks focused on the static plateau elasticity [Tempel et al. 1996, Shin et al. 2004a, Tharmann et al. 2007]; the frequency dependent loss modulus representing the viscous dissipation in such networks has been largely ignored so far. It is yet to be resolved how transiently cross-linking proteins affect the frequency dependent viscoelastic response of cross-linked actin networks in the biologically most relevant elasticity dominated intermediate frequency regime.

The transient cross-links formed by ABPs are characterized by an off-rate, k_{off}, which typically corresponds to frequencies in an intermediate regime of several mHz up to a few Hz [Marston 1982, Miyata et al. 1996, Vignjevic et al. 2006]. In a comparable frequency regime, cells show increasing viscous dissipation [Dheng et al. 2006, Massiera et al. 2007] which is a feature that does not appear in the frequency spectrum of covalently cross-linked networks. This suggests that transient cross-links might trigger an important relaxation mechanism in cytoskeletal networks of semi-flexible polymers.

This chapter focuses on the transient nature of actin/ABP interactions and elucidates the impact of cross-linker unbinding events on the viscoelastic response of actin networks which are transiently cross-linked by ABPs. In section 4.1.1 it is demonstrated that thermal energy is sufficient to entail cross-linker unbinding

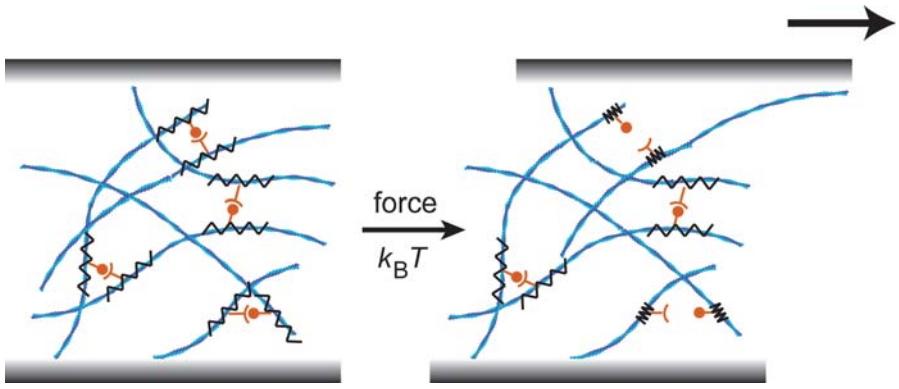

Figure 4.1: If a cross-linked actin network is subjected to shear deformations, unbinding of transient cross-links can be triggered either by force or thermal energy (k_BT). This unbinding process entails a loss of elasticity in the local actin filament configuration as indicated by the stretched and relaxed springs, respectively.

events (see sketch in Fig. 4.1). It is shown that this relaxation process determines the dynamic network response at intermediate frequencies. A simple semi-phenomenological model is introduced in section 4.1.2 and employed to quantify the viscoelastic frequency spectrum. It is demonstrated, that the dynamic viscoelastic response sensitively depends on the microscopic interaction potential of actin/ABP bonds. Conversely, this interaction potential can – for simple network geometries – be obtained from the macroscopic frequency spectrum as demonstrated in section 4.1.3. Depending on the microstructure of the reconstituted network, a macroscopic deformation can be transmitted to the microscopic level of single filaments and individual cross-linking molecules in an affine or non-affine manner [I]. In either case, large forces may evoke rupturing of the non-covalent actin/ABP bond. This is adressed in section 4.1.4 of this chapter. For the non-linear response of actin/fascin bundle networks the cross-linker density and the force loading rate are observed to be equivalent. This is used to introduce a generalized description of the viscoelastic frequency response with a master curve (section 4.2). Finally, the transient character of actin/ABP bonds in combination with kinetic trapping effects can give rise to meta-stable network configurations and complex relaxation processes (section 4.3).

[I] Compare the discussion on actin/fascin bundle networks in section 3.3.2.

4.1 Thermal and forced unbinding of transient cross-links

In polymer networks distinct molecular mechanisms can lead to a relaxation of external (or internal) stresses on different time scales; depending on whether energy is stored or dissipated, elastic or viscous behavior can be evoked [De Gennes 1979, Rubinstein and Colby 2003]. The linear response of entangled actin solutions is well-understood (compare section 2.2.3). Thermal bending fluctuations of single actin filaments dominate the viscoelastic response at high frequencies while the plateau elasticity is attributed to confinement effects that are induced by the surrounding filaments. The diffusive motion of filaments along their contour is the main mechanism that is responsible for the relaxation of stresses at low frequencies.

The corresponding relaxation processes are complicated if cross-linking molecules are introduced. Many synthetic polymer networks are covalently cross-linked resulting in a predominantly elastic response over a broad frequency range – the covalent cross-links suppress the single polymer diffusion present in entangled solutions. Therefore, the frequency dependent viscoelastic behavior of a covalently cross-linked polymer network is expected to reach a constant level of elasticity at low frequencies while viscous effects become negligible. In contrast, if transient cross-links are present (i.e. physical cross-links based on electrostatic interactions or van-der-Waals forces), a pronounced minimum and maximum in the viscous dissipation is observed for flexible polymer networks in a frequency range of $0.01 - 10$ Hz [Sjibesma et al. 1997, van der Gucht et al. 2003]. This feature in the viscous dissipation is always accompanied by a decrease in elasticity at low frequencies; nevertheless, the viscoelastic response in this frequency regime is dominated by the network elasticity. Moreover, the "stickiness" of polymer sidegroups gives rise to additional friction processes in both asymptotic frequency regimes [Leibler et al. 1991, Tanaka and Edwards 1992, Rubinstein and Semenov 2001]. In transiently cross-linked cytoskeletal networks the semi-flexible nature of the biopolymers complicates a theoretical description of their viscoelastic properties (compare section 3.3). Additionally, the cross-linking proteins can fully dissociate from the filaments and reach new cross-linking positions by diffusion. As a consequence, the molecular mechanisms responsible for the behavior at intermediate ($f \approx k_{\mathrm{off}}$) and low frequencies ($f < k_{\mathrm{off}}$) are poorly understood. A molecular understanding of these mechanisms is still missing but urgently needed to rationalize the mechanical properties of living cells.

4.1.1 Dominance of cross-linker unbinding at intermediate frequencies

Proteins such as fascin, α-actinin, filamin or rigor-HMM create non-covalent cross-links in actin networks. In actin/fascin and actin/HMM networks these cross-links interconnect distinct bundles and/or filaments in a pointwise manner. For these networks, the viscous dissipation $G''(f)$ exhibits a pronounced minimum at an intermediate frequency $f_{\min}$, whose exact position depends on the cross-link density (Fig. 4.2).

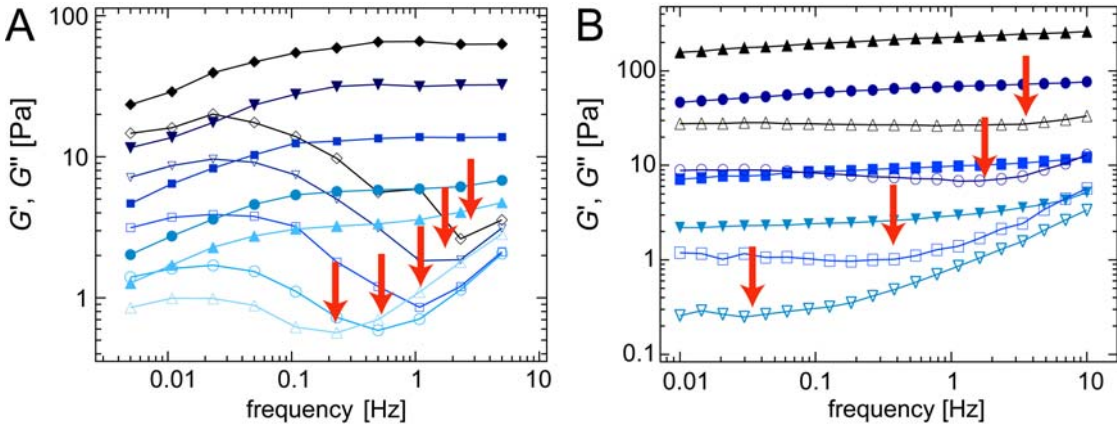

Figure 4.2: Frequency spectra for (A) actin/rigor-HMM networks ($c_a = 19\,\mu$M, $R = 0.0076$ (upright triangles) up to $R = 0.143$ (diamonds)) and (B) actin/fascin networks ($c_a = 9.5\,\mu$M, $R = 0.05$ (downright triangles) up to $R = 0.5$ (upright triangles)). Closed symbols denote $G'(f)$, open symbols denote $G''(f)$. The red arrows mark local minima in the loss modulus, $G''_{\min} = G''(f_{\min})$.

The elastic response of these cross-linked networks differs from the expectation for covalently cross-linked networks: although the elastic modulus $G'(f)$ is constant for sufficiently large frequencies $f > f_{\min}$, it decreases significantly at lower frequencies. This decrease in the elasticity as well as the increase in the viscous dissipation is more pronounced for isotropically cross-linked actin/HMM networks where the cross-link density is significantly higher (compare Fig. 4.2A and B). Here, the viscous dissipation even reaches a clear maximum around $f_{\max} \approx 0.03\,$Hz (Fig. 4.3A). This time scale is independent of the cross-link density; however, the maximal amount of low-frequency energy dissipation increases linearly with the cross-link density [Tharmann et al. 2007]. The transient nature of actin/HMM cross-links becomes also evident in a step-stress experiment. Such an experiment is conducted for a strongly cross-linked actin/HMM network ($R = 0.1$) as depicted in Fig. 4.3B. At intermediate time scales ($\approx 40 - 60\,$s) the network exhibits significant creep similar to a viscous fluid.

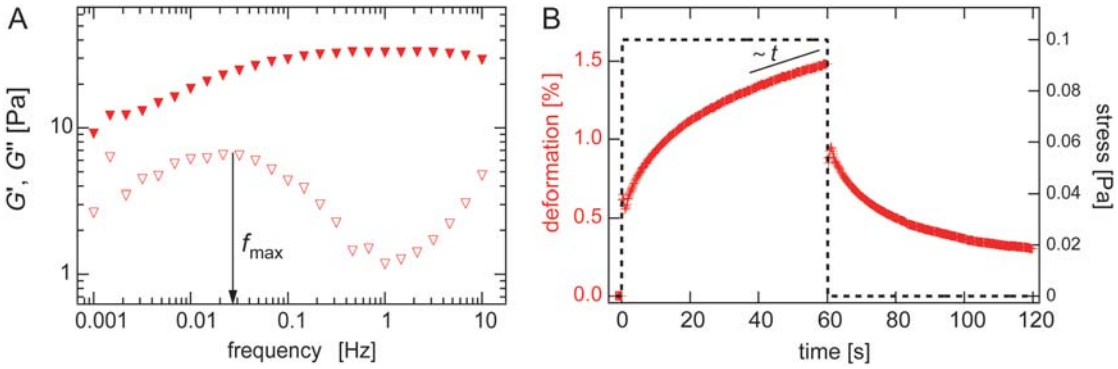

Figure 4.3: (A) Extended frequency spectrum of a transiently cross-linked actin/HMM network ($R = 0.1$). A clear maximum in the viscous dissipation is located at $f_{\max} \approx 0.03$ Hz. (B) A stress puls of 0.1 Pa height and 60 s duration is applied to a transiently cross-linked actin/HMM network ($R = 0.1$) and the resulting deformation is recorded. This step-stress experiment reveals significant creep behavior at time scales of $\approx 40 - 60$ s.

To shed light on the molecular origin of the viscoelastic response of transiently cross-linked actin networks, the possible molecular mechanisms involved should be tuned independently. A mechanism of energy dissipation that is always present in polymer networks is friction due to viscous drag of individual filaments. The viscosity of the solvent can be increased by the addition of glycerol. As a consequence, the time scale of the single filament relaxation regime should be shifted according to the increase in solvent viscosity. Indeed, for the cross-linked network the minimum in the viscous dissipation relocates as the viscosity of the solvent is increased by glycerol (Fig. 4.4A). However, over the whole frequency range the addition of glycerol does not significantly affect the elastic network response.

It is important to note, that the viscous dissipation depends on the solvent viscosity only at frequencies $f > f_{\min}$ while e. g. the maximal dissipation at $f_{\max} \approx 0.03$ Hz remains unchanged. Obviously, single filament fluctuation is not sufficient to rationalize the complex dissipation behavior of a cross-linked polymer network. In fact, another molecular mechanism has to be considered. Recall that the maximum in the viscous dissipation is located around $f_{\max} \approx 0.03$ Hz independent of the cross-link density. The cross-links are created by rigor-HMM which is known to form a non-covalent bond to the biopolymer actin with a typical off-rate $k_{\text{off}} \approx 0.09\,\text{s}^{-1}$ [Marston 1982]. As this off-rate is on the order of $f_{\max}$, the binding kinetics of the cross-linking protein HMM might give rise to additional mechanisms in the network accounting for the observed frequency dependence of the viscoelastic moduli for frequencies $f \approx f_{\min}$.

It was shown before that the bond between actin and ABPs can be forced to unbind by mechanical load [Miyata et al. 1996, Guo and Guilford 2006,

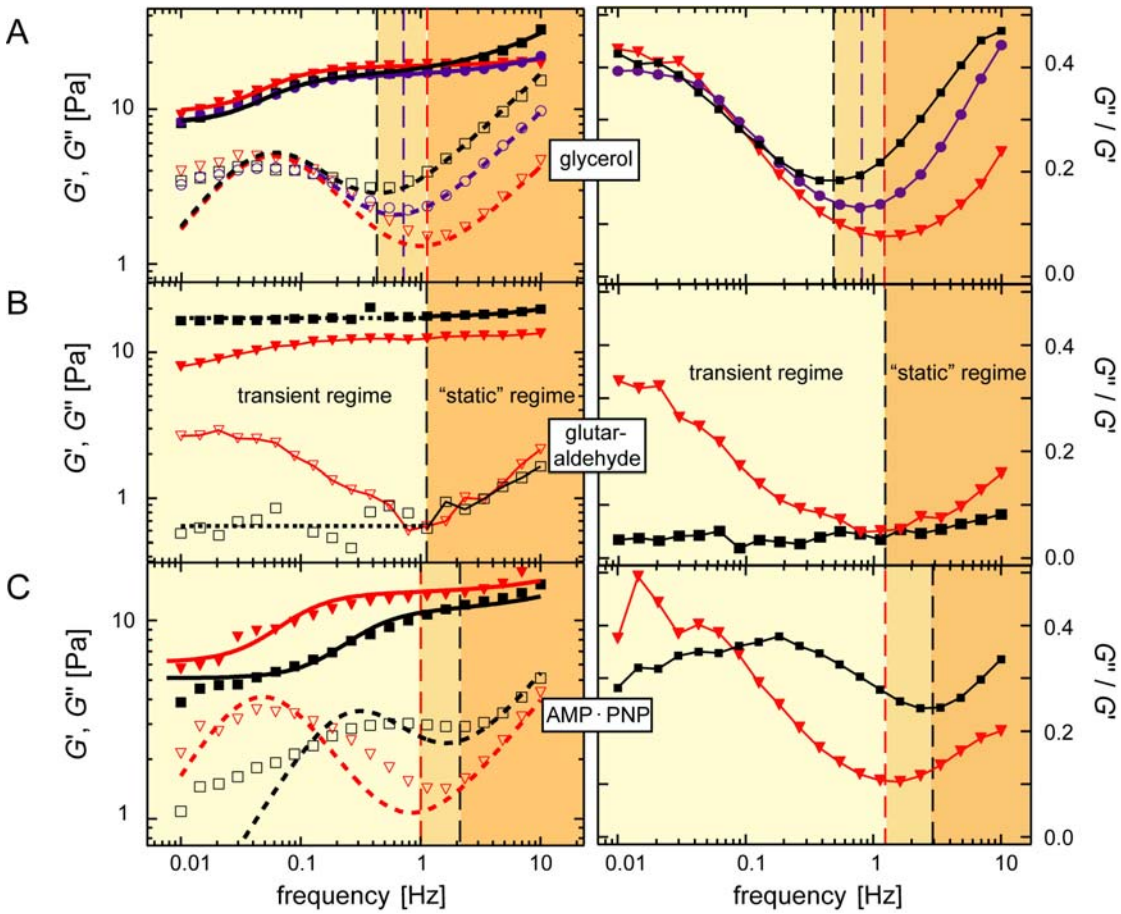

Figure 4.4: Viscoelastic frequency response for actin/HMM networks ($c_a = 9.5\,\mu$M, $R = 0.1$). The left column shows the storage (closed symbols) and the loss modulus (open symbols) while the same data is depicted in the right column in a loss factor representation. The full and dashed lines in (A) and (C) represent a global best fit using equations (4.4) and (4.5) on page 55. Fit parameters are adjusted as they are controlled experimentally. (A) Distinct amounts of glycerol (0 % (triangles), 25 % (circles) and 50 % (squares) are added to increase the solvent viscosity. (B) 0.1 % glutaraldehyde is added to fix the actin/HMM bond. The resulting viscoelastic response (squares) is compared to a non-fixed network (triangles). The dotted lines are constant fits to guide the eyes. (C) 2 mM AMP·PNP (squares) is added to a standard ATP sample (triangles) to tune the off-rate of the actin/HMM bond. (A), (B), (C): The vertical lines represent the transition from the transient cross-link regime to the "static" cross-link regime.

Ferrer et al. 2008]. However, the transient nature of an actin/ABP bond should also allow for spontaneous unbinding events in thermal equilibrium. Thus, thermal unbinding of distinct cross-links could be the molecular reason for the observed behavior of both viscoelastic moduli in the linear response regime. To verify this

hypothesis a fixation of the ABP/actin bond would be of avail. Glutaraldehyde is able to create a covalent linkage between neigboring proteins by the formation of a Schiff base. It is commonly used for fixation purposes of cells and other biomaterials [Fernandez et al. 2007] and can be employed to create a chemical bond between HMM and actin. Indeed, as depicted in Fig. 4.4B, the minimum in the viscous dissipation can be suppressed by the addition of 0.1 % glutaraldehyde. At the same time, the decrease in the network elasticity at low frequencies, which is observed in the absence of glutaraldehyde, is almost completely suppressed. This suggests that the minimum in the viscous dissipation marks the frequency below which the transient character of the cross-links starts to dictate the viscoelastic response of the network.

The covalent fixation of an actin/ABP bond using glutaraldehyde has an extreme effect on the viscous dissipation. A more subtle method to affect the viscous response of a cross-linked polymer network might be given by only slightly changing the binding kinetics of the cross-linking molecule. HMM is a formidable choice for a model cross-linking molecule since it possesses an ATP binding site besides the actin binding domain (compare section 2.1.4). Binding of AMP·PNP [II], a non-hydrolizable ATP-analogon, can induce a conformational change in the actin binding site (Fig. 4.5) and therefore increases the off-rate of the actin/HMM bond from $0.09\,\mathrm{s}^{-1}$ to $1.8\,\mathrm{s}^{-1}$ [Marston 1982].

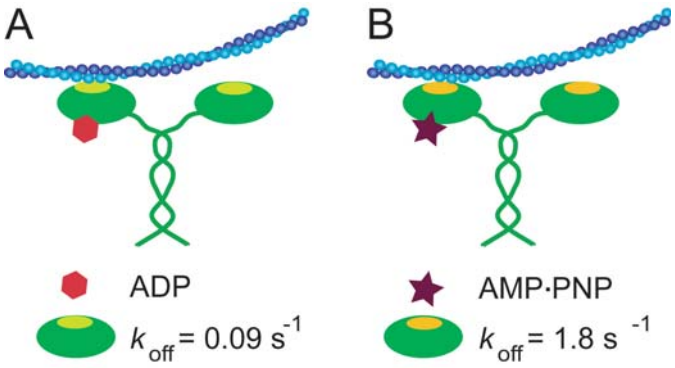

Figure 4.5: The binding affinity of HMM towards actin can be modulated by the binding of either (A) ADP or (B) non-hydrolizable AMP·PNP. The given off-rates for the actin binding domain of HMM are taken from [Marston 1982].

To quantitatively analyze how altered binding kinetics of the cross-linking molecule influence the viscoelastic response, a network with 2 mM AMP·PNP is compared to a network which contains only ADP-HMM. First, the addition of AMP·PNP to a cross-linked actin/HMM network changes the position of both the minimum and the maximum of the viscous dissipation (Fig. 4.4C). However, for frequencies $f > f_{\mathrm{min}}$ the viscoelastic response seems almost unaffected. Second, the frequency at which the network elasticity starts to drop is also shifted with

[II] adenosine 5'-(β,γ-imido)triphosphate

the increase in k_{off}. This strongly suggests that these two features have the same molecular origin.

4.1.2 Modelling the frequency response of isotropically cross-linked networks

The results presented so far imply that thermal unbinding of distinct cross-links triggers a relaxation mechanism which influences the elastic and the viscous properties of the network simultaneously. This calls for a simple semi-phenomenological description to quantify the observed effects. The static network elasticity G_0 of an isotropically cross-linked semi-flexible polymer network can be described by an affine stretching model [MacKintosh et al. 1995] as

$$G_0 \sim \frac{\kappa_0^2}{k_{\text{B}} T \xi^2 l_{\text{c}}^3} \tag{4.1}$$

where κ_0 denotes the bending modulus of a single actin filament, ξ is the mesh-size of the network and l_{c} describes the average distance between two cross-links. Hence, the term $\frac{1}{l_{\text{c}}^3}$ describes the density of cross-links which is proportional to the number of cross-link points, N. Thus, equation (4.1) can be rewritten to

$$G_0 \sim \frac{\kappa_0^2 \cdot N}{k_{\text{B}} T \xi^2} \tag{4.2}$$

which reduces to the simple scaling argument $G_0 \sim N$, which is valid for constant bending modulus and mesh size. These conditions are fulfilled as for the actin/HMM system bundling of filaments does not occur. As a consequence, the mesh size of actin/HMM networks is also independent of the cross-link density as long as the filament density is kept constant [III]. This linear dependence of the network elasticity on the cross-link density allows for

- a simple linear description of the contribution of unbinding events to the network elasticity
- a direct comparison of the experimental scaling relation $G_0 \sim R^{1.2}$ [Tharmann et al. 2007, Luan et al. 2008] with the scaling relation $N \sim R^x$ obtained from modelling – which should give $x = 1.2$ to be consistent

In thermal equilibrium, an ensemble of N cross-links exhibits statistical unbinding events whose probability is determined by the cross-linker off-rate, k_{off}. This spontaneous unbinding can be described in analogy to a unimolecular reaction:

$$\text{AB} \xrightarrow{k_{\text{off}}} \text{A} + \text{B} \tag{4.3}$$

[III] In this thesis only data sets with a constant filament density are discussed.

where AB describes the bound configuration between the actin filaments (A) and the cross-linker (B) that can dissociate with a rate k_{off}. Herein, the rebinding process is assumed to be fast enough to provide a constant equilibrium number of cross-links: the unbinding process is only limited by the lifetime of the actin/ABP bond and not by the reformation of new bonds [IV]. This results in an exponential decay of intact cross-links over time, $t \geq 0$: $N(t) \sim N \cdot e^{-k_{\mathrm{off}} \cdot t}$ which can be translated into the frequency domain using a Fourier transformation yielding the complex function $\widehat{N}(f)$. Since the linear relation $G_0 \sim N$ holds for actin/HMM networks, the real part $\Re(\widehat{N}(f))$ represents the loss of elasticity due to cross-link unbinding:

$$G'(f) = G_0 - a \cdot \frac{N k_{\mathrm{off}}}{\frac{k_{\mathrm{off}}^2}{4\pi^2} + f^2} + b \cdot \left(\frac{f}{f_0}\right)^{3/4} \tag{4.4}$$

where the last term represents the fluctuation of single filaments in semi-flexible polymer networks [Morse 1998, Gisler and Weitz 1999]. The time scale of this relaxation mode is set by the factor f_0 which is a function of the solvent viscosity η [Rubinstein and Colby 2003]. The imaginary part of $\widehat{N}(f)$ contributes to the viscous part of the frequency spectrum where it competes with the single filament relaxation:

$$G''(f) = c \cdot \frac{N f}{\frac{k_{\mathrm{off}}^2}{4\pi^2} + f^2} + d \cdot \left(\frac{f}{f_0}\right)^{3/4} \tag{4.5}$$

The key parameters are the cross-linker off-rate which is known from independent experiments [Marston 1982] and the number of cross-links; the prefactors a and c include the amount of energy that is released and dissipated by unbinding of a single cross-link [V], b and d depend on the density of filaments in the network which is kept constant during a set of measurements.

The best fit for the cross-linker concentration series shown in Fig. 4.2A is obtained for $k_{\mathrm{off}} \approx 0.3\,\mathrm{s}^{-1}$ (Fig. 4.6), which is in excellent agreement with values determined by biochemical means [Marston 1982] considering that the unbinding rate of a cross-link point should be twice as high as the off-rate of a single actin/HMM bond [VI]. Not only the maximal amount of dissipated energy, $G''(f_{\mathrm{max}})$, is quantitatively reproduced by this simple model but also the position of minimal viscous dissipation as well as the dependencies of both quantities on k_{off} and N.

[IV] For simplicity, an explicite description of the rebinding process is neglected.

[V] Note, that the absolute values of a and N (and thus also c) are ambiguous; only the product $a \cdot N$ is directly set by the fit result. However, a is globally fixed for all data sets shown and the scaling relations discussed here as well as all conclusions drawn remain unaffected by the ambiguity in the absolute values of these fitting parameters.

[VI] A cross-link point is considered to be "open" as soon as one of the two actin/HMM bonds unbinds.

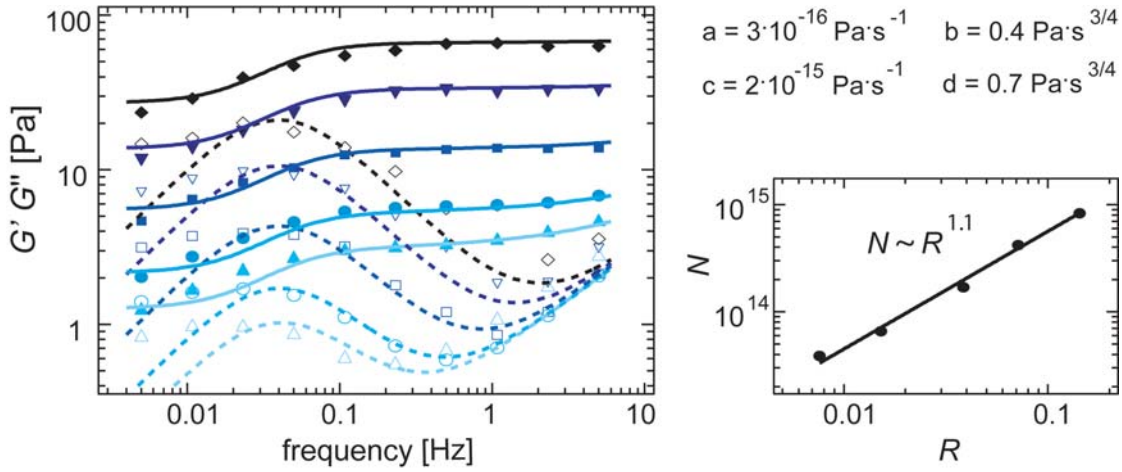

Figure 4.6: Elastic (full symbols) and viscous (open symbols) response for actin/rigor-HMM networks as a function of frequency ($c_a = 19\,\mu$M, $R = 0.0076$ (upright triangles) up to $R = 0.143$ (diamonds)). The full and dashed lines represent a global best fit using equations (4.4) and (4.5). The fitting parameters a, b, c and d are kept constant, only the cross-link density N is varied in order to reproduce the R-series. Here, $k_{off} \approx 0.3\,s^{-1}$ and $N \sim R^{1.1}$ is obtained from the fit in excellent agreement with the experimental finding $G_0 \sim R^{1.2}$ [Tharmann et al. 2007].

In all experiments, at very high frequencies $f \gg \frac{k_{off}}{2\pi}$ the viscous response is unaffected by the stress release mediated by unbinding events. Vice versa, a variation of the solvent viscosity results only in a shift of the single filament relaxation regime without affecting the off-rate of the cross-linking molecules. Consistently, only the known solvent viscosity needs to be considered to reproduce the viscoelastic network response in the presence of glycerol (Fig. 4.4A): By the addition of glycerol the viscosity of the solvent η is increased up to 6-fold for 50 % glycerol [Dorsey 1940]. Due to this change in the viscosity, the time scale of the single filament relaxation regime, $1/f_0$, is shifted. From the resulting apparent increase of b and d with the solvent viscosity a scaling $f_0 \sim 1/\eta$ can be obtained as expected [Rubinstein and Colby 2003] – which is also quantitatively consistent with the experimental changes in the solvent viscosity.

In conclusion, the minimum in the viscous dissipation can be identified as a direct result of the competition between local stress release triggered by thermal cross-link unbinding and friction which is induced by the fluctuations of single filaments. Importantly, the decay in the elastic response is also correctly reflected by the global fit. The mechanism of local stress release becomes increasingly important when approaching $f \approx \frac{k_{off}}{2\pi}$ where the contribution of thermal unbinding events, $\widehat{N}(f)$, is most pronounced and the viscous dissipation becomes maximal. If the off-rate of the cross-linking molecule is altered (Fig. 4.4C), the maximum in the

viscous dissipation is shifted, accordingly [VII].

The position of minimal dissipation therefore provides an excellent definition for the plateau elasticity in transiently cross-linked networks. At the time scale of $f \approx f_{\min}$ a transiently cross-linked network can best be regarded to be a mostly elastic material. These observations imply a well-defined transition between two generic frequency regimes: If the system is deformed with a frequency much faster than $f_{\min}$, cross-linker unbinding is too slow to significantly modify the viscoelastic response of the network, the cross-links themselves appear to be "static" and unbinding kinetics are more or less irrelevant (Fig. 4.4). However, if the deformation is imposed slow enough, the transient nature of the cross-links will dictate both the elastic and the viscous response of the network. The amount of energy which is dissipated in molecular unbinding and the ensuing stress release is determined by the density and the lifetime of the cross-links as indicated by the color scheme in Fig. 4.7.

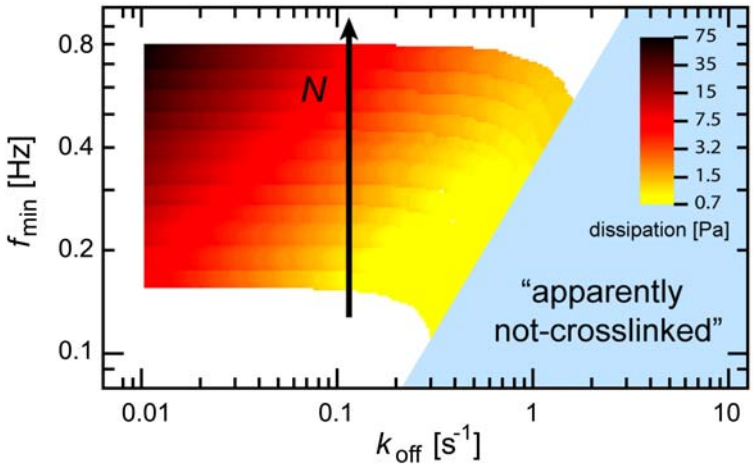

Figure 4.7: Schematic representation of the state diagram of transiently cross-linked actin/HMM networks. The transition frequency $f_{\min}$ from which on the network response is dictated by the transient nature of the cross-linker molecule is shown as a function of either the cross-linker off-rate, k_{off}, or the cross-linker density, N. As argued in the main text, this frequency marks the transition from the transient regime to the "static" cross-link regime. The maximum dissipation in the transient regime that results from cross-linker unbinding is encoded in the color scheme.

A moderate variation of the off-rate hardly affects the transition frequency $f_{\min}$; however, the maximal energy dissipation can be tuned over two orders of magnitude. A change in cross-linker density N affects both, the transition frequency from the transient to the "static" regime and the amount of maximal dissipation. At

[VII] The fits were obtained using literature values for k_{off} at 2 mM AMP·PNP [Marston 1982]

high cross-linker off-rates or low cross-link densities (indicated by the blue panel) the network behaves "apparently non-cross-linked". In this regime, a minimum in the viscous dissipation does not occur any more and a plateau regime in the network elasticity is lacking.

Local stress release triggered by thermal cross-link unbinding fully accounts for the dissipation behavior in a frequency range of $\frac{k_{\text{off}}}{2\pi}$ up to at least 10 Hz. However, at frequencies $f < \frac{k_{\text{off}}}{2\pi}$ the macroscopic network elasticity is systematically overestimated and the viscous dissipation is underestimated in Fig. 4.4 and Fig. 4.6. Interestingly, the viscous dissipation reaches a maximum at $f \approx \frac{k_{\text{off}}}{2\pi}$ in both the microscopic and the macroscopic response; yet, the macrorheological spectrum is still dominated by the elastic properties of the remaining cross-links while the locally obtained frequency spectra exhibit a low frequency regime resembling that of entangled actin solutions (Fig. 4.8). This result is independent of the type of microrheological technique: Magnetic tweezer microrheology (Fig. 4.8A) and dynamic light scattering (Fig. 4.8B, DLS spectrum measured by Wolfgang Michel [VIII]) report the same qualitative behavior, i.e. a crossing-over to a regime dominated by viscous properties at low frequencies $f < \frac{k_{\text{off}}}{2\pi}$.

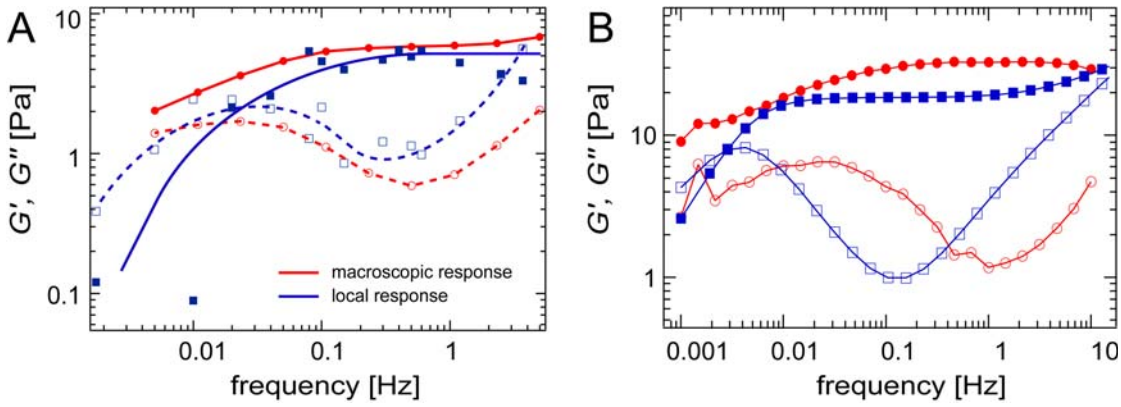

Figure 4.8: Direct comparison of a macroscopic (red circles) and microscopic (blue squares) frequency spectrum for transiently cross-linked actin/HMM networks. Full symbols denote $G'(f)$, open symbols denote $G''(f)$. A macrorheological spectrum (red circles) is compared to a local spectrum (blue squares) obtained by (A) with magnetic tweezer microrheology ($R = 0.015$) or (B) dynamic light scattering ($R = 0.1$).

This finding suggests, that a third local mechanism of relaxation has to be considered for the network response at very low frequencies. With increasing probability of unbinding events a considerable amount of filaments is "set free". For flexible polymer networks the local mechanism of "sticky reptation" has been described accounting for slow relaxations in physically cross-linked networks [Leibler et al.

[VIII] Arbeitsgruppe Ott, Lehrstuhl für biologische Experimentalphysik, Universität des Saarlandes

1991, Rubinstein and Semenov 2001]. Therefore, for frequencies $f < \frac{k_{\mathrm{off}}}{2\pi}$ local filament reorientation or even diffusion/reptation might also occur in transiently cross-linked semi-flexible polymer networks. Although this local relaxation mechanism is partially masked on the macroscopic scale, it could account for the observed deviation of the experimental data from our simplified model which does not include local filament diffusion/reptation events.

It is important to note, that the observed transient unbinding effects described here do not permanently change the material properties – underlining the thermal nature of the process. Transient cross-links provide maximal energy dissipation without permanently altering the microstructure of the network. The tunability of the viscous dissipation in an elasticity dominated frequency regime allows for local reorganization processes and creates an adaptive material which is able to absorbe mechanical shocks on the microscopic scale without causing structural failure. In fact, this extraordinary material property might be an important advantage for living cells employing transiently cross-linked biopolymer networks instead of covalently cross-linked structures which would be much too brittle.

4.1.3 Influence of the actin/ABP interaction potential

Transient cross-links guarantee structural and mechanical adaptability at long time scales while ensuring an elastic network response at time scales that are short compared to the cross-linker off-rate. Nature offers a huge variety of actin binding proteins (ABPs) to cross-link and tailor the microstructure and the mechanical properties of the cytoskeleton. In order to achieve high versatility, cells make use of the inherent biochemical differences of diverse ABPs. These differences manifest themselves in distinct interaction potentials, which can be manipulated by forces acting on the actin/ABP bond - a strategy cells can pursue by creating internal stresses [Wang et al. 2002]. The dynamic interplay between actin filaments and ABPs is set by biochemical parameters such as the binding energy E_{B}, the cross-linker on- and off-rate k_{on} and k_{off}, and the position of the transition state Δx, which represents the characteristic bond length (Fig. 4.9).

Typically, these parameters are determined by a combination of biochemical and single molecule studies [Evans 1998, Schlierf and Rief 2006]. For further progress in a microscopic understanding of cellular mechanics, it needs to be shown whether these biochemical properties of the cross-linking molecules are closely linked to their mechanical function.

As networks formed by rigor-HMM are homogeneous and isotropically cross-linked, the network elasticity depends solely on one length scale, which is the cross-linker distance l_{c} [Tharmann et al. 2007, Luan et al. 2008]. Furthermore, the biochemical interaction of actin and HMM has been characterized in great detail [Marston 1982]. This makes actin/HMM networks ideal for a quan-

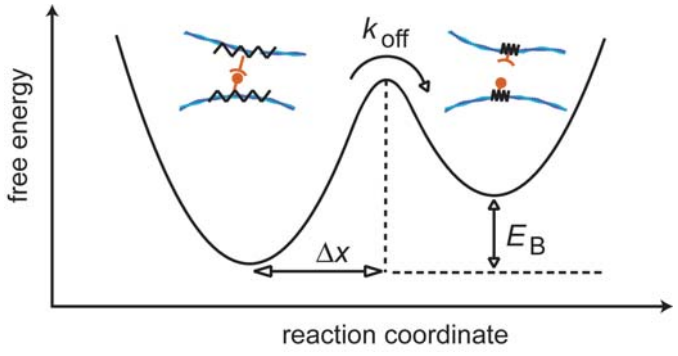

Figure 4.9: A transient bond can unbind due to thermal activation or upon force application. The transient actin/ABP cross-link can be characterized by an interaction potential. The key parameters are the cross-linker off-rate k_{off}, the binding energy E_{B} and the position of the transition state Δx.

titative analysis of the viscoelastic network response. In a cross-linker concentration series as depicted in Fig. 4.10A the cross-linker off-rate is constant – which makes this set of measurements ideal to determine k_{off}. The total number of cross-links N is set by experimental conditions. As discussed in section 4.1.2, the scaling relation $G_0 \sim N \sim R^{1.2}$ describes the static network elasticity G_0 and correlates the number of cross-links N with the experimental control parameter R. With this constraint, the best reproduction of the data set is obtained for $k_{\mathrm{off}} \approx (0.30 \pm 0.05)\,\mathrm{s}^{-1}$ (compare section 4.1.2). The same result is obtained if the actin concentration is varied at a fixed cross-linker concentration (e. g. $R = 0.1$) as depicted in Fig. 4.10B. Here, $k_{\mathrm{off}} \approx (0.23 \pm 0.05)\,\mathrm{s}^{-1}$ is obtained which agrees well with the result obtained from the R-series. Note, that in the actin concentration series the impact of single filament fluctuations becomes more pronounced with increasing actin concentrations – representing the increasing density of actin filaments. At higher filament densities the entanglement length decreases which facilitates the formation of cross-links at a given cross-linker concentration. Thus, in the actin concentration series the effective cross-linker density is increased, too. This makes this experiment qualitatively very similar to the R-series discussed before. In both cases, the variation of the cross-link density allows for the extraction of the cross-linker off-rate of individual actin/HMM bonds. This finding confirms that the time scale at which the energy dissipation in the cross-linked network is minimal is set not only by the static density of the cross-links but also by the dynamic off-rate of the actin/ABP bond.

In addition, since cross-linker unbinding determines the frequency response of transiently cross-linked networks, the characteristic binding energy of the cross-link should be obtainable from the temperature dependence of frequency sweeps. The results discussed in section 4.1.1 demonstrate that thermal energy is sufficient to drive the actin/HMM bond across the potential barrier. The binding energy E_{B} is lost every time an unbinding event occurs between the cross-linking molecule and

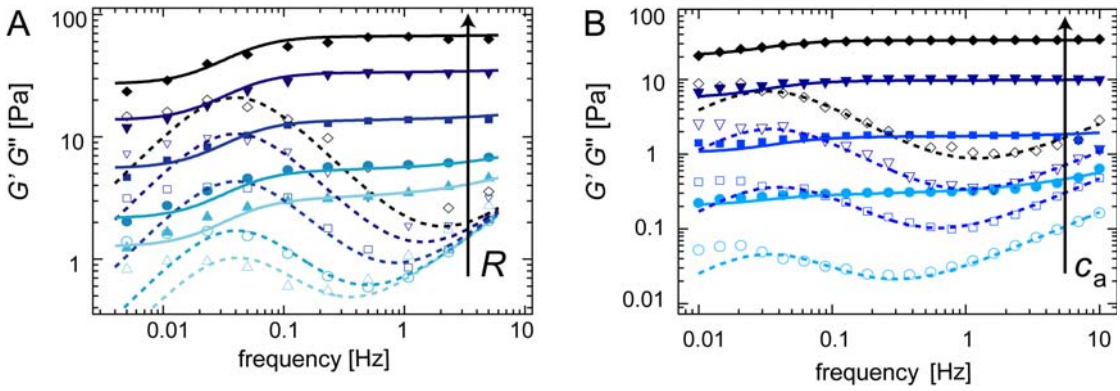

Figure 4.10: Either a cross-linker concentration series (A, fixed $c_a = 19\,\mu$M) or an actin concentration series (B, fixed $R = 0.1$) can be employed to extract the cross-linker off-rate from the viscoelastic spectrum of transiently cross-linked actin/HMM networks. Closed symbels denote $G'(f)$, open symbols denote $G''(f)$. The full and dashed lines represent a global best fit using equations (4.4) and (4.5).

the actin filament. E_B characterizes the cross-link and sets the total ratio of bound to unbound molecules. This gives rise to an inherent temperature dependence of the binding constant $K \sim \exp(-E_B/k_BT)$. Thus, investigating the frequency spectrum of a cross-linked actin network at different temperatures should be an appropriate approach to determine the binding energy of a single cross-link.

A series of linear response measurements in a temperature range of $10 - 30\,^\circ$C is analyzed as depicted in Fig. 4.11A. Starting at $21\,^\circ$C, where the network was polymerized, the sample temperature is modified using a protocol of oscillating temperature steps ($T = 21 \rightarrow 15 \rightarrow 25 \rightarrow 10 \rightarrow 30\,^\circ$C) providing adequate time for thermal equilibration (Fig. 4.11C). This protocol guarantees that a putative change in the observed network response is purely due to thermal effects and not superimposed by time dependent changes like sample "ageing" (compare section 4.3). As depicted in Fig. 4.11A, a continuous decrease in both viscoelastic moduli is observed with increasing temperature T. A reproduction of the data set by the model described in section 4.1.2 results in a constant off-rate, $k_{off} \approx 0.3\,s^{-1}$, a decrease of the static elasticity G_0 with increasing T (Fig. 4.11B) and a shift of the time scale of the single filament relaxation regime, $t_0 = 1/f_0$ (compare section 4.1.2). This time can be normalized by the solvent viscosity η yielding $\frac{t_0}{\eta}$. This parameter is almost independent of T (Fig. 4.11B), indicating that the observed shift in this time scale with respect to T is simply given by the temperature dependence of the solvent viscosity.

As the static plateau modulus G_0 of isotropically cross-linked actin networks depends solely on the total number of cross-links, the following relation holds: $G_0 \sim N \sim K \cdot R$. The temperature dependence of the binding constant K is

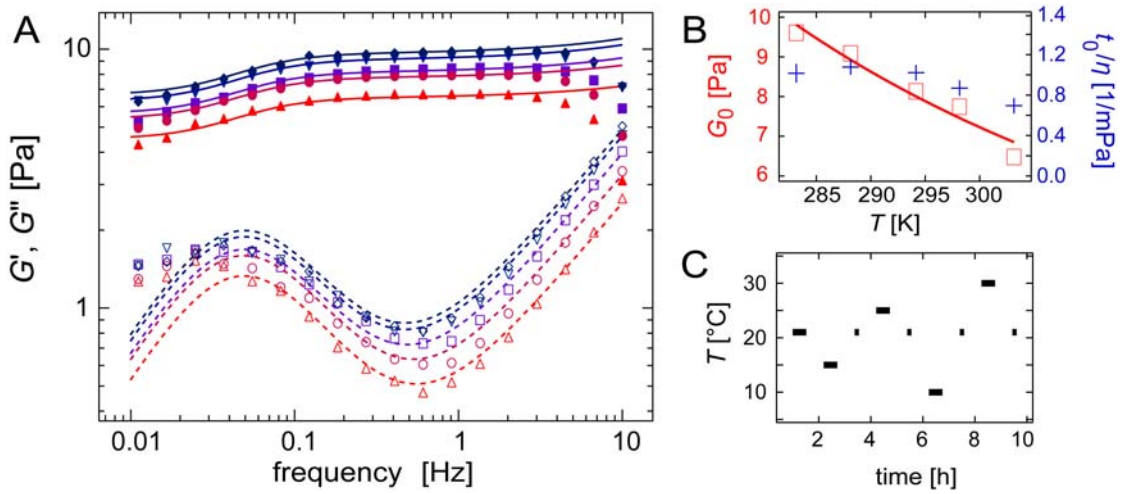

Figure 4.11: (A) Frequency response of actin/HMM networks ($c_a = 9.5\,\mu M$, $R = 0.1$) at distinct temperatures (10 °C (diamonds) up to 30 °C (upright triangles)). Closed symbols denote $G'(f)$, open symbols denote $G''(f)$. The full and dashed lines represent the model used to evaluate the macromechanical response as described in section 4.1.2. (B) Plateau modulus G_0 (squares) and the normalized time t_0/η (crosses) as a function of temperature. η denotes the viscosity of water. (C) Temperature-oscillation protocol as described in the main text. Frequency sweeps (bars) are taken at 21, 15, 25, 10 and 30 °C. Before the next temperature jump, the network is brought back to its initial temperature of 21 °C in order to assure reversibility (dots).

given by an Arrhenius law, thus $G_0 \sim \exp(-E_B/k_BT)$. Therefore, the binding energy of the actin/HMM bond can be directly extracted from $G_0(T)$ by fitting an exponential decay to the data as shown in Fig. 4.11B. $E_B \approx (-13 \pm 2)\,\mathrm{kJ{\cdot}mol^{-1}}$ is obtained in good agreement with literature values [Highsmith 1977, Marston 1982]. A similar temperature dependence was reported for actin networks cross-linked by α-actinin [Tempel et al. 1996]. There, the complicated and heterogeneous microstructure of α-actinin networks (compare section 3.1.1) had defied a quantitative comparison of the macroscopic network elasticity with the cross-linker affinity. However, the results on actin/HMM networks presented here clearly demonstrate that the binding energy of a single cross-link determines the temperature dependence of the network response of transiently cross-linked actin networks.

While cells can only passively react to changes in the temperature of their environment, adjusting the local density or composition of cross-linking molecules gives them the possibility to actively tune their mechanical properties. Another strategy to actively control cytoskeletal mechanics is given by creating internal forces. It was shown, that living cells exploit molecular motors to create and maintain a certain level of internal stress to increase the elastic response of the

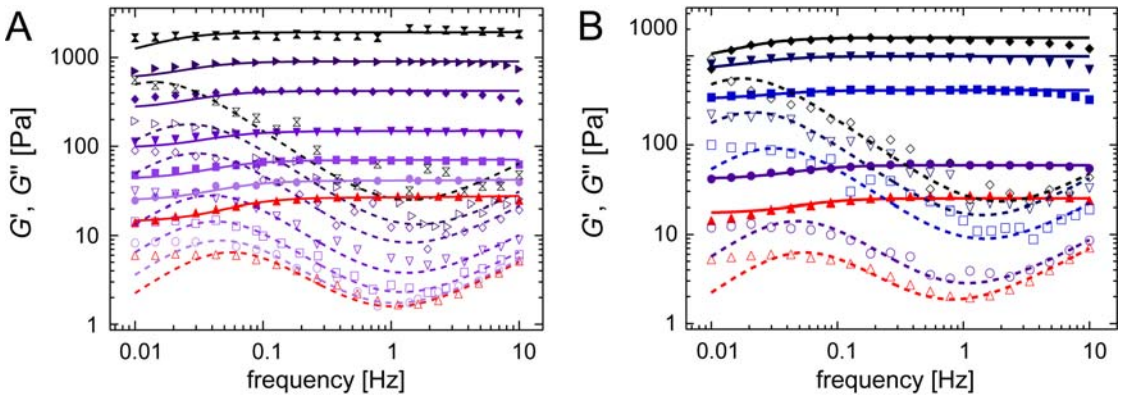

Figure 4.12: Frequency response of actin/HMM networks ($c_a = 9.5\,\mu$M) at distinct levels of prestress σ_0. Closed symbols denote $G'(f)$, open symbols denote $G''(f)$. The full and dashed lines represent the model used to evaluate the macromechanical response as described in section 4.1.2. (A) $R = 0.1$: $\sigma_0 = 0\,$Pa (upright triangles) up to $\sigma_0 = 20\,$Pa (butterflies)), (B) $R = 0.2$: $\sigma_0 = 0\,$Pa (upright triangles) up to $\sigma_0 = 15\,$Pa (diamonds).

cytoskeleton [Wang et al. 2002]. However, it remains to be analyzed how external or internal forces acting on cytoskeletal networks affect the binding kinetics of cross-linking molecules and therefore the dynamic viscoelastic network response.

A microscopic parameter which dictates the sensitivity of a transient actin/ABP bond towards forces is the characteristic bond length, Δx. This parameter marks the position of the transition state of the binding/unbinding process. Having demonstrated that the viscoelastic response of a transiently cross-linked actin/HMM network is set by the off-rate and the binding energy of the HMM/actin bond, it is now addressed if the bond length Δx influences the network mechanics. If this is case, the bond length should be obtainable from the macroscopic network response by employing the force dependence of the binding kinetics of the cross-linker.

Single molecule studies have demonstrated that the rupture force of a single molecular bond depends on the force loading rate in a logarithmic manner [Evans and Ritchie 1997]. There, a variation of the force loading rate allows for shifting the rupture force distribution and thus determining Δx. A similar principle should also be applicable for actin/ABP bonds in cross-linked networks – however, instead of studying the loading rate dependence of the rupture force, the application of a constant "prestress" [Gardel et al. 2006] should already be sufficient to characterize the cross-linker unbinding process in the presence of external force. Therefore, the frequency dependence of the viscoelastic network response of densely cross-linked actin/HMM networks ($R = 0.1$ and $R = 0.2$) in the presence of varying external prestress σ_0 is analyzed (Fig. 4.12A and B).

As depicted in (Fig. 4.13A), the static network elasticity increases linearly with

the prestress, $G_0 \sim \sigma_0$. Furthermore, the global fit of the prestress series requires an increase of the stress relaxation parameters $a(\sigma_0 = 0) = 3 \cdot 10^{-16}\,\mathrm{Pa \cdot s^{-1}}$ and $c(\sigma_0 = 0) = 2 \cdot 10^{-15}\,\mathrm{Pa \cdot s^{-1}}$ in proportion with the prestress σ_0 (Fig. 4.13B); however, $\frac{a}{c} = \text{const}$. This shows, that the amount of dissipated energy upon cross-link unbinding as well as the loss in the network elasticity are both enhanced in the presence of prestress - with the same dependence on σ_0 [IX].

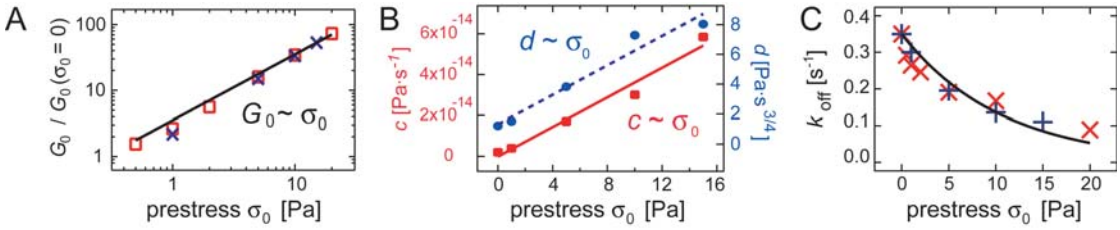

Figure 4.13: Fitting parameters for prestressed actin/HMM networks as obtained for the data sets depicted in Fig. 4.12A and B. (A) Enhancement of the network elasticity $G_0/G_0(\sigma_0 = 0)$ as a function of prestress σ_0. A linear relation is observed for both cross-linker densities ($R = 0.1$ (squares) and $R = 0.2$ (crosses)). (B) Stress relaxation parameter c and single filament relaxation parameter d increase linear with the prestress σ_0. (C) Cross-linker off-rate k_{off} as a function of prestress for two different actin/HMM networks ($R = 0.1$ ($\times$) and $R = 0.2$ ($+$)).

Concomitant with the enhanced network elasticity an exponential decrease of the apparent cross-linker off-rate is observed (Fig. 4.13C) for both cross-linker densities studied here. In an isotropically cross-linked actin network the macroscopic stress will be transduced to single actin/ABP bonds following the geometry of the network. Depending on the orientation of the cross-link relative to the direction of the applied force, a distribution of force vectors will be present. Partially, they will stabilize or destabilize the bonds. With the simplified assumption that stabilizing and destabilizing forces of identic magnitude are equally probable, a decrease in the apparent cross-linker off-rate of the network with increasing force can be rationalized (see appendix). With that an Arrhenius law

$$k_{\mathrm{off}}^{F} = k_{\mathrm{off}}^{0} \cdot \exp\left(-\sigma_0/\sigma^*\right) \tag{4.6}$$

can be fitted to the observed decay of k_{off} in Fig. 4.13C. Here, k_{off}^{F} and k_{off}^{0} denote the cross-linker off-rate in the presence and absence of external force and σ^* is the characteristic decay stress. The magnitude of force that is transduced to a single bond is given by the level of prestress as $F \sim \sigma_0$. In a Bell model [Bell 1978], the characteristic bond length is described by the position of the transition state Δx.

[IX] The same scaling behavior is observed for the parameter $d(\sigma_0 = 0) = 0.08\,\mathrm{Pa \cdot s^{3/4}}$ which describes the high frequency regime that is dominated by the fluctuations of single filaments.

As a consequence, the experimentally determined decay stress σ^* can be related with the Bell prediction and the following relation can be assumed to hold

$$\frac{\sigma_0}{\sigma^*} = \frac{F \cdot \Delta x}{k_\mathrm{B} T}. \tag{4.7}$$

In order to extract the bond length Δx from this relation, the ratio F/σ_0 has to be determined for any level of prestress. It is assumed, that F/σ_0 depends only on the network geometry and not on the magnitude of the applied force. Therefore, the point of bond rupturing is chosen to determine this ratio since the rupture stress $\sigma_{0,\mathrm{r}}$ and the rupture force F_r are experimentally accessible: For actin/HMM networks the rupture force of a single bond was determined to be $F_\mathrm{r} \approx 8\,\mathrm{pN}$, the corresponding rupture stress is $\sigma_{0,\mathrm{r}} \approx 30 - 40\,\mathrm{Pa}$ [Tharmann et al. 2007] for $R = 0.14$. Hence, the bond length Δx can directly be calculated from the decay stress $\sigma^* = (10.6 \pm 1.3)\,\mathrm{Pa}$ to be $\Delta x \approx (1.9 \pm 0.7)\,\mathrm{nm}$. This is in excellent agreement with literature values obtained from microscopic studies of the actin/HMM bond. There, a bond length $\Delta x_\perp = 0.5\,\mathrm{nm}$ [Nishizaka et al. 2000] and $\Delta x_\parallel = 2\,\mathrm{nm}$ [Guo and Guilford 2006] was reported – depending on whether the force was applied orthogonally to the binding direction [Nishizaka et al. 2000] or in a parallel manner [Guo and Guilford 2006]. Indeed, these simple considerations give a reasonable value $\Delta x_\perp < \Delta x < \Delta x_\parallel$. This might reflect the fact, that in an isotropically cross-linked network a distribution of various force directions is present. However, simulations might be necessary to determine this force distribution in detail.

4.1.4 Non-linear response: force-induced unbinding

In section 4.1.3 it was demonstrated that the interaction potential of an actin/ABP bond determines the viscoelastic reponse of transiently cross-linked actin networks. While thermal energy is sufficient to drive the unbinding reaction of the cross-link across the potential barrier, the application of prestress was shown to shift the effective cross-linker off-rate of the network by partially stabilizing and destabilizing actin/ABP bonds. As a consequence, sufficiently large external forces should also allow for cross-linker unbinding events.

The viscoelastic response of cross-linked or bundled actin networks and even entangled actin solutions retains a highly non-linear character at large stresses [Gardel et al. 2004a, Gardel et al. 2006] and thus strains. The degree and type of non-linearity – hardening or weakening [X] – crucially depends on the measurement protocol [Semmrich et al. 2008] and the network microstructure. The molecular origin of this non-linear behavior is still elusive and vehemently

[X] i.e. with respect to strain or stress

discussed; a generic description (if possible at all) would have to account for the microscopic differences in the network structures as well as for the subtle interplay of cross-linker unbinding events and the persistence length of actin filaments and bundles, respectively.

The simplest approach to correctly probe the non-linear elasticity of actin networks is given by applying a constant shear rate $\mathrm{d}\gamma/\mathrm{d}t$. This method largely avoids artifacts induced by viscous creep, which in principle is not neglectable in transiently cross-linked actin networks. The resulting stress σ is reported and from the smoothed $\sigma(\gamma)$ relation the differential modulus $K = \partial\sigma/\partial\gamma$ is calculated [Semmrich et al. 2008] and analyzed as a function of strain. At low strains linear response is observed for all kinds of actin networks, i.e. $K \approx$ const (regime I, dashed lines in Fig. 4.14A and B). However, beyond a critical deformation γ_c non-linear deformations start to set in (regime II, compare section 3.3.2) [XI]. For many network configurations strain-hardening is observed and the differential modulus increases roughly with a power law, $K \sim \gamma^x$ (blue line in Fig. 4.14); the exponent x can be used to describe the degree of hardening. Finally, at high deformations $\gamma > \gamma_{max}$ the network is irreversible damaged and plastic deformations occur (regime III).

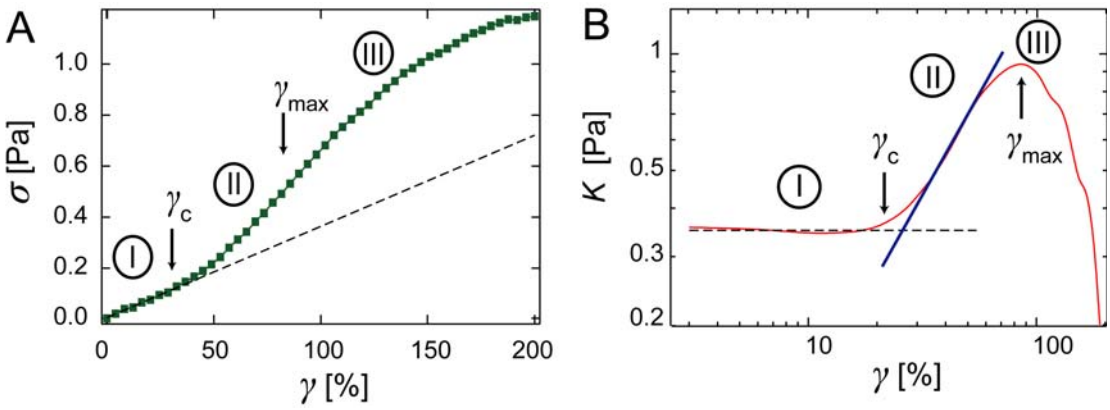

Figure 4.14: Typical non-linear strain-hardening response of actin networks. From the stress-strain relation $\sigma(\gamma)$ shown in (A) the differential modulus K is calculated and depicted as a function of strain in (B). Three different regimes emerge as described in the text.

Isotropically cross-linked actin/HMM networks [Tharmann et al. 2007] and bundled actin/PEG networks [Tharmann et al. 2006] both exhibit a strain-hardening response in the non-linear deformation regime. The degree of hardening

[XI] For a quantitative analysis the following definition of γ_c is used: γ_c marks the critical deformation at which the differential modulus K deviates by 5 % from its value in the linear regime.

decreases with increasing concentrations of the additive in both cases, i.e. with increasing cross-link density in the case of actin/HMM networks [THARMANN et al. 2007] and with increasing actin bundle thickness/stiffness in the case of actin/PEG networks [THARMANN et al. 2006] [XII], respectively. In order to analyze the interplay of increasing cross-link density and bundle thickness/stiffness on the non-linear response, actin/fascin bundle networks are investigated where both parameters can be simultaneously increased as a function of R (compare section 3.3.1 and 3.3.2). The same qualitative trend as described above is also observed for actin/fascin bundle networks; however, here the variability in the degree of hardening is much more pronounced: With increasing fascin concentration R the non-linear response of actin/fascin bundle networks exhibits a full transition from strain-hardening to strain-weakening as depicted in Fig. 3.17 on page 44. The same data set is shown again in a renormalized version in Fig. 4.15A to enhance the visibility of the effect. In actin/fascin networks the bundles are transiently cross-linked with fascin molecules, the degree of cross-linking among individual bundles depends on the fascin concentration (see section 3.3.2). With increasing R the bundle stiffness as well as the connectivity of individual bundles is enhanced. Thus, at high fascin concentrations a macroscopic deformation will lead to forced unbinding of interconnecting fascin molecules even before non-linear deformations of the stiff bundles can be evoked.

The same effect on the non-linear response can be achieved by applying different strain rates to a bundle network with fixed microstructure ($R = 0.1$) as shown in Fig. 4.15B. Varying the strain rate by two orders of magnitude leads to a continuous change in the degree of strain-hardening. When the bundle network is sheared with very low strain rates, detaching of fascin molecules is very likely on the timescale of the experiment (e. g. $\approx 100\,\mathrm{s}$ in the case of $\mathrm{d}\gamma/\mathrm{d}t = 0.125\,\%\mathrm{s}^{-1}$). Therefore, the remaining number of connection points between fascin bundles might become too low to evoke strain hardening as in the case of higher shear rates. This underlines the non-universal behavior of the non-linear response of semi-flexible polymer networks, qualitative similar observations are even reported for purely entangled actin solutions where cross-links are lacking and a putative stickiness of actin filaments is hypothesized to account for the non-linear response of the solution [SEMMRICH et al. 2007]. Even if the molecular mechanism responsible for the strain hardening remains yet to be understood, the non-linear response of semi-flexible polymer networks can be tuned both geometrical parameters of the network and experimental conditions including the polymer bending rigidity, cross-link density, binding kinetics and compliance of the cross-linker as well as the strain rate and sample

[XII] The bundle network formed by the depletion agent PEG only exhibits "virtual" cross-links between the bundles, i.e. attractive forces that are due to the entropic depletion effect. These virtual cross-links should be mechanically weak compared to physical cross-links as they are created by ABPs.

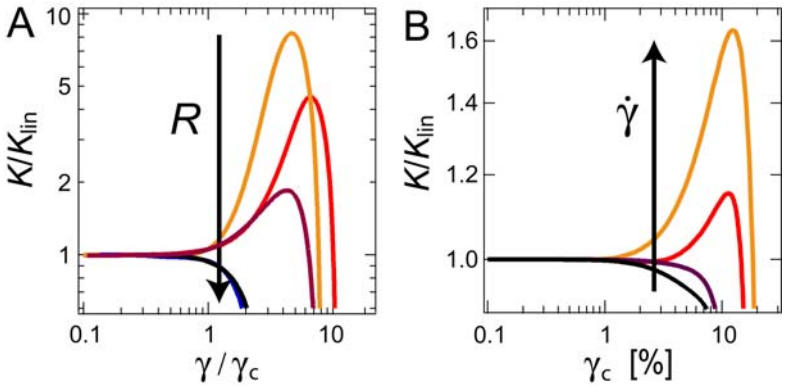

Figure 4.15: The differential modulus K of actin/fascin bundle networks is normalized by its value in the linear regime and shown as a function of strain. The non-linear response can be tuned from hardening to weakening at a fixed strain rate $\mathrm{d}\gamma/\mathrm{d}t = 6.25\%s^{-1}$ by varying the fascin concentration ($R = 0.02$ up to $R = 0.5$) as shown in (A) as well as for fixed $R = 0.1$ tuning the strain rate ($\mathrm{d}\gamma/\mathrm{d}t = 0.125, 1.25, 6.25, 12.5\,\%\mathrm{s}^{-1}$) as depicted in (B). $c_\mathrm{a} = 9.5\,\mu\mathrm{M}$ for all curves shown.

temperature.

In the experiments on actin/fascin bundle networks discussed so far, the shear rate measurements were conducted in such a way, that the non-linear reponse was completely tuned from strain-hardening to weakening by either tuning the cross-linker density or the shear rate. With varying shear rates the net force loading rate that is sensed by a single actin/ABP cross-link during the shear experiment is changed, too. This should manifest itself in a shifted rupture force distribution in the transiently cross-linked network. For a single molecular bond a linear increase of the rupture force with the logarithm of the loading rate, $F_\mathrm{max} \sim \ln(\mathrm{d}F/\mathrm{d}t)$, would be expected from the Bell prediction [Bell 1978, Evans and Ritchie 1997]. To further investigate the dependence of F_max on the loading rate in transiently cross-linked networks, a weakly bundled network is chosen where the density of bundle interconnection points is low ($R = 0.05$). For this network type strain-hardening is observed for all strain rates applied (Fig. 4.16).

The maximum strain the bundle network can endure without being irreversibly damaged is independent from the strain rate, $\gamma_\mathrm{max} \approx (22 \pm 1)\,\%$. The maximum stress $\sigma_\mathrm{max} = \sigma(\gamma_\mathrm{max})$ the bundle network can withstand depends logarithmically on the strain rate $\mathrm{d}\gamma/\mathrm{d}t$ as depicted in the inset of Fig. 4.16. The maximum force a single fascin molecule connecting two bundles can hold is given by $F_\mathrm{max} \sim \sigma_\mathrm{max} l_\mathrm{c}^2$ whereas l_c denotes the average distance of two neighboring bundle interconnection points being fixed for a given R. For the data presented here the proportionality $\mathrm{d}F/\mathrm{d}t \sim \mathrm{d}\gamma/\mathrm{d}t$ holds at the point of rupture γ_max (see appendix). Therefore, the Bell-prediction is reproduced well – indicating that forced unbinding of actin/fascin

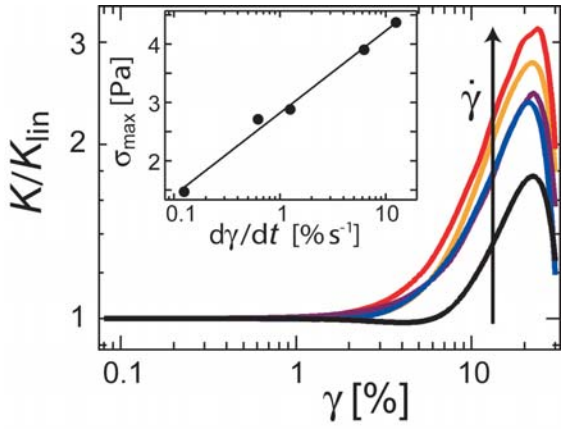

Figure 4.16: Differential modulus K normalized by its value in the linear regime as a function of strain. A weakly bundled actin/fascin network ($R = 0.05$, $c_a = 9.5\ \mu$M) is examined at different strain rates ($d\gamma/dt = 0.125, 0.625, 1.25, 6.25, 12.5\ \%s^{-1}$). The inset shows the maximum stress σ_{max} as a function of the strain rate.

bonds gives rise to the observed strain rate dependence. As the macroscopic deformation is transmitted in a non-affine way to the bundle cross-linking points (compare section 3.3.2), not all interconnecting fascin molecules will be loaded with the same force during a strain rate experiment. Surprisingly, the Bell prediction is still fulfilled.

These results show that force-induced rupturing of single actin/ABP bonds limits the stability of transiently cross-linked actin networks under mechanical load. Moreover, the rate dependent cross-linker unbinding behavior observed in complex networks is also reported from single molecule studies – indicating that collective phenomena can be largely neglected. The complete tunability of the non-linear response by either the cross-linker concentration or the shear rate suggests that the viscoelastic response of purely bundled actin networks might be equally determined by the cross-linker concentration – as also observed for the simpler actin/HMM system – and the chosen time scale of the experiment. The transient nature of actin/fascin bonds introduces the cross-linker off-rate as an important time scale (compare section 4.1.1). For actin/fascin bonds in filopodia this off-rate was determined to be $k_{off} \approx 0.12\,s^{-1}$ [Aratyn et al. 2007]; however experimental uncertainties in *in vivo* assays may cause this value to be slightly different in an *in vitro* experiment. The off-rates of several actin/ABP bonds are compared in table 4.1. As it turns out, these off-rates span less than one decade. This suggests, that unbinding of cross-linking molecules is an ubiquitous mechanism, which dictates the dynamic properties of isotropically cross-linked actin networks at biological relevant time scales of several seconds.

In conclusion, the transient character of actin/ABP bonds gives rise to a delicate sensitivity of cytoskeletal mechanics towards external or internal forces. This might provide a central mechanism living cells can exploit for mechanosensing tasks. As distinct ABPs differ in their biochemical properties such as the off-rate, binding energy or bond length, the corresponding actin/ABP interaction potentials provide

ABP	unbinding rate	reference
HMM	$0.09\,\mathrm{s}^{-1}$	[Marston 1982]
fascin	$0.12\,\mathrm{s}^{-1}$	[Aratyn et al. 2007]
α-actinin	$0.44\,\mathrm{s}^{-1}$	[Goldmann and Isenberg 1993]
filamin	$0.61\,\mathrm{s}^{-1}$	[Goldmann and Isenberg 1993]

Table 4.1: The off-rates for different actin/ABP bonds all lie within a relatively narrow frequency window of less than one decade.

a formidable basis to tailor the dynamic viscoelastic response of the cytoskeleton, not only in thermal equilibrium but also under mechanical load.

4.2 Master curve descriptions

In an actin solution the semi-flexible nature of the actin filaments causes a separation of length scales and therefore time scales [Hinner et al. 1998, Morse 1998]. The addition of ABPs alters the structure of entangled actin solutions. Depending on the molecular structure of the cross-linking molecule, isotropically cross-linked networks [Tharmann et al. 2007], purely bundled networks (see section 3.1.2.2 or [Purdy et al. 2007]) or heterogeneous composite phases are created (compare section 3.1.1 or [Shin et al. 2004a]). Concomitant with the structural change new length and time scales are introduced. While the microstructure of such complex reconstituted actin networks mainly determines the elastic response (compare section 3.3), the length dependence of the persistence length of individual bundles [Claessens et al. 2006, Tharmann et al. 2006] has to be considered as well (compare section 3.3.2).

In section 4.1.4 an equivalence of cross-linker concentration and time was demonstrated for the non-linear response of actin/fascin bundle networks. Moreover, in section 4.1.1 it was shown that the frequency response of transiently cross-linked networks is dictated by the density and lifetime of cross-links. In both cases the impact of cross-link unbinding becomes more pronounced with increasing cross-link density. These findings suggest that a generalized description of the frequency response of transiently cross-linked networks by a master curve might be possible. Such a master curve construction, i.e. the creation of an extended frequency spectrum spanning several orders of magnitude in frequency, relies on the superposition of distinct frequency spectra which are obtained under different experimental conditions. A prominent example known from flexible polymers is the superposition of frequency spectra which are acquired at different sample temperatures. For cross-linked networks of semi-flexible polymers such a superposition principle has not been validated yet.

The following considerations are first applied to bundled actin/fascin networks. Then, the applicability of a similar master curve construction is discussed for isotropically cross-linked actin/HMM networks and composite actin/α-actinin networks. In all cases, an impartial criterion is needed to obtain appropriate parameters for a putative generalization process of the frequency response. In section 4.1.2 it was demonstrated that the local minimum in the viscous dissipation marks the time scale at which the viscoelastic response of a transiently cross-linked network is equally dominated by thermal cross-linker unbinding events and single polymer fluctuations. Therefore, this minimum position in the loss modulus is an ideal candidate representing both the cross-link density and the cross-linker off-rate as well as single polymer properties.

The miminum position $(f_{\min}|G''^*)$ [XIII] together with the corresponding value of the storage modulus G'^* [XIV] is determined for actin/fascin networks in the bundle phase. For samples below the bundling transition such a minimum in the viscous dissipation is not observable – thermal cross-linker unbinding is negligible at such low fascin concentrations [XV]. Therefore, $f_{\min}$ is obtained by creating a "best match" overlay of the frequency spectra. Normalizing the frequency spectra by these values results in a master curve which shows two different regimes corresponding to distinct network types. At low rescaled frequencies the master curve corresponds to networks in the purely bundled phase (Fig. 4.17A, rescaled $G'(f)$ shifted up for clarity). This regime contains a pronounced plateau region in the storage modulus $G'(f)$ accompanied by a clear minimum in the loss modulus $G''(f)$. A maximum in the viscous dissipation as observed for actin/HMM networks cannot be identified in this master curve since this feature is also lacking in the unshifted frequency spectra. It can only be speculated whether the master curve construction shown here would also be valid towards lower frequencies where local reptation effects start to set in. However, the increasing bundle thickness at higher R-values suggests that bundle reptation should get more and more slowed down with respect to R – which would be consistent with the superposition principle of cross-linker concentration and time employed here.

Networks before the bundling threshold also show a common frequency dependence similar to a purely entangled actin solution (Fig. 4.17B). For an actin concentration of $c_{\mathrm{a}} = 9.5\,\mu$M this bundling threshold R^* is located at $R^* \approx 0.01$ (section 3.1.2.2). Indeed, the scaling parameters obtained for the master curve construction follow a conjoint power law $G'^* \sim (f_{\min})^x$, $G''^* \sim (f_{\min})^x$ in the bundle phase, while dropping off this relation for values $R < R^*$ (see Fig. 4.17C). For the bundle phase a linear relation between the scaling parameters, $x = 1$, is obtained. This is an indication of self-similarity as also observed in other soft matter systems [Trappe and Weitz 2000]. Fascin networks with $R < R^*$ can also be rescaled with a common power law between the scaling parameters, however $x \approx 1/2$. As in this regime the tube model can be applied to describe the mechanical response (compare section 3.1.2.2), the addition of few fascin molecules seems to only slightly modify the network properties which does not give a self-similar structure. The corresponding part of the master curve, $f/f_{\min} > 10^3$, shows a regime $\sim f^{0.5}$ in both viscoelastic moduli right before the crossing-over, $f_{\mathrm{cross}} \sim 1/\tau_{\mathrm{e}}$, where τ_{e} denotes the entanglement time. While the molecular origin of this behavior is still unclear, it is expected for cross-linked semi-flexible polymer networks in an intermediate frequency regime resulting from tensions in the

[XIII] $G''^* = G''(f_{\min})$

[XIV] $G'^* = G'(f_{\min})$

[XV] This is fully consistent with the generic occurrence of a weakly cross-linked regime at low ABP concentrations, which is still dominated by the entanglement length l_{e} (compare section 3.1).

network [Morse 1998]. It is also reported for entangled actin networks from two-point microrheological experiments [Liu et al. 2006] and interpreted to be due to the diffusive dissipation of long-wavelength longitudinal fluctuations. Only at very short time scales $t \ll \tau_e$, and therefore very high frequencies beyond the crossing-over of $G'(f)$ and $G''(f)$, i.e. around 1 kHz, a scaling $\sim f^{0.75}$ due to undisturbed relaxations along single filaments would be expected [Morse 1998, MacKintosh et al. 1995, LeGoff et al. 2002b] and is also detected experimentally [Gisler and Weitz 1999].

From a single macrorheological experiment it is difficult to extract the crossing-over time τ_e with a decent accuracy. The master curve presented in this work would in principle offer enough reliable data points – albeit normalizing both moduli to the same absolute value cancels out the desired information. In fact, re-shifting the rescaled storage modulus might give the wrong impression that both moduli do not cross over at all in the frequency range probed. Therefore, it is helpful to calculate the loss factor $\tan(\delta) = G''(f)/G'(f)$. The shape of the loss factor curves drastically changes at $R^* = 0.01$ (large symbols in the inset of Fig. 4.18). This again is in agreement with the bundling transition reported before. Moreover,

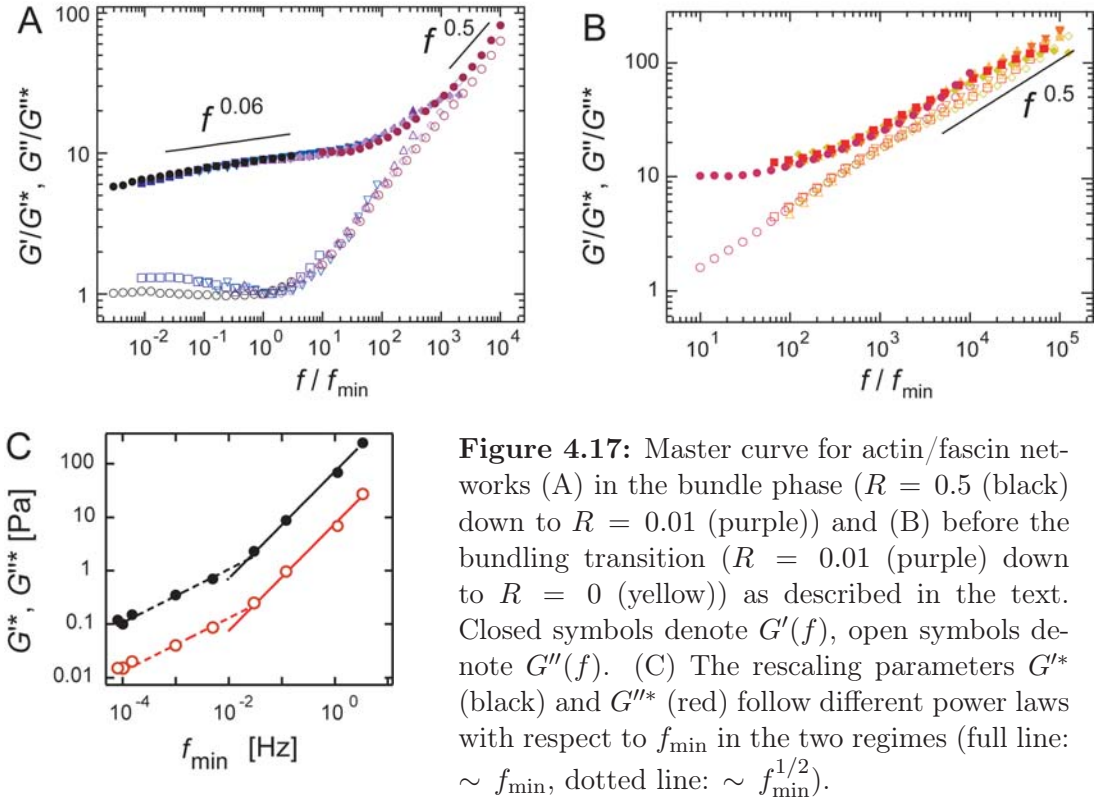

Figure 4.17: Master curve for actin/fascin networks (A) in the bundle phase ($R = 0.5$ (black) down to $R = 0.01$ (purple)) and (B) before the bundling transition ($R = 0.01$ (purple) down to $R = 0$ (yellow)) as described in the text. Closed symbols denote $G'(f)$, open symbols denote $G''(f)$. (C) The rescaling parameters G'^* (black) and G''^* (red) follow different power laws with respect to $f_{\min}$ in the two regimes (full line: $\sim f_{\min}$, dotted line: $\sim f_{\min}^{1/2}$).

these curves can also be generalized (Fig. 4.18) requiring only one single rescaling parameter, namely the same $f_{\min}$ as used for the master curves shown in Fig. 4.17.

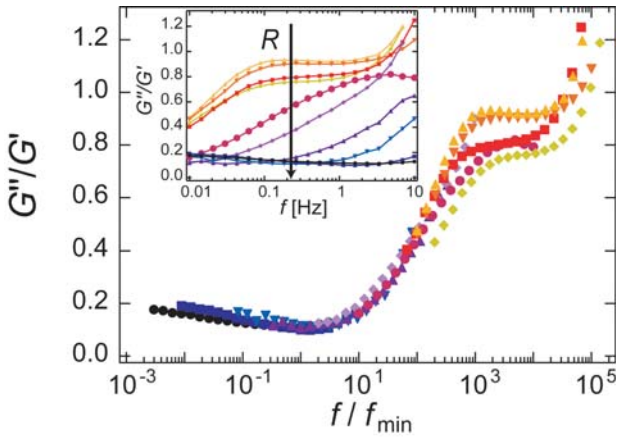

Figure 4.18: Generalized loss factor curve for actin/fascin networks. The unshifted curves are depicted in the inset, the symbols and colors used correspond to those in Fig. 4.17A and B.

For a rescaled frequency range of $10^3 - 10^4$ the loss factor master curve exhibits a plateau. In this regime the viscoelastic moduli show the same frequency dependence and have comparable absolute values. For even higher rescaled frequencies the loss factor finally reaches values larger than 1, indicating that a crossing-over to a viscous dominated regime, $f > 1/\tau_e$, does exist but is not sufficiently accessible with macrorheological methods – not even by the application of the cross-linker concentration/time superposition. Yet, the rescaled loss factor curves unambiguously show that the $f^{0.5}$ regime observed for actin/fascin networks is indeed an analytical power law as the Kramers-Kronig relations are fulfilled implying an intermediate asymptotic regime. Possibly, the frequency behavior at intermediate times might be strongly dependent on the network architecture as a regime $\sim f^{0.75}$ has been described for actin networks in a composite phase, as obtained by the cross-linker scruin [Gardel et al. 2004b].

Thus the mesoscopic network structure does not only determine the plateau modulus but also the frequency behavior of semi-flexible polymer networks. Despite the fact that for composite networks a master curve description was reported [Gardel et al. 2004b], this is not a generic feature for cross-linked actin networks. Isotropically cross-linked actin/HMM networks do not allow a master curve construction based on a concentration/time superposition. There, the network elasticity is enhanced by simply decreasing the cross-linker distance l_c – without any overall change in the network structure [Tharmann et al. 2007]. Thus, structural self-similarity does not apply for isotropically cross-linked networks.

Matters are complicated for heterogeneous actin/α-actinin networks. The bundle clusters formed by α-actinin exhibit a fractal dimension (compare section 3.1.1); the fractal nature of these clusters is retrievable in the whole network on length

scales up to 150 μm. Therefore, structural self-similarity should be applicable for actin/α-actinin networks – at least in the clustered bundle phase. A clear minimum in the viscous dissipation $G''(f)$ cannot be observed in the distinct frequency spectra of actin/α-actinin networks. Thus, a best-match overlay of these frequency spectra is used to decide whether or not the actin/α-actinin system can be described with a master curve. Accordingly, shifting parameters a, b and c are determined from this best-match overlay which indeed gives a reasonable master curve $a \cdot G'(c \cdot f)$, $b \cdot G''(c \cdot f)$ (Fig. 4.19). The virtually same shifting procedure can be applied to data sets at high and low temperature (see inset of Fig. 4.19) resulting in two distinct master curves that appear to be effectively shifted against each other. This can be rationalized by the fact that a change in temperature alters the effective cross-linker concentration (see section 3.1.1) which again underlines the principle of cross-linker-concentration/time superposition.

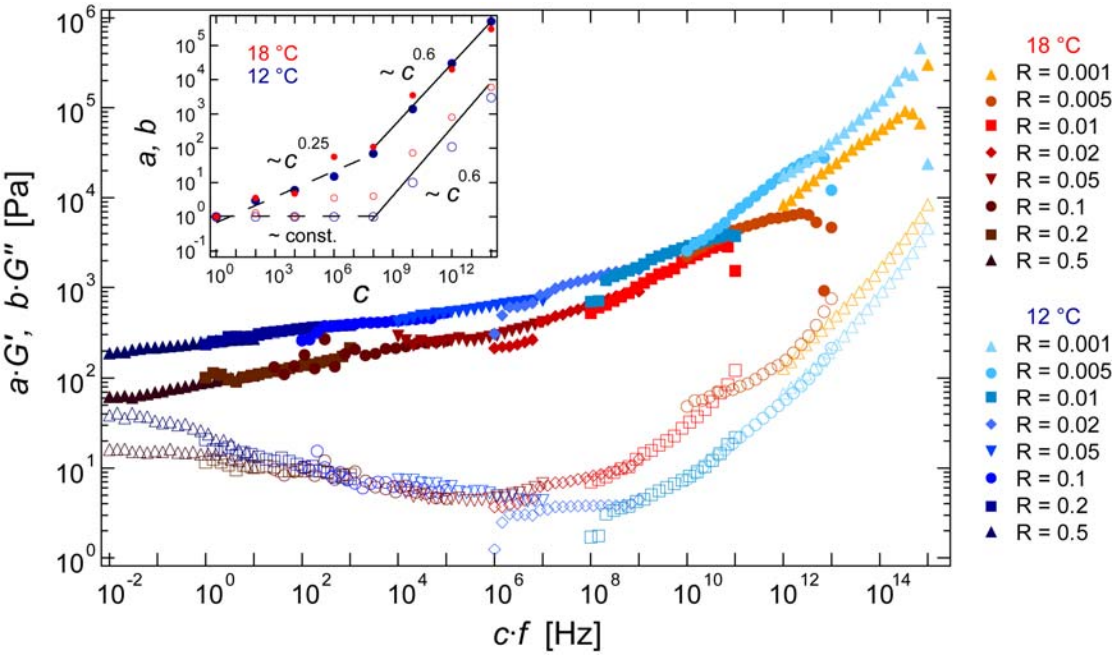

Figure 4.19: Master curves for actin/α-actinin networks at two distinct temperatures (18 °C: red color scheme, 12 °C: blue color scheme). Inset: the shifting parameters a (closed symbols) and b (open symbols) follow different scaling relations below and above $R = 0.02$ which roughly corresponds to the onset of bundle formation.

The mathematical relation between the shifting parameters is not linear as observed for the self-similar actin/fascin system. Moreover, in the composite and clustered bundle phase the loss moduli of actin/α-actinin networks can be directly shifted on top of each other without adjusting the absolute values at all (i.e. $b \approx$ const. in these regimes). Although a reasonable overlay of the actin/α-actinin

frequency spectra can be created, a mathematical consistent master curve construction [XVI] is only possible if one intrinsic parameter determines structure *and* mechanical behavior at the same time. This is the case for actin/fascin networks in the bundle phase: Increasing the fascin concentration R "magnifies" all system properties including the mechanical parameters of its constituting bundles. This creates a self-similar network that can be described by the principle of cross-linker concentration/time superposition introduced here. The resulting master curve description broadens the measurable frequency window over 8 orders of magnitude simply by altering the typical network length scales tuning R – fully equivalent to the principle of temperature/time superposition that is known for classical flexible polymer networks [Rubinstein and Colby 2003].

[XVI] i.e. a rescaling process with a linear relation between the scaling parameters

4.3 Retarded equilibration in bundle networks

In the previous sections of this thesis it was shown that unbinding of transiently cross-linking molecules dictates the non-linear network response as well as the linear frequency behavior at intermediate time scales. In the following section it is demonstrated that on very long time scales, i.e. in the course of several hours, the non-static nature of actin/ABP bonds can also lead to spatial cross-linker reorganizations throughout the whole network. In section 4.3.1 this is discussed for actin/fascin bundle networks where the influence of cross-link unbinding events can also be identified in the autocorrelation function obtained from dynamic light scattering. The temporal evolution of actin/fascin bundle networks indicate that meta-stable but well-defined initial states exist which have not reached full equilibrium. A similar retarded equilibration of a bundle network is described in section 4.3.2. There, it is demonstrated that kinetic arrest in localized aggregates of bundles can lead to a meta-stable network configuration which slowly equilibrates over time. These findings demonstrate, that the commonly accepted belief of fully equilibrated *in vitro* network formations has to be questioned. Finally, the complex dynamics observed for bundled actin networks is compared to phenomenological descriptions in the conceptional framework of soft glassy materials.

4.3.1 Actin/fascin networks: Aging and cross-linker unbinding

When the linear response of an actin/fascin bundle network ($R = 0.1$) is recorded over several hours, a slight but significant and continuous drop of both viscoelastic moduli is observed (Fig. 4.20A). Concomitant with the change in the absolute values of the moduli, the shape of the loss modulus is altered, too. While at age $t = 0\,\mathrm{h}$ a clear minimum in the viscous dissipation can be observed this feature shifts to lower frequencies and becomes less pronounced with increasing sample age. The time evolution of the plateau elasticity $G_0 = G'(0.01)\,\mathrm{Hz}$ is depicted in the inset of Fig. 4.20B and exhibits a roughly inverse sigmoidal shape. This suggests that after an initial meta-stable state reorganizations in the network configuration start to set in after $\approx$ 2 hours [XVII] but seem to fade out after $\approx$ 8 hours.

$G''(f)$ is significantly flattening with increasing sample age and the shape of the loss factor curve changes in a non-conformal way (see Fig. 4.20B): The uprise in the loss factor at low frequencies vanishes over time. Therefore, rescaling of neither the frequency spectra nor of the loss factor curves is possible with respect to sample age. In comparison to the master curve discussed in section 4.2, this suggests that the observed change in the viscoelastic response cannot be attributed

[XVII] This and all following times are given with respect to the time point of full polymerization.

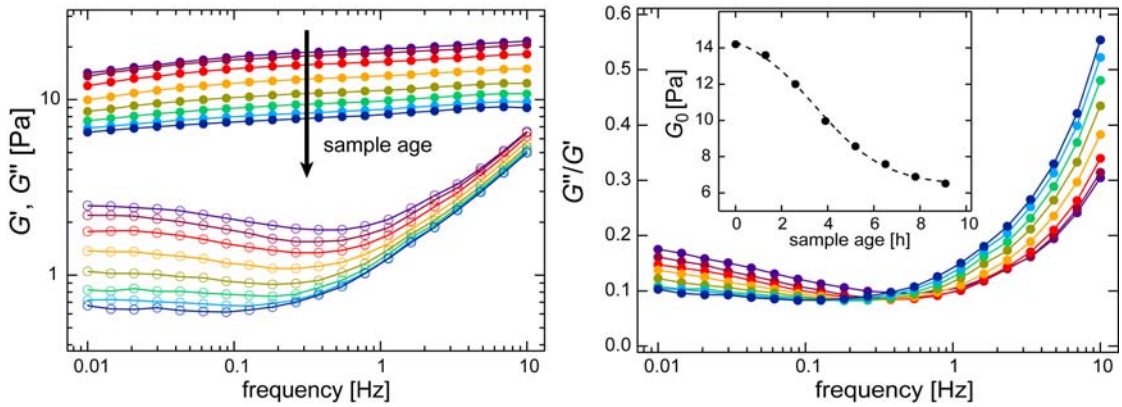

Figure 4.20: Temporal evolution of the frequency response of an actin/fascin bundle network ($c_a = 9.5\,\mu$M, $R = 0.1$). (A) Closed symbols denote $G'(f)$, open symbols denote $G''(f)$. The color scheme encodes the sample age ranging from 0 h (purple) to 9.1 h (blue) after polymerization has been terminated. (B) Loss factor representation of the frequency spectra depicted in (A): The uprise at low frequencies vanishes over time. The inset shows the plateau elasticity G_0 as a function of sample age, the dashed line represents a sigmoidal fit to the data.

to a significant overall change in the network structure. This is confirmed by phase contrast microscopy images (see appendix) and SAXS experiments [Semmrich] which both demonstrate that the meshsize of the network and the bundle thicknesses remain unaffected even though the viscoelastic network response evolves with time.

Recall, that actin/fascin bundle networks exhibit point-to-point cross-links between distinct bundles, which are also formed by fascin. Therefore, in analogy to transiently cross-linked HMM-networks the observed flattening of $G''(f)$ (which is accompanied by a shift in the minimum to smaller frequencies) can be a signature of either

1. decreasing cross-linking degree or

2. decreasing amount of released energy per cross-linker unbinding event

with increasing sample age. On large time scales the complete dissociation of cross-linking fascin molecules [XVIII] from the bundle cross-link points becomes feasible. Recent single bundle experiments reveal that fascin bundles are not saturated with fascin molecules for fascin concentrations $R \leq 0.2$ [Claessens et al. 2008]. This suggests that an uptake of unbound fascin molecules into unsaturated bundles

[XVIII] i.e. simultaneous detachment of both binding sites from the two cross-linked bundles

might in principle be possible. This uptake process will be opposed by an energy barrier much larger than k_BT requiring long times – which would be consistent with the observed meta-stable configuration of actin/fascin networks. As soon as all cross-link points have been depleted, this reorganization process should indeed come to an end. However, actin/fascin networks with saturated bundles ($R = 0.5$) also show a temporal evolution of the network elasticity towards smaller G_0 values similar to the $R = 0.1$ network depicted in Fig. 4.20 which seems to contradict the hypothesis of decreasing cross-link density.

Interestingly, the temporal evolution of actin/fascin bundle networks from a meta-stable initial state to a configuration with lower network elasticity can be accelerated if the bundle network is exposed to high deformations as depicted in Fig. 4.21: The decrease in the viscoelastic moduli in Fig. 4.20A is significantly enhanced. This indicates that the proposed reorganization is facilitated by external forces and demonstrates that cross-link unbinding plays a central role in the context of this retarded equilibration process.

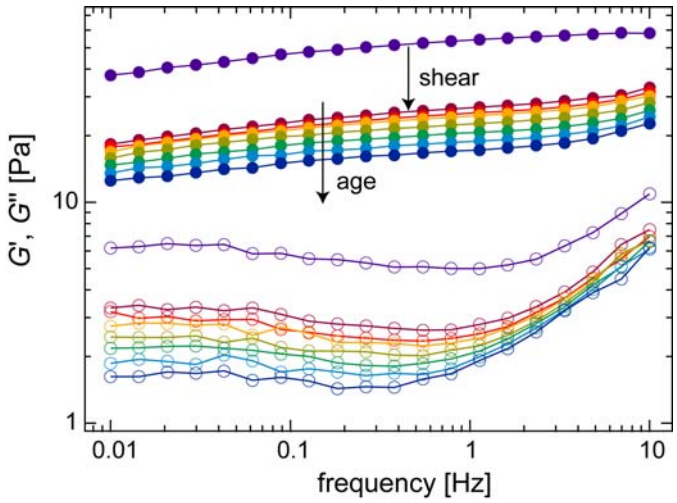

Figure 4.21: The passive retarded equilibration of an actin/fascin bundle network ($c_a = 9.5\ \mu$M, $R = 0.1$) can be accelerated by mechanical load: After the meta-stable state is reached, the network is sheared beyond the critical point (i.e. $\gamma_c < \gamma < \gamma_{max}$) and the subsequent temporal evolution is recorded. Closed symbols denote $G'(f)$, open symbols denote $G''(f)$. The color scheme encodes the sample age ranging from 0 h (purple) to 9.1 h (blue) after polymerization has been terminated.

To further analyze the complex "ageing" behavior of actin/fascin bundle networks, the network dynamics should be investigated more in detail. Dynamic light scattering (DLS) is an ideal tool to determine the dynamics of a colloidal sample within a broad frequency range. DLS reports a qualitative similar ageing behavior of actin/fascin bundle networks as observed in macrorheology. For

a scattering vector of 90 ° DLS probes the correlation of local sample fluctuations on a length scale of $\approx$ 50 nm. As depicted in Fig. 4.22, the correlation function for actin/fascin networks in the bundle phase, $c_{\mathrm{I}}(t,\tau)$ [XIX], exhibits a pronounced plateau at intermediate times ($\tau = 1 - 10\,\mathrm{s}$) [XX]. This plateau extends to higher times with increasing sample age t and is followed by a steep decrease to zero.

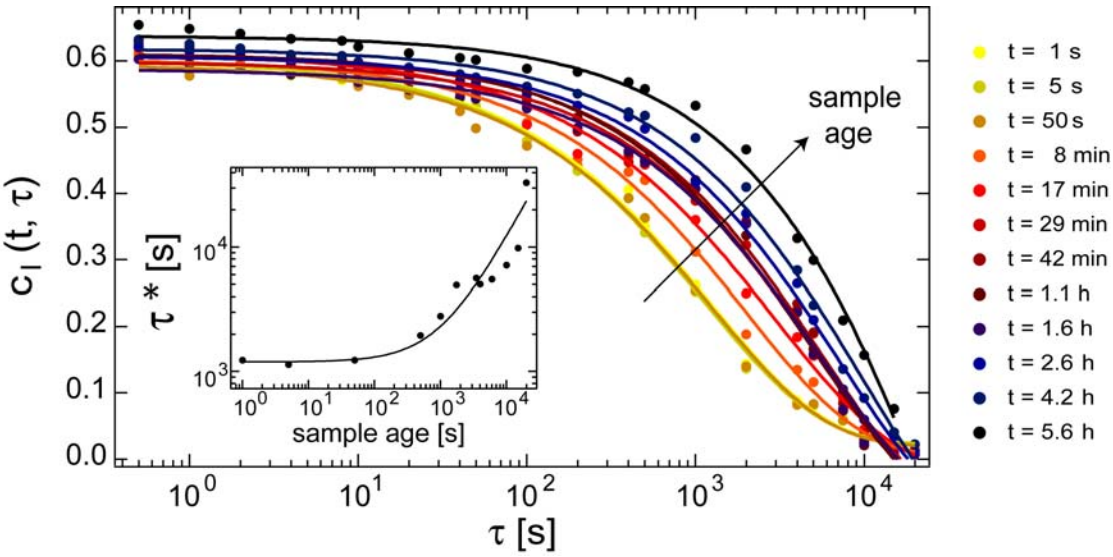

Figure 4.22: Temporal evolution of the network dynamics for an actin/fascin bundle network ($c_{\mathrm{a}} = 9.5\,\mu\mathrm{M}$, $R = 0.1$). The correlation function $c_{\mathrm{I}}(t,\tau)$ is depicted as a function of correlation time τ. The color scheme encodes the sample age t. The inset shows the increase in the decay time τ^* with respect to sample age which roughly follows a linear relation.

To quantify the time scale τ^* of the underlying decorrelation process a stretched exponential

$$c_{\mathrm{I}}(t,\tau) \sim \exp\left(-\tau/\tau^*\right)^{\alpha} \tag{4.8}$$

is fitted to the correlation function. The data set depicted in Fig. 4.22 can be globally fitted with a fixed stretch exponent $\alpha = 0.63$; only the characteristic decay time τ^* is shifted to higher values with increasing sample age, the time dependence of τ^* roughly follows a linear relation: $\tau^*(t) = \tau_0^* + a \cdot t$. Despite this well-defined behavior, the molecular origin of the observed slow-down in the network dynamics remains elusive as the time scale of the decorrelation process, $\tau^* \approx 10^3 - 10^4\,\mathrm{s}$ is considerably larger than the lifetime of a single actin/fascin bond ($\tau_{\mathrm{fascin}} = 1/k_{\mathrm{off}}^{\mathrm{fascin}} \approx 8\,\mathrm{s}$; compare section 4.1.4).

[XIX] see section 2.3.4 for details

[XX] corresponding to the frequency regime of the elastic plateau in the viscoelastic frequency spectrum

Yet, the rheological results discussed before imply that unbinding of cross-linking fascin molecules has to play an important role for the observed "ageing" of actin/fascin bundle networks. Thermal unbinding events of cross-linking fascin molecules should in principle also be detectable in the correlation function obtained from DLS. In the following, the correlation function is analyzed at a given correlation time $\tau = \text{const}$ as a function of sample age t. [XXI] Due to thermal fluctuations of actin/fascin bundles, the correlation function is subjugated to thermal noise as depicted in Fig. 4.23A. While purely thermal noise follows a Gaussian distribution, unbinding events should systematically lead to lower levels of correlation. Indeed, exactly such a behavior is observed if distinct time intervals of the correlation function are statistically analyzed (Fig. 4.23B-D). The asymmetry in the fluctuation spectrum becomes less pronounced with sample age which would be consistent with both, a decreasing frequency or impact of unbinding events.

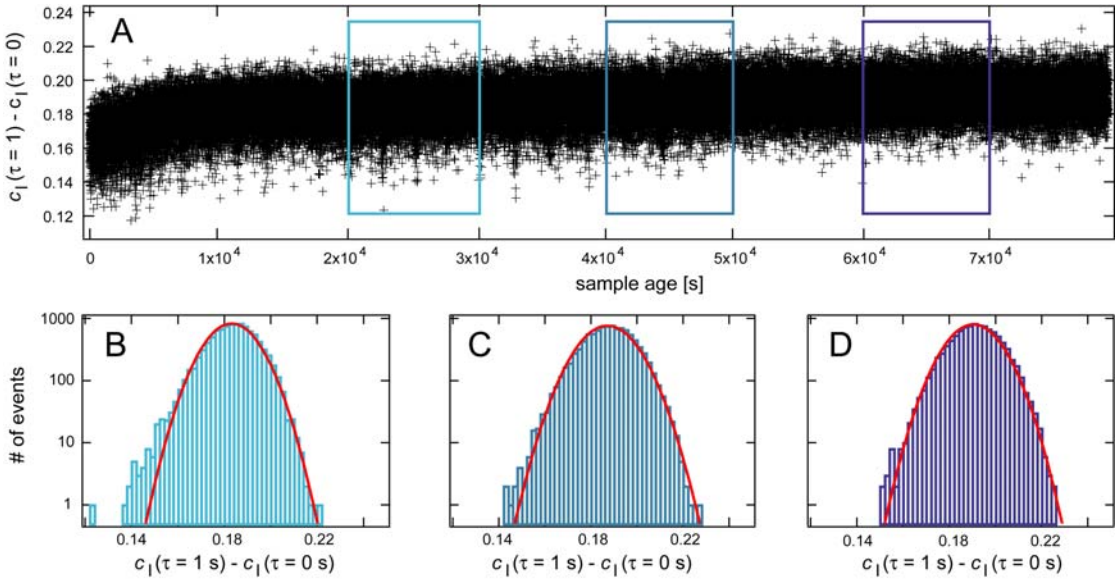

Figure 4.23: (A) Corrected correlation function for an actin/fascin network in the bundle phase ($c_a = 9.5\,\mu$M, $R = 0.1$) as a function of sample age. The thermal fluctuations are statistically analyzed for three different time intervals (B - D). Gaussian functions (red lines) are fitted to the distributions to determine their asymmetry.

In conclusion, thermal cross-linker unbinding can also be detected in the correlation function obtained from DLS, their occurrence – or at least their impact – is fading over time. This correlates well with the macrorheological behavior: the flattening in the loss modulus as well as the decrease in the plateau elasticity is

[XXI] To correct for the "blurriness" of the speckle pattern, the data is normalized by the autocorrelation function $c_I(\tau = 0)$.

consistent with a decreasing impact of cross-linker unbinding events. This decreasing impact may result from a decreasing cross-link density with increasing sample age. However, the macrorheologial observations would also be consistent with the DLS data if the inital network configuration of actin/fascin bundle networks would bear low levels of internal stress as e. g. observed for bundled actin/filamin networks [SCHMOLLER et al. 2008a]. Then, thermal cross-linker unbinding events can locally release this stress and drive the network towards a fully equilibrated state. As soon as such thermal cross-linker unbinding events have released all internal stress between the bundles, the observed ageing process should fade out as observed. A final decision whether an overall decrease in the cross-linker density or a local release of internal stress is responsible for the complex retarded equilibration of actin/fascin bundle networks is not possible on the basis of the current experimental information. Yet, the results presented so far clearly demonstrate that *in vitro* reconstituted actin networks do not necessarily have to have reached their final equilibrium configuration right after the polymerization process.

4.3.2 Actin/α-actinin networks: Kinetic trapping and thermal curing

In the previous section it was demonstrated that the viscoelastic response of actin/fascin networks in the bundle phase exhibits a temporal evolution from a meta-stable initial state to a significantly different final state. This ageing process is a good indication that the initial network configuration is not fully equilibrated – although the network structure of actin/fascin bundle networks is very homogeneous and does not undergo major rearrangements in the bundle distribution over time. For actin/α-actinin networks drastic inhomogeneities in the network microstructure occur at high R (section 3.1.1) where a pure bundle phase is observed. Pronounced mesoscopic heterogeneities such as bundle clustering are neither reported nor expected for fully equilibrated actin networks which suggests that also actin/α-actinin networks in the bundle phase may not have reached full equilibrium right after polymerization.

Interestingly, the structural patterns formed, i.e. the occurrence of clusters and their shape, and the concomitant mechanical properties are highly reproducible even in this strongly heterogeneous phase of actin/α-actinin networks at high R. Yet, the viscoelastic response of a bundle cluster network critically depends on the initial conditions at which the network is formed (Fig. 4.24A and B): If an α-actinin network ($R = 0.5$) is polymerized at low temperature only a moderately larger elasticity ($G_0^{\text{initial}}(12\,^\circ\text{C}) \approx 35\,\text{Pa}$ [XXII]) is observed compared to polymerization at high temperature ($G_0^{\text{initial}}(21\,^\circ\text{C}) \approx 20\,\text{Pa}$). However, if the same 12 °C network

[XXII] For actin/α-actinin networks $G_0 = G'(0.01\,\text{Hz})$ is used.

is treated by an intermediate heating step to 21 °C a significantly higher plateau modulus, $G_0^{\text{final}}(12\,°\text{C}) \approx 200$ Pa, is obtained when the network is brought back to its initial temperature. The same final network elasticity $G_0^{\text{final}}(12\,°\text{C})$ is reached if the sample is polymerized at the high temperature and subsequently cooled to 12 °C. This indicates that the polymerization at 12 °C results in a kinetically trapped structure, which can be cured by temporarily lowering the binding affinity of the cross-linking molecules. This is achieved by the transient heating step and allows for a faster spatial equilibration of the cross-linking molecules.

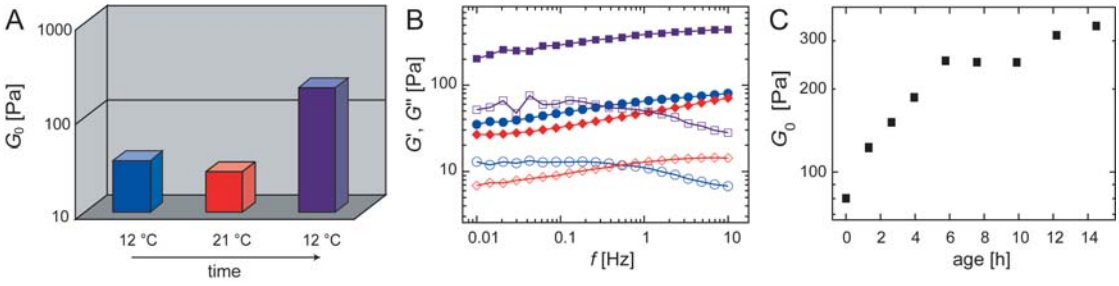

Figure 4.24: An actin/α-actinin bundle cluster network ($c_a = 9.5\,\mu$M, $R = 0.5$) is investigated: (A) Plateau modulus G_0 at different temperatures: After polymerization at 12 °C (blue) a heating step up to 21 °C (red) followed by re-cooling to 12 °C (purple) was applied. (B) The frequency spectra corresponding to the plateau moduli shown in (A) are compared directly after polymerization at 12 °C (blue circles), after heating to 21 °C (red diamonds) and after re-cooling to 12 °C (purple squares). Closed symbols denote G', open symbols denote G''. (C) Retarded temporal equilibration at 12 °C: The plateau modulus G_0 is shown as a function of the sample age.

Consistently, a very slow increase over $\approx$ 15 h to approximately the same high elastic modulus $G_0^{\text{final}}(12\,°\text{C}) \approx 250$ Pa is observed for samples that have been polymerized at 12 °C (Fig. 4.24C). This phenomenon is not limited to an initial temperature of 12 °C – the network exhibits an identical behavior at higher temperatures (see appendix). The presented data show that a well-defined final state of the system exists. This final state is determined by the effective cross-linker concentration – which in turn is set by the temperature-dependent binding affinity of the cross-linking molecule. In all cases, the starting conditions and the subsequent sample treatment dictate how fast this final state is reached.

In section 3.1.1 it was shown that the bundle clusters formed exhibit fractal character. Their fractal dimension of $d \approx 1.8$ indicates that the meta-stable bundle cluster phase is the result of kinetic aggregation and growth effects [Meakin 1983, Weitz and Oliveria 1984]. Still, a quantitative modelling of the complex kinetics driving the formation of the network will be necessary: The polymerization and treadmilling of the filaments and the formation of cross-links and bundles occur simultaneously. In addition, the binding of the cross-linking molecules is

dynamic with a well-defined off-rate, which – to a certain extent – should also allow for disassembly. Yet, the clusters themselves are stable and unaffected by the temperature sweeps as confirmed by confocal microscopy (see appendix). This either indicates that the bundle clusters represent an equilibrium structure - which seems unlikely - or that their kinetic arrest is too strong to be overcome by the temperature circle.

For the following discussion it is crucial to recall that two aspects of the network microstructure dictate the mechanical response of actin bundle networks: the degree of bundling *and* the degree of cross-linking (compare section 3.3). The typical single filament behavior $\sim f^{0.75}$ observed for actin solutions or actin/HMM networks at high frequencies cannot be observed in the frequency spectrum of actin/α-actinin networks in the bundle cluster phase [XXIII] – underlining that in these cluster networks all actin filaments are organized into bundles.

Interestingly, the thermal curing as well as the retarded temporal equilibration of the system both result in a pronounced change in the viscoelastic spectrum. The frequency spectra of the two 12 °C networks in Fig. 4.24B both exhibit a maximum in the loss modulus at low frequencies. Increasing viscous dissipation at low frequencies is a signature for a transiently cross-linked network, the position of this "unbinding peak" is given by the cross-linker off-rate while its height is set by the cross-link density (compare section 4.1.2). Unlike the data obtained at 12 °C, the spectrum taken at 21 °C does not show such a low-frequency peak in the viscous dissipation. It rather resembles the featureless shape of frequency spectra obtained for bundled filamin networks [Schmoller et al. 2008b], which do not possess point-like cross-links between the bundles. This suggests that at 21 °C the network is not effectively cross-linked [XXIV] while at 12 °C cross-links between the bundles are formed.

Moreover, after heating and subsequent cooling both components of the viscoelastic frequency spectrum are shifted to higher absolute values while retaining their overall shape. In other words, the *degree* of cross-linking is significantly enhanced by the transient heating step. This increase of the cross-link degree accounts for both the mere shift of the frequency spectra and the increased plateau elasticity [XXV]: The applied temperature cycle (12 °C → 21 °C → 12 °C) leads to an increased interconnectivity between the bundles. When their affinity is transiently lowered during the temperature sweep, α-actinin molecules that have been trapped in the clustered bundles during the polymerization at 12 °C might be able to escape and can now form mechanically more effective cross-links outside the clusters.

[XXIII] At lower α-actinin concentrations this single filament regime can clearly be identified (compare Fig. 4.19)

[XXIV] The shape of the frequency spectrum is indeed similar to those of composite networks that are formed at intermediate R, where a low local elasticity was observed (compare section 3.2.1).

[XXV] compare isotropically cross-linked actin/HMM networks as discussed in section 4.1.2

Simulations (compare section 3.2.2) show that the mechanical properties of cluster networks are highly sensitive on the interconnnectivity, i.e. the cross-link density between single bundles and bundle clusters (Fig. 4.25A). This demonstrates that the number of "equillibrated" α-actinin molecules does not have to be very large to account for the observed effect – is consistent with the observation that the large bundle clusters are preserved after the temperature cycle.

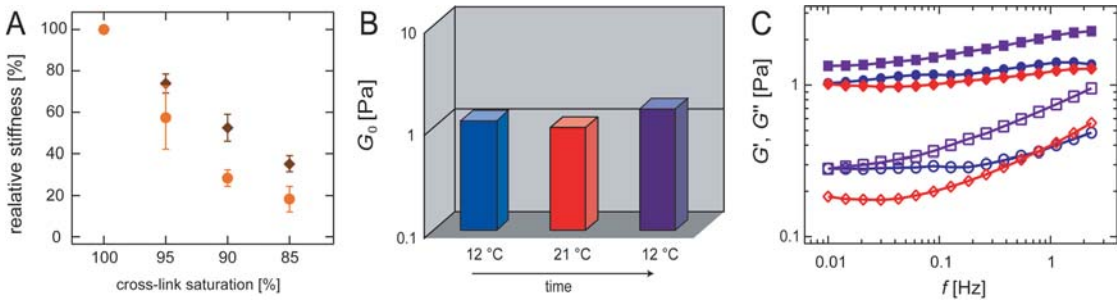

Figure 4.25: (A) Finite element simulations of cross-linked bundle networks with decreasing cross-link density: Circles denote networks with a high degree of heterogeneity (30 % of the material is redistributed into one central cluster), diamonds denote homogeneous networks. (B) Plateau modulus G_0 of a composite α-actinin bundle network ($c_a = 9.5\,\mu$M, $R = 0.02$) at different temperatures. After polymerization at 12 °C (blue) a heating to 21 °C (red) followed by re-cooling to 12 °C (purple) was applied. (C) Frequency spectra of the $R = 0.02$ network shown in (B) directly after polymerization at 12 °C (blue circles), after heating to 21 °C (red diamonds) and after re-cooling to 12 °C (purple squares). Closed symbols denote G', open symbols denote G''.

In contrast to this third cross-linker concentration regime of cross-linked actin/α-actinin networks ($R > R^{\#}$, compare section 3.1.1) where kinetic effects play an important role, networks without clusters $R < R^{\#}$ are virtually unaffected by the starting conditions (Fig. 4.25B and C) which indicates their thermally well-equilibrated nature. This agrees well with the observation that actin/α-actinin networks in the composite phase are – if at all – only very sparsely cross-linked as also indicated by the low local network elasticity (compare section 3.2.1). Interestingly, isotropically cross-linked actin/HMM networks do not exhibit ageing or temperature hysteresis phenomena, either. In comparison to the retared equilibration of actin/fascin networks in the bundle phase these findings suggest that the formation of bundles, i.e. an alternative configuration for the cross-linking ABPs besides the cross-link points, is responsible for the observed complex kinetic trapping and ageing processes. The mechanical behavior of such networks sensitively depends on the transient nature and in particular on the binding affinity of the cross-linking molecule. In combination with kinetic trapping effects, this gives rise to a delicate temperature memory of the network elasticity and retarded temporal

equilibration.

4.3.3 Complex dynamics in actin networks vs soft glassy rheology

Not only reconstituted actin bundle networks exhibit complex dynamics at various time scales. Living cells are an outstanding example of biological and physical complexity; therefore, it is even more astonishing that the frequency response of whole cells is rather simple – at least at a first glimpse. Due to the featureless shape of both viscoelastic moduli [Fabry et al. 2001, Fabry et al. 2003] the viscoelastic response of living cells is often described by a simple power law behavior representing a broad distribution of relaxation times. In a recent review [Lenormand and Fredberg 2006] it is stated that *"no distinct internal time scale can typify protein–protein interactions within the living cytoskeleton, and the response is scale-free."*

As a consequence, a phenomenological model called "soft glassy rheology" (SGR) has been introduced [Sollich 1998] and was proposed to rationalize the featureless viscoelastic spectrum of living cells [Fabry and Fredberg 2003, Bursac et al. 2005]. The basic idea is that the viscoelastic response of the living cytoskeleton is determined by an energy landscape that is extremely rough and exhibits plenty of local minima. Fast and frequent hopping processes between these distinct minima are thought to give rise to a frequency response that follows a power-law $G'(f) \sim G''(f) \sim f^x$ over a broad range of frequencies. The power law exponent x is correlated with a so-called "noise temperature" Θ via $\Theta = 1 + x$. Typical values for Θ lie within a quite narrow range between 1.1 and 1.4 – depending on the cell type and/or stiffness; exponents $x \approx 1$ are supposed to indicate that the glass transition is approached.

As depicted in Fig. 4.26A, the frequency dependent elastic response of actin/fascin networks can roughly be approximated by a power law. The resulting noise temperatures Θ are depicted in Fig. 4.26B as a function of the relative fascin concentration, R. At high R, i.e. in the bundle phase, the low value of $\Theta \approx 1.1$ would – in the context of SGR – indicate proximity to the glass transition ("frozen" state). In contrast, at low R corresponding to the weakly cross-liked single filament phase the system would be considered to be in the "molten" state and $\Theta \approx 1.4$. Note, that the full range of Θ-values that is reported for cells can be reproduced with only one cross-linking molecule *in vitro*.

Although the simplicity of such a description is appealing, it is questionable what (if anything) can be learned from such a purely phenomenlogical approach. If the right presentation is chosen many similarities to colloidal and glassy materials can be constructed. In Fig. 4.26 such a questionable presentation is chosen on

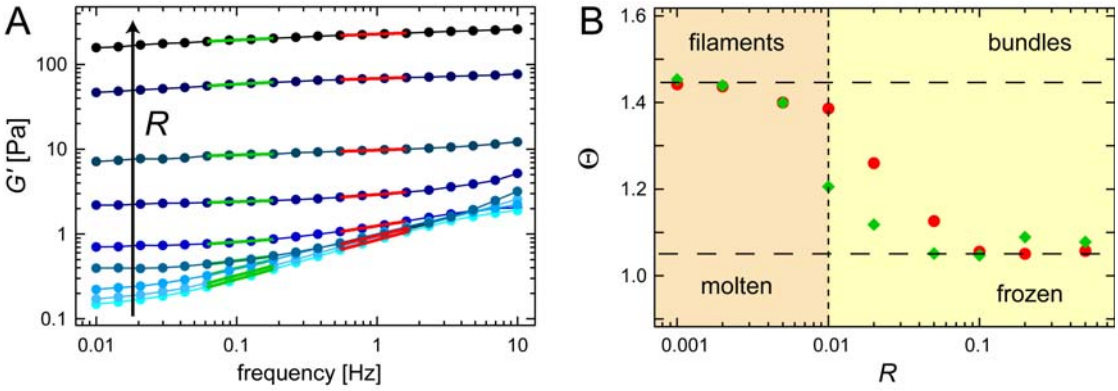

Figure 4.26: (A) The elastic frequency response of an actin/fascin bundle network can be approximated by a power law. The resulting noise temperature values Θ are depicted in (B) and exhibit a transition from a "molten" regime at low R to a "frozen" regime close to the glass transition at high R. The transition point depends on the exact frequency position that is used for the evaluation as indicated by the green (0.1 Hz) and red (1 Hz) lines and symbols. The horizontal lines indicate the asymptotic regimes, the vertical line represents the bundling transition in actin/fascin networks.

purpose to illustrate the ambiguity of the SGR description. As explained in detail in this thesis, the mechanical properties of actin/fascin networks can be understood in terms of a microscopic single filament picture; a qualitative description by the relatively vague SGR is dispensible. A detailed molecular description of the frequency response of cross-linked and bundled actin networks might be difficult to develop, yet it this is the sole promising approach for understanding the complex viscoelastic behavior of cytoskeletal networks. A recently suggested extension of the classical worm-like chain description of semi-flexible polymers [Kroy and Glaser 2007] might indeed be helpful for a qualitative understanding of entangled actin solutions [Semmrich et al. 2007] where well-defined characteristic time scales of the system are elusive. For transiently cross-linked actin networks, however, the cross-linker off-rate is a well-defined intrinsic time scale which largely dictates the viscoelastic network response and therefore has to be thorougly considered in modelling approaches.

In the living cell many cross-linking molecules with slightly different biochemical properties are used simultaneously. As a consequence, the broad distribution of relaxation times observed in cells can already result from small differences in the off-rates of different cross-linking proteins. A featureless frequency spectrum in both viscoelastic moduli can e. g. be generated by simply mixing the two bundling ABPs fascin and filamin in equal concentrations [Schmoller et al. 2008b]. This way, even the power law exponent x and with this the noise temperature Θ can be adjusted (Fig. 4.27).

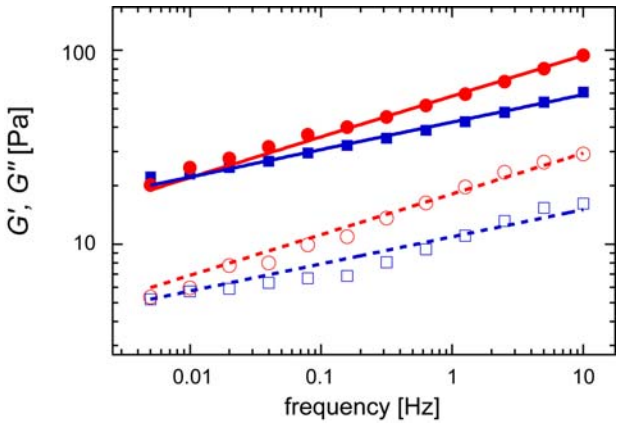

Figure 4.27: Frequency response of composite actin/fascin/filamin networks. Closed symbols denote $G'(f)$, open symbols denote $G''(f)$. Each frequency spectrum is fitted with a power law which results in $\Theta = 1.21$ for $R_{\text{fascin}} = R_{\text{filamin}} = 0.05$ (red symbols and lines) and $\Theta = 1.14$ for $R_{\text{fascin}} = 0.05$, $R_{\text{filamin}} = 0.2$ (blue symbols and lines).

In addition, aggregation phenomena can result in kinetic arrest of metastable structures and local stress release gives rise to slow retarded equilibration processes as described in section 4.3.2 and 4.3.1, respectively. Living cells achieve a rearrangement of the cytoskeleton with the help of actin depolymerization agents and molecular motors, which complicates the picture. In this context – from a more philosophical point of view – the SGR model definitely has a valid point: the energy landscape of a living cell *is* highly complicated. Yet, exactly this biological complexity calls for increasingly complex *in vitro* model systems in order to correlate the macroscopic response of living cells with microscopic events.

5 Outlook

Cells show remarkable polymorphism in the structural organization of their cytoskeleton. This polymorphism is directly related to the different specialized tasks of cytoskeletal elements and often attributed to the local activation of different actin cross-linking and/or bundling proteins (ABPs). As demonstrated in this thesis, structural polymorphism of actin networks can already be induced by a single ABP. By adjusting the relative concentration of this ABP different structural phases can be generated which in turn set the macromechanical response of the reconstituted actin network. It remains to be shown how mixtures of different ABPs affect the structural organization of actin networks. It is an interesting question if a combination of different ABPs would give rise to new structural elements that are not observed in reconstituted systems which contain only one type of ABP. In particular, the interplay of different ABPs could be synergistic, competitive or independent. For example, composite fascin/α-actinin networks are suggested to show synergistic/cooperative behavior [Tseng et al. 2005] while in fascin/filamin networks the cross-linkers contribute independently to both the network structure and mechanics [Schmoller et al. 2008b]. To this date it remains elusive whether these qualitatively different results are a consequence of the particular combination of ABPs and what could be the molecular origin of this difference. The precise type of the ABP-interplay might well depend on both the respective subclasses of the mixed ABPs and their relative concentration. It seems reasonable to assume that a combination of two (mainly) bundling ABPs exhibits a different behavior than a combination of a pure cross-linker with a bundling protein. The well-characterized actin/HMM and actin/fascin system discussed in this thesis are an excellent starting point for a detailed analysis of complex actin networks with multiple cross-linking proteins.

Besides networks with multiple cross-linkers, composite networks containing other biopolymers in addition to actin are yet to be characterized. The steric interaction of actin filaments with other biopolymers such as neurofilaments or microtubules might lead to different network formations compared to the structures that are observed if actin is polymerized alone. Reconstituted actin/MT networks have recently drawn attention in cytoskeletal research [Brangwynne et al. 2008]. However, a clean systematic investigation of the structural patterns formed in such composite networks is missing. It would definitely lift the structural characterization of reconstituted cytoskeletal networks to the next higher level of

complexity.

Despite the rich polymorphism of actin networks that can be created *in vitro*, the physical origin of the transitions between the different structural and mechanical phases is still poorly understood. In this thesis the first parameterization of the cross-link transition from a generic weakly cross-linked phase at low cross-linker concentrations to an isotropically cross-linked phase is presented and related to microscopic network parameters. It turns out, the cross-link transition occurs at a well-defined point, i.e. when the average distance between cross-linking points matches the persistence length of actin filaments. As a consequence, the local deformation mode of the network changes. While at low cross-link densities the network response is still dominated by the entropic suppression of filament fluctuations, at high cross-link densities the network elasticity is set by the mechanical stretching of single filaments. In the framework of this thesis, the bundling transition in actin/fascin networks could also be parameterized; however, a microscopic understanding of the obtained relation has still to be developed. The simultaneous variation of both important length scales, i.e. the cross-linker distance *and* the persistence length, calls for a detailed theoretical analysis of the experimental data presented in this study. Only by accounting for the subtle interplay between entropic and enthalpic contributions, the bundling transition and the concomitant change in the local deformation mode might be properly understood.

This change in the local deformation mode has been demonstrated in this thesis for the bundling transition of actin/fascin networks. Here, the high stiffness of actin/fascin bundles implicates that bending modes become energetically preferrable in comparison to stretching deformations. Concomitantly, the long and straight shape of the stiff bundles suggests that the local deformation field should acquire a strongly non-affine character. Such non-affine deformations were indeed assumed in section 3.3.2 for the theoretical modeling of the bundle network elasticity. However, a direct demonstration of such non-affine deformations in bundle networks is still missing. A shear cell experiment in combination with confocal microscopy might allow for the 3-dimensional characterization of the deformation field in bundle networks by optically following the microscopic displacement of labeled actin bundles under shear. This could help settle the ongoing discussions on the microscopic origin of the elasticity in actin networks.

Similar insights into the tunability of the local deformation field could also be gained by the systematic creation of composite networks whose constituents exhibit significantly different but well-defined persistence lengths. Such tailored composite networks with well-defined properties could be obtained by mixing two different biopolymer systems, e.g. isotropically cross-linked actin/HMM networks with different amounts of stiff microtubules (MTs). Since MTs exhibit persistence lengths that are comparable to or even larger than those of actin/fascin bundles, the dom-

inating microscopic deformation mode in a composite actin/HMM/MT network should sensitively depend on the MT content and can possibly be completely tuned from affine stretching to non-affine bending. In combination with the structural investigation of composite actin/MT networks suggested before, this might provide an even more realistic (and of course much more complex) model system for the cytoskeleton. Such a refined model system would be a valuable tool to verify or improve the conclusions drawn from reconstituted actin networks – the cytoskeleton surely is one of the most complex composite biomaterials.

The formation of composite phases might be a central strategy in cell mechanics. In this thesis it was described that embedding stiff actin bundles into soft networks of actin filaments can provide the needed mesoscopic toughness while the local network elasticity remains low. This might facilitate the intracellular transport of vesicles or organelles which is achieved by molecular motors that have to drag their cargo through the cytoskeletal meshwork. This hypothesis could be directly tested *in vitro*: Processive myosin V motors could be employed to transport "artificial cargo" such as engineered complexes of quantum dots or labelled proteins through actin networks of comparable macroscopic stiffness but different microstructure. By following the fluorescence signal of the quantum dots the transport efficiency of the myosin motors could be correlated with the local network elasticity and network mesh size giving insight into the relevance of the cellular microstructure for transport processes.

A dense meshwork of actin filaments might impede cellular trafficking. However, it is important to note that cytoskeletal networks are transiently cross-linked. Thus, local unbinding of cross-linked filaments in response to the force exerted by forward pressing motor proteins might give way to obstructed cargo. This hypothesis could be tested by comparing traficking assays as suggested above using different cross-linker molecules but similar network geometries. Then, the cross-linker off-rate will be the pivotal parameter in this experiment. Engineered mutants of actin cross-linking proteins, i.e. slight modifications in the actin binding domain of α-actinin, will extend the available toolbox and allow for an advanced modeling of cytoskeletal processes *in vitro*.

In this thesis it is shown that external load can indeed trigger forced unbinding events of transient cross-links. The transient character of cytoskeletal cross-links limits the mechanical stability of the cytoskeleton under force. There is growing evidence that forced and thermal cross-linker unbinding are the dominating processes in cytoskeletal networks both under mechanical load and in thermal equilibrium. For actin/fascin bundle networks typical Bell behavior of the rupture force is demonstrated in this thesis, similar results can be obtained using actin/HMM networks [Tharmann]. The typical rupture forces of single actin/ABP bonds are in the range of several pN. Such forces could also give rise to (partial) unfolding

of cross-linking proteins. It is still under debate whether or not (partial) unfolding of cross-linker molecules adds additional compliances to the viscoelasticity of the cytoskeleton. Although this seems more and more unlikely, it is difficult to completely rule out cross-linker unfolding in cytoskeletal networks at this point of experimental research. Stimulated by the findings on actin/fascin networks presented here, other groups have started to investigate the rupture behavior of actin networks cross-linked by other ABPs. Indeed, recent experiments on cross-linked actin/filamin networks before the bundling transition [Kasza] reproduce the Bell scaling observed in the actin/fascin system. Since filamin is a highly compliant cross-linking molecule this indicates that even for this flexible cross-linker unbinding dominates over unfolding *in vitro* and suggests that unbinding might also be the dominant process used for mechanosensing tasks *in vivo*.

Realistic 3-dimensional simulations of transiently cross-linked networks of semiflexible polymer networks might help to answer these questions, i.e. determining the local deformation field in cross-linked networks considering thermal cross-linker unbinding events and filaments of different stiffness. So far, such detailed 3-dimensional simulations of actin networks are not available. The implementation of thermal energy is a major complication but is crucial for the correct consideration of thermally activated cross-linker unbinding events. A recently started collaboration with the group of Prof. A. Wall[I] has already indicated highly promising possibilities: the experimentally determined fluctuation spectrum of a single actin filament (discretized by several Timoshenko beams using finite element methods) can be reproduced with astonishing accuracy. Based on the experimental insights into the dynamics of transiently cross-linked networks presented in this thesis a realistic representation of thermally undulating actin networks might indeed be possible in the near future. This will allow for a detailed analysis of the stretching/unfolding behavior of cross-linkers in comparison to cross-linker unbinding dynamics and the visualization of the deformation field. Such simulations will be a great complementary tool to the experimental *in vitro* approach presented here and will give quantitative insight into the physical principles in cell mechanics.

In conclusion, there are still many unsolved puzzles regarding the equilibrium properties of reconstituted cytoskeletal networks. Systematic investigations of (equilibrium) cytoskeletal networks under well-controlled conditions is mandatory to elucidate so far unconsidered physical principles that govern the structural organization and the viscoelastic response of living cells. Several other groups working on reconstituted cytoskeletal systems – and especially theorists – proclaim that equilibrium actin networks are already sufficiently understood. They suggest that experimental research should go beyond equilibrium networks and move on to investigate the viscoelastic properties of networks where molecular motors actively

[I] Lehrstuhl für numerische Mechanik, TU München

rearrange the network microstructure. However, the results presented in this thesis clearly demonstrate that the properties of equilibrated actin networks are all but completely understood. A further complication arises from the recent observation that in many cases *in vitro* reconstitutions of cytoskeletal networks do not necessarily result in fully equilibrated structures. This underlines the importance of the *bottom up* approach described here since only in well-defined model systems the observed effects can be reliably traced back to their molecular origin.

Appendix

@section 3.1.2.2: Cosedimentation assay for actin/fascin bundle networks

Co-sedimentation assays are performed to confirm the organization of actin/fascin mixtures into bundles at high fascin concentrations as observed using fluorescence microscopy. Actin/fascin samples are mixed at a distinct molar ratio of fascin to actin before initiating polymerization. G-actin polymerization is induced by adding 10-fold F-buffer followed by gentle mixing. The samples (200 μl) are polymerized for 1 h at room temperature and centrifuged with a table-top centrifuge (Beckman Coulter Microfuge 18) at 12,000 g for 15 min.

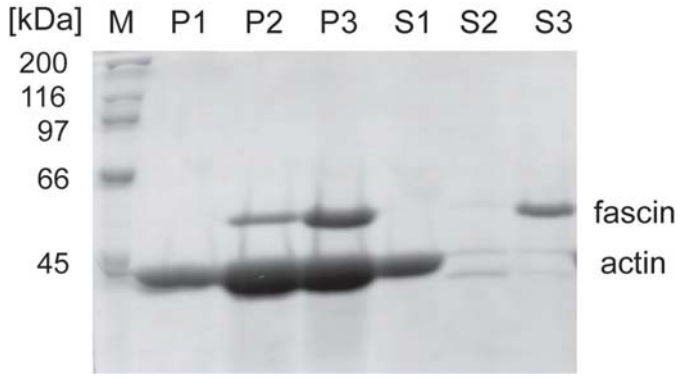

Figure 5.1: Co-sedimentation assay of actin/fascin bundle networks. The picture shows a scanned image of a SDS/polyacrylamide gel. The sample numbers, 1, 2 and 3, correspond to $R = 0$, $R = 0.1$ and $R = 0.5$ respectively at fixed $c_a = 9.5\,\mu$M. S, supernatant after centrifugation; P, pellet after centrifugation. M, marker.

After centrifugation the supernatant is separated from the pellet, the pellets are resuspended in F-buffer. Supernatants (S) and pellets (P) of all samples are analyzed by electrophoresis using a 12 % SDS/polyacrylamide gel. The gel is stained with Coomassie brilliant blue for protein band visualization. As the gel depicted in Fig. 5.1 shows, the supernatant of both bundled networks investigated ($R = 0.1$ and $R = 0.5$) does not exhibit an actin band which demonstrates that only bundles are formed at high fascin concentrations.

@section 3.3.2: Exemplaric derivation of the scaling relation for the plateau modulus of actin/fascin bundle networks

As described in section 3.3.2, by assuming non-affine deformations the linear elastic modulus is given by

$$G_0 \sim \nu k_\perp \delta_{\mathrm{na}}^2 \tag{5.1}$$

Substituting the polymer density $\nu \sim 1/\xi^2 l_\mathrm{c}$, the bending rigidity of a bundle of N intermediately coupled filaments $k_\perp \sim \frac{\kappa}{l_\mathrm{c}^3} \sim \frac{N\kappa_\mathrm{f} l_\mathrm{c}^2}{l_\mathrm{c}^3}$ [II] and non-affine deformation $\delta_{\mathrm{na}} \sim \gamma L_\mathrm{B}$ in equation (5.1) one obtains

$$G_0 \sim \frac{N}{\xi^2 l_\mathrm{c}^2} \tag{5.2}$$

The cross-linker distance is given as $l_\mathrm{c} \sim R^{-y} l_\mathrm{e}$. As a result of the intermediate coupling of the filaments in the bundle, the entanglement length is given as $l_\mathrm{e} \sim (N\kappa_\mathrm{f}\xi^4)^{1/3}$. Accordingly, equation (5.2) is modified to

$$G_0 \sim \frac{N}{\xi^2 R^{-2y} N^{2/3} \xi^{8/3}} \tag{5.3}$$

which can be simplified to

$$G_0 \sim \frac{N^{1/3} R^{2y}}{\xi^{14/3}} \tag{5.4}$$

Using $\xi \sim c_\mathrm{a}^{-1/2} R^x$ for the mesh size and $D \sim N^{1/2} \sim R^x$ for the bundle diameter equation (5.4) can be rewritten to

$$G_0 \sim R^{2x/3} R^{2y} c_\mathrm{a}^{7/3} R^{-14x/3} \tag{5.5}$$

which can be simplified to

$$G_0 \sim R^{2y-4x} c_\mathrm{a}^{7/3} \tag{5.6}$$

which corresponds to the final relation given in equation (3.5) on page 43 where $z = 2y - 4x$ and $w = 7/3$.

[II] Note, that the deformation mode length λ is set equal to l_c and the spacing of fascin molecules within the bundles is assumed to be constant.

@section 4.1.3: Apparent off-rate in a cross-linked network under prestress

In prestressed actin/HMM networks a decrease in the off-rate with respect to external prestress is observed (see Fig 4.12E in section 4.1.3). In single molecule experiments with rigor HMM, such an decrease of the cross-link off-rate in the presence of mechanical load has already been reported [Guo and Guilford 2006] – consistent with a catch-slip mechanism of the actin/HMM bond. However, a simple approximation shows that in a network of cross-linked actin filaments the network geometry gives rise to a decrease in the apparent cross-linker off-rate in the presence of mechanical load. Moreover, this decrease in the apparent cross-linker off-rate is independent of the particular binding mechanism and therefore a geometrical effect. In the following, the effective off-rate is calculated for a model system where the cross-links experience forces of constant magnitude but with random algebraic sign: $F^{\pm} = \pm F_0 \sim \pm \sigma_0$. This extremely simplified model is able to rationalize the counterintuitive dependence of the off-rate on external force – at least in a qualitative manner. The actual force distribution will be much more complex.

If the forces $F^{\pm} = \pm F_0 \sim \pm \sigma_0$ load an ensemble of N_Σ bonds, two different off-rates $k_{\text{off}}^{+} = k_{\text{off}} \cdot \exp(+F \cdot \Delta x / k_{\text{B}}T)$ and $k_{\text{off}}^{-} = k_{\text{off}} \cdot \exp(-F \cdot \Delta x / k_{\text{B}}T)$ emerge: $N_\Sigma = N^+ + N^-$. Here N^+ denotes the number of cross-links with enhanced off-rate (destabilized fraction) and N^- denotes the number of cross-links with lowered off-rate (stabilized fraction).

This defines an effective off-rate $k_{\text{off}}^{\text{eff}}$ for the whole ensemble of N_Σ cross-links:

$$k_{\text{off}}^{\text{eff}} \cdot N_\Sigma = k_{\text{off}}^{+} \cdot N^+ + k_{\text{off}}^{-} \cdot N^- \tag{5.7}$$

For constant on-rates [III], $k_{\text{on}}^{+} = k_{\text{on}}^{-}$, the two populations N^+ and N^- equilibrate according to the difference in their off-rates

$$\frac{N^+}{N^-} = \frac{k_{\text{off}}^{-}}{k_{\text{off}}^{+}} \tag{5.8}$$

Eliminating N^- in equation (5.8) results in

$$N^+ = N_\Sigma \cdot \frac{k_{\text{off}}^{-}}{k_{\text{off}}^{+} + k_{\text{off}}^{-}} \tag{5.9}$$

Together with equation (5.7) and (5.8) one obtains

$$k_{\text{off}}^{\text{eff}} = 2 \cdot \frac{k_{\text{off}}^{+} \cdot k_{\text{off}}^{-}}{k_{\text{off}}^{+} + k_{\text{off}}^{-}} \tag{5.10}$$

[III] This assumption is reasonable since during the binding process a cross-linking protein does not feel any external force acting on the actin filaments.

which results in the apparent off-rate

$$k_{\text{off}}^{\text{eff}} = 2 \cdot \frac{k_{\text{off}}^{0}}{\exp(+F \cdot \Delta x / k_{\text{B}}T) + \exp(-F \cdot \Delta x / k_{\text{B}}T)} \tag{5.11}$$

which can be rewritten to $k_{\text{off}}^{\text{eff}} = k_{\text{off}}^{0} / \cosh(F \cdot \Delta x / k_{\text{B}}T) < k_{\text{off}}^{0}$.

@section 4.1.4: Loading rate dependence of $f_{\max}$

In the shear rate experiment discussed in section 4.1.4, the force loading rate $\mathrm{d}f/\mathrm{d}t$ is proportional to $\mathrm{d}\sigma/\mathrm{d}t$ as force is proportional to stress, $f \sim \sigma$. Since the experiments were conducted using a constant shear rate $\mathrm{d}\gamma/\mathrm{d}t = \text{const}$, the linear relation $\gamma \sim t$ holds. Thus, $\mathrm{d}\sigma/\mathrm{d}t \sim \mathrm{d}\sigma/\mathrm{d}\gamma = K$. At the point of rupture the data shows that $K_{\max}$ [IV] $\sim d\gamma/dt$. A linear relation $K_{max} \sim \mathrm{d}\gamma/\mathrm{d}t$ fits the data reasonably well; only the lowest loading rate does not follow the linear relation (see Fig. 5.2). This can be physically understood as for the very low loading rate ($\mathrm{d}\gamma/\mathrm{d}t = 0.125\,\%\mathrm{s}^{-1}$) viscous flow occurs in networks where the cross-linking degree is low ($R = 0.05$). As a consequence the apparent increase in the sample stress is decreased by the viscous flow resulting in an underestimation of $K_{\max}$. Because of that, the second slowest loading rate $\mathrm{d}\gamma/\mathrm{d}t = 0.625\,\%s^{-1}$ has to be seen as a lower limit that can be used to investigate a sample with $R = 0.05$.

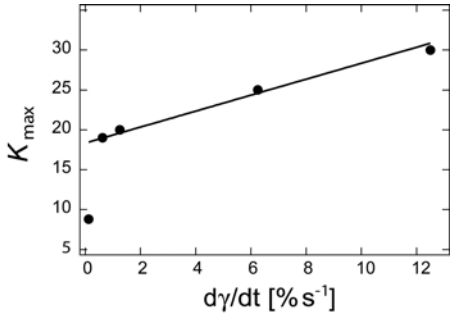

Figure 5.2: Differential modulus at the point of rupture $K_{\max} = K(\gamma_{\max})$ as a function of loading rate $\mathrm{d}\gamma/\mathrm{d}t$. A linear relation holds reasonably well.

[IV] $K_{\max} = K(\gamma_{\max})$

@section 4.3.1: Structure of actin/fascin bundle networks

Actin/fascin bundle networks do not undergo detectable alterations in the overall network structure with respect to sample age as depicted in Fig. 5.3.

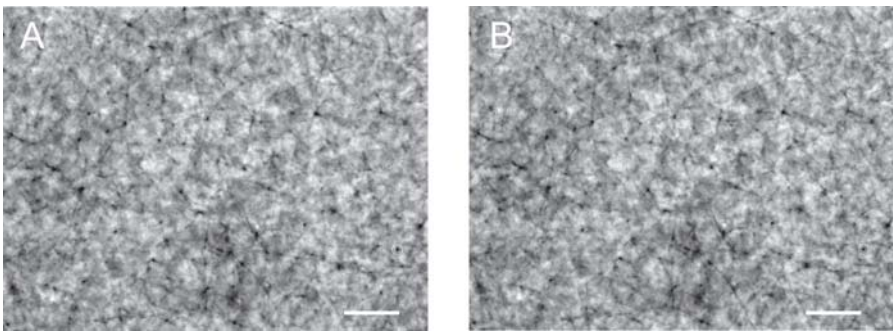

Figure 5.3: Phase contrast micrograph of an actin/fascin bundle network ($c_a = 9.5\,\mu$M, $R = 0.1$) (A) in the meta-stable state (4 h after polymerization) and (B) in the fully equilibrated state (16 h after polymerization). Scale bars represents $50\,\mu$m.

@section 4.3.2: Thermal hysteresis and thermal curing of actin/α-actinin bundle cluster networks

The hysteresis behavior and thermal curing demonstrated in section 4.3.2 for an actin/α-actinin network in the bundle cluster phase is independent from the initial temperature. The effects observed for an initial temperature of 12 °C can be reproduced for a higher initial temperature (Fig. 5.4A-D).

In order to investigate the stability of actin/α-actinin clusters towards temperature, an actin/α-actinin bundle cluster network ($c_a = 4.25\,\mu$M and $R = 0.5$) is polymerized at 10 °C and observed with confocal microscopy. A typical cluster occuring in such networks is shown in Fig. 5.5A. After 60 min of polymerization, the network is heated up to 30 °C and equilibrated for 30 minutes. To compensate for drift, a comparable confocal layer in the bundle cluster is chosen after this heating procedure. As shown in Fig. 5.5B the heterogeneous network structure is stable despite the drastic temperature change, only minimal changes in the network configuration occur. Note, that bleaching effects might have changed the absolute fluorescence intensities.

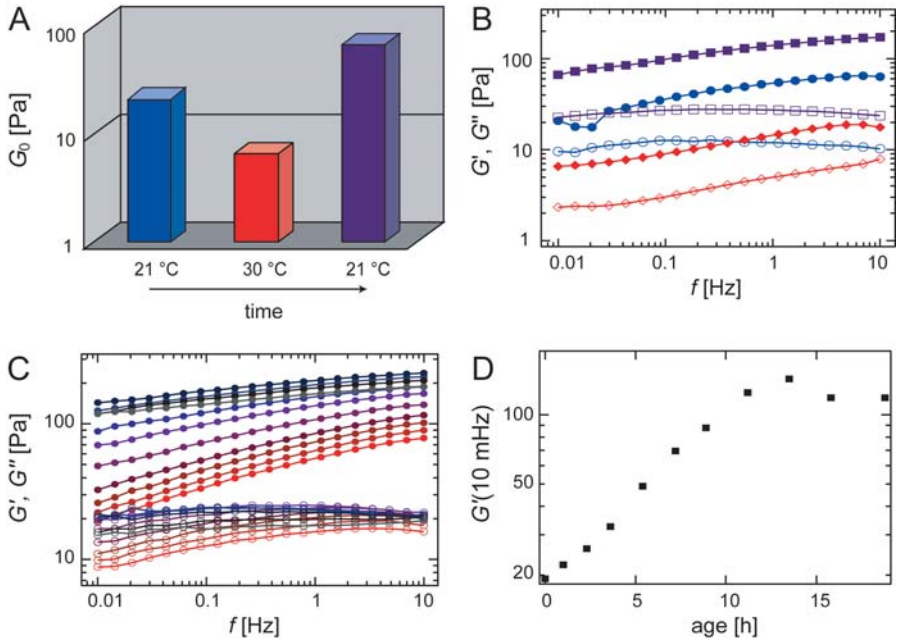

Figure 5.4: (A) Plateau modulus G_0 at different temperatures: After polymerization at 21 °C (blue) a heating step up to 30 °C (red) followed by re-cooling to 21 °C (purple) was applied. (B) The frequency spectra corresponding to the plateau moduli shown in (A) are compared directly after polymerization at 21 °C (blue circles), after heating to 30 °C (red diamonds) and after re-cooling to 21 °C (purple squares). Closed symbols denote G', open symbols denote G''. (C) Temporal equilibration at 21 °C. (D) The plateau modulus G_0 as determined from the spectra in (C) is shown as a function of the sample age.

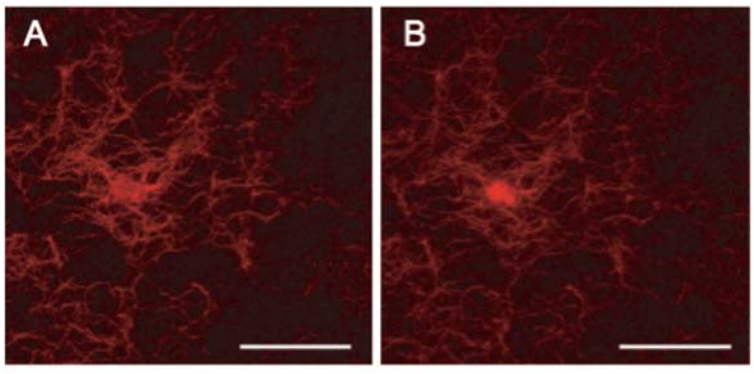

Figure 5.5: Confocal images (projections of 30 μm height) of an actin/α-actinin network bundle cluster network ($c_a = 4.25\,\mu$M and $R = 0.5$) at 10 °C (A) and 30 °C (B). Scale bars represent 50 μm.

Bibliography

[Aratyn et al. 2007] Aratyn, Y. S., T. E. Schaus, E. W. Taylor and G. G. Borisy (2007). *Intrinsic Dynamic Behavior of Fascin in Filopodia*. Mol. Biol. Cell, 18:3928–3940.

[Bartles et al. 1998] Bartles, J. R., L. Zheng, A. Li, A. Wierda and B. Chen (1998). *Small Espin: A Third Actin-bundling Protein and Potential Forked Protein Ortholog in Brush Border Microvilli*. J. Cell Biol., 143(1):107–119.

[Bathe et al. 2008] Bathe, M., C. Heussinger, M. M. A. E. Claessens, A. R. Bausch and E. Frey (2008). *Cytoskeletal Bundle Mechanics*. Biophys. J., 94(8):2955–2964.

[Bausch and Kroy 2006] Bausch, A. R. and K. Kroy (2006). *A Bottom-up Approach to Cell Mechanics*. Nature Phys., 2:231–238.

[Bell 1978] Bell, G. I. (1978). *Models for Specific Adhesion of Cells to Cells*. Science, 200 (4342):618–627.

[Bendix et al. 2008] Bendix, P.M., G. Koenderink, D. Cuvelier, Z. Dogic, N. Koeleman, W. Brieher, C. Field, L. Mahadevan and D. Weitz (2008). *A Quantitative Analysis of Contractility in Active Cytoskeletal Protein Networks*. Biophys. J., 94:3126–3136.

[Borukhov et al. 2005] Borukhov, I., R. Bruinsma, W. Gelbart and A. Liu (2005). *Structural polymorphism of the cytoskeleton: A model of linker-assisted filament aggregation*. Proc. Natl Acad. USA, 102:3673–3678.

[Brangwynne et al. 2008] Brangwynne, C. P., G. H. Koenderink, F. C. MacKintosh and D. A. Weitz (2008). *Nonequilibrium Microtubule Fluctuations in a Model Cytoskeleton*. Phys. Rev. Lett., 100:118104.

[Bursac et al. 2005] Bursac, P. Lenormand, G., B. Fabry, M. Oliver, D. A. Weitz, V. Viasnoff, J. Butler and J. Fredberg (2005). *Cytoskeletal Remodelling and Slow Dynamics in the Living Cell*. Nature Mat., 4:557.

[Claessens et al. 2006] Claessens, M. M. A. E., M. Bathe, E. Frey and A. R. Bausch (2006). *Actin-binding Proteins Sensitively Mediate F-actin Bundle Stiffness*. Nature Mat., 5:748–753.

[Claessens et al. 2008] Claessens, M. M. A. E., C. Semmrich, L. Ramos and A. R. Bausch (2008). *Helical Twist Controls the Thickness of F-actin Bundles*. Proc. Natl Aca. Sci. USA, 105:6590–6595.

[Craig et al. 1982] Craig, S. W., C. L. Lancashire and J. A. Cooper (1982). *Preparation of Smooth-muscle α-actinin*. Methods Enzymol., 85:316–321.

[De Gennes 1979] De Gennes, P.-G. (1979). *Scaling Concepts in Polymer Physics*. Cornell University Press, Ithaca.

[Dheng et al. 2006] Dheng, L., X. Trepat, J. Butler, J. Millet, K. G. Morgan, D. A. Weitz and J. Fredberg (2006). *Fast and Slow Dynamics of the Cytoskeleton*. Nature Mat., 5:636–640.

[Doi and Edwards 1986] Doi, M. and S. F. Edwards (1986). *The Theory of Polymer Dynamics*. Clarendon Press, Oxford.

[Dorsey 1940] Dorsey, N. E. (1940). *Properties of Ordinary Water-Substance*. Hafner Publishing Co., New York.

[Duri et al. 2005] Duri, A., H. Bissig, V. Trappe and L. Cipelletti (2005). *Time-resolved Correlation Measurements of Temporally Heterogeneous Dynamics*. Phys. Rev. E, 72:051401.

[Engler et al. 2006] Engler, A. J., S. Sen, H. L. Sweeney and D. D. E. (2006). *Matrix Elasticity Directs Stem Cell Lineage Specification*. Cell, 126:677–689.

[Evans 1998] Evans, E. (1998). *Energy Landscapes of Biomolecular Adhesion and Receptor Aanchoring at Interfaces Explored with Dynamic Force Spectroscopy*. Faraday Discussions, 111:1–16.

[Evans and Ritchie 1997] Evans, E. and K. Ritchie (1997). *Dynamic Strength of Molecular Adhesion Bonds*. Biophys. J., 72 (4):1541–1555.

[Fabry and Fredberg 2003] Fabry, B. and J. J. Fredberg (2003). *Remodeling of the Airway Smooth Muscle Cell: Are we Built of Glass?*. Resp. Physiol. Neurobi., 137:109–124.

[Fabry et al. 2001] Fabry, B., G. N. Maksym, J. P. Butler, M. Glogauer, D. Navajas and J. J. Fredberg (2001). *Scaling the Microrheology of Living Cells*. Phys. Rev. Lett., 87(14):148102.

[Fabry et al. 2003] Fabry, B., G. N. Maksym, J. P. Butler, M. Glogauer, D. Navajas, N. A. Taback, E. J. Millet and J. J. Fredberg (2003). *Time Scale and Other Invariants of Integrative Mechanical Behavior in Living Cells*. Phys. Rev. E, 68:041914.

[Fernandez et al. 2007] Fernandez, P., L. Heymann, A. Ott, N. Aksel and P. A. Pullarkat (2007). *Shear Rheology of a Cell Monolayer*. New Journal of Physics, 9:419.

[Ferrer et al. 2008] Ferrer, J. M., H. Lee, J. Chen, B. Pelz, F. Nakamura, R. D. Kamm and M. J. Lang (2008). *Measuring Molecular Rupture Forces Between Single Actin Filaments and Actin-binding Proteins*. Proc. Natl Acad. Sci. USA, 105:9221–9226.

[Frey 2001] Frey, E. (2001). *Physics in Cell Biology: Actin as a Model System for Polymer Physics*. Adv. in Solid State Phys., 41:345–356.

[Gardel et al. 2006] Gardel, M. L., F. Nakamura, J. H. Hartwig, J. C. Crocker, T. P. Stossel and D. A. Weitz (2006). *Prestressed F-actin Networks Cross-linked by Hinged Filamins Replicate Mechanical Properties of Cells*. Proc. Natl Acad. Sci. USA, 103:1762–1767.

[Gardel et al. 2004a] Gardel, M. L., J. H. Shin, F. C. MacKintosh, L. Mahadevan, P. Matsudaira and D. A. Weitz (2004a). *Elastic Behavior of Cross-linked and Bundled Actin Networks*. Science, 304:1301–1305.

[Gardel et al. 2004b] Gardel, M. L., J. H. Shin, F. C. MacKintosh, L. Mahadevan, P. A. Matsudaira and D. A. Weitz (2004b). *Scaling of F-Actin Network Rheology to Probe Single Filament Elasticity and Dynamics*. Phys. Rev. Lett., 93 (18):188102.

[Gisler and Weitz 1999] Gisler, T. and D. A. Weitz (1999). *Scaling of the Microrheology of Semidilute F-Actin Solutions*. Phys. Rev. Lett., 82:1606.

[Goldmann and Isenberg 1993] Goldmann, W. H. and G. Isenberg (1993). *Analysis of Filamin and α-actinin Binding to Actin by the Stopped Flow Method*. FEBS, 336(3):408–410.

[van der Gucht et al. 2003] Gucht, J. van der, N. A. M. Besseling, W. Knoben, L. Bouteiller and M. A. Cohen Stuart (2003). *Brownian Particles in Supramolecular Polymer Solutions*. Phys. Rev. E, 67:051106.

[Guo and Guilford 2006] Guo, B. and W. H. Guilford (2006). *Mechanics of Actomyosin Bonds in Different Nucleotide States are Tuned to Muscle Contraction*. Proc. Natl Acad. Sci. USA, 103 (26):9844–9849.

[Heussinger et al. 2007] Heussinger, C., M. Bathe and E. Frey (2007). *Statistical Mechanics of Semiflexible Bundles of Wormlike Polymer Chains*. Phys. Rev. Lett., 99:048101.

[Heussinger and Frey 2006a] Heussinger, C. and E. Frey (2006a). *Floppy Modes and Non-affine Deformations in Random Fiber Networks*. Phys. Rev. Lett., 97:105501.

[Heussinger and Frey 2006b] Heussinger, C. and E. Frey (2006b). *Stiff Polymers, Foams, and Fiber Networks*. Phys. Rev. Lett., 96:17802.

[Highsmith 1977] Highsmith, S. (1977). *The Effects of Temperature and Salts on Myosin Subfragment-1 and F-Actin Association*. Arch. Biochem. Biophys., 180:404–408.

[Hinner et al. 1998] Hinner, B., M. Tempel, E. Sackmann, K. Kroy and E. Frey (1998). *Entanglement, Elasticity, and Viscous Relaxation of Actin Solutions*. Phys. Rev. Lett., 81:2614–2617.

[Howard 2001] Howard, J. (2001). *Mechanics of Motor Proteins and the Cytoskeleton*. Sinauer Associates, Inc.

[Huisman et al. 2007] Huisman, E.M., T. van Dillen, P. R. Onck and E. van der Giessen (2007). *Three-Dimensional Cross-Linked F-Actin Networks: Relation between Network Architecture and Mechanical Behavior*. Phys. Rev. Lett., p. 208103.

[Janmey et al. 1986] Janmey, P. A., J. Peetermans, K. S. Zaner, P. S. Stossel and T. Tanaka (1986). *Structure and Mobility of Actin Filaments as Measured by Quasielastic Light Scattering, Viscometry, and Electron Microscopy*. J. Biol Chem., 261(18):8357–8362.

[Kasza] Kasza, K. personal information.

[Kroy and Glaser 2007] Kroy, K. and J. Glaser (2007). *The Glassy Wormlike Chain*. New Journal of Physics, 9:416.

[Kurokawa et al. 1990] Kurokawa, H., W. Fujii, K. Ohmi, T. Sakurai and Y. Nonomura (1990). *Simple and Rapid Purification of Brevin*. Biochem. Bioph. Res. Co., 168(2):451–457.

[Landau and Lifschitz 1975] Landau, L. and E. Lifschitz (1975). *Lehrbuch der Theoretischen Physik Band VII: Elastizitätstheorie*. Akademie-Verlag Berlin.

[Landau and Lifschitz 1979] Landau, L. and E. Lifschitz (1979). *Lehrbuch der Theoretischen Physik Band V: Statistische Physik Teil 1*. Akademie-Verlag Berlin.

[LeGoff et al. 2002a] LeGoff, L., O. Hallatschek, E. Frey and F. Amblard (2002a). *Tracer Studies on F-actin Fluctuations*. Phys. Rev. Lett., 89(25):258101.

[LeGoff et al. 2002b] LeGoff, V., F. Amblard and E. Furst (2002b). *Motor-Driven Dynamics in Actin-Myosin Networks*. Phys. Rev. Lett., 88(1):018101.

[Leibler et al. 1991] Leibler, L., M. Rubinstein and R. H. Colby (1991). *Dynamics of Reversible Networks*. Macromolecules, 24:4701–4707.

[Lenormand and Fredberg 2006] Lenormand, G. and J. J. Fredberg (2006). *Deformability, Dynamics, and Remodeling of Cytoskeleton of the Adherent Living Cell*. Biorheology, 43:1–30.

[Lieleg 2005] Lieleg, O. (2005). *Untersuchung des Phasenverhaltens und der mikro-mechanischen Eigenschaften von Biopolymer-Netzwerken*. Master's thesis, TU München.

[Liu et al. 2006] Liu, J., M. L. Gardel, K. Kroy, E. Frey, B. D. Hoffman, J. C. Crocker, A. R. Bausch and A. D. Weitz (2006). *Microrheology Probes Length Scale Dependent Rheology*. Phys. Rev. Lett., 96:118104.

[Lowey et al. 1969] Lowey, S., H. S. Slayter, A. G. Weeds and H. Baker (1969). *Substructure of the Myosin Molecule*. J. Mol. Biol., 42:1–29.

[Luan et al. 2008] Luan, Y., O. Lieleg, B. Wagner and A. Bausch (2008). *Micro- and Macrorheological Properties of Isotropically Cross-linked Actin Networks*. Biophys. J., 94:688–693.

[MacKintosh et al. 1995] MacKintosh, F. C., J. Käs and P. A. Janmey (1995). *Elasticity of Semiflexible Biopolymer Networks*. Phys. Rev. Lett., 75:4425–4428.

[Marston 1982] Marston, S. B. (1982). *The Rates of Formation and Dissociation of Actin-Myosin Complexes*. Biochem. J., 203:453–460.

[Massiera et al. 2007] Massiera, G., K. M. Citters, P. Biancaniello and J. C. Crocker (2007). *Mechanics of Single Cells: Rheology, Time Dependence and Fluctuations*. Biophys. J., 93:3703–3713.

[Meakin 1983] Meakin, P. (1983). *Formation of Fractal Clusters and Networks by Irreversible Diffusion-Limited Aggregation*. Phys. Rev. Lett., 51(13):1119–1121.

[Miyata et al. 1996] Miyata, H., R. Yasuda and K. Kinosita (1996). *Strength and Lifetime of the Bond between Actin and Skeletal Muscle alpha-actinin Studied with an Optical Trapping Technique*. Biochim. Biophys. Acta, 1290 (1):83–88.

[Morse 1998] Morse, D. C. (1998). *Viscoelasticity of Concentrated Isotropic Solutions of Semiflexible Polymers*. Macromol., 31:7030–7043.

[Nishizaka et al. 2000] Nishizaka, T., R. Seo, H. Tadakuma, K. Kinosita and S. Ishiwata (2000). *Characterization of Single Actomyosin Rigor Bonds: Load Dependence of Lifetime and Mechanical Properties*. Biophys. J., 79 (2):962–974.

[Odijk 1983] Odijk, T. (1983). *On the Statistics and Dynamics of Confined or Entangled Stiff Polymers*. Macromol., 16:1340–1344.

[Ono et al. 1997] Ono, S., Y. Yamakita, S. Yamashiro, P. T. Matsudaira, J. R. Gnarra, T. Obinata and F. Matsumura (1997). *Identification of an Actin Binding Region and a Protein Kinase C Phosphorylation Site on Human Fascin*. J. Biol. Chem., 272:2527–2533.

[Purdy et al. 2007] Purdy, K.R., J. Bartles and G. Wong (2007). *Structural Polymorphism of the Actin-Espin System: A Prototypical System of Filaments and Linkers in Stereocilia*. Phys. Rev. Lett., 98:058105.

[Rubinstein and Colby 2003] Rubinstein, M. and R. H. Colby (2003). *Polymer Physics*. Oxford University Press.

[Rubinstein and Semenov 2001] Rubinstein, M. and A. N. Semenov (2001). *Dynamics of Entangled Solutions of Associating Polymers*. Macromolecules, 34:1058–1068.

[Schilling et al. 2004] Schilling, J., E. Sackmann and A. Bausch (2004). *Digital Imaging Processing for Biophysical Applications*. Rev. Sci. Instr., 75(9):2822–2827.

[Schlierf and Rief 2006] Schlierf, M. and M. Rief (2006). *Single-Molecule Unfolding Force Distributions Reveal a Funnel-Shaped Energy Landscape*. Biophysical Journal, 90:L33–35L.

[Schmoller 2008] Schmoller, K. (2008). *in preparation*. Master's thesis, TU München.

[Schmoller et al. 2008a] Schmoller, K. M., O. Lieleg and A. R. Bausch (2008a). *Internal Stress in Kinetically Trapped Actin Bundle Networks*. Soft Matter, accepted.

[Schmoller et al. 2008b] Schmoller, K.M., O. Lieleg and A. Bausch (2008b). *Cross-linking Molecules Modify Composite Actin Networks Independently*. Phys. Rev. Lett., accepted.

[Semmrich] Semmrich, C. *unpublished data*.

[Semmrich et al. 2007] Semmrich, C., J. Glaser, R. Merkel, A. R. Bausch and K. Kroy (2007). *Glass Transition and Rheological Redundancy in F-Actin Solutions*. Proc. Natl Acad. Sci. USA, 104 (51):20199–20203.

[Semmrich et al. 2008] Semmrich, C., R. J. Larsen and A. R. Bausch (2008). *Non-linear Mechanics of Entangled F-actin Solutions*. Soft Matter, preprint.

[Shin et al. 2004a] Shin, J. H., M. L. Gardel, L. Mahadevan, P. Matsudaira and D. A. Weitz (2004a). *Relating Microstructure to Rheology of a Bundled and Cross-linked F-actin Network in vitro*. Proc. Natl Acad. Sci. USA, 101:9636–9641.

[Shin et al. 2004b] Shin, J. H., L. Mahadevan, P. T. So and P. Matsudaira (2004b). *Bending Stiffness of a Crystalline Actin Bundle*. J. Mol. Biol., 337:255–261.

[Sjibesma et al. 1997] Sjibesma, R. P., F. H. Beijer, L. Brunsveld, B. J. B. Folmer, J. H. K. K. Hirschberg, R. F. M. Lange, J. K. L. Lowe and E. W. Meijer (1997). *Reversible Polymers Formed from Self-Complementary Monomers Using Quadruple Hydrogen Bonding*. Science, 278:1601.

[Sjöblom et al. 2008] Sjöblom, B., A. Salmazo and K. Djinovic-Carugo (2008). *α-actinin Structure and Regulation*. Cell. Mol. Life Sci., Epub ahead of print.

[Sollich 1998] Sollich, P. (1998). *Rheological Constitutive Equation for a Model of Soft Glassy Materials*. Phys. Rev. E, 58(1):738–759.

[Spudich and Watt 1971] Spudich, J. A. and S. Watt (1971). *Regulation of Rabbit Skeletal Muscle Contraction .1. Biochemical Studies of Interaction of Tropomyosin-Troponin Complex with Actin and Proteolytic Fragments of Myosin*. J. Biol. Chem., 246:4866–71.

[Tanaka and Edwards 1992] Tanaka, F. and S. F. Edwards (1992). *Viscoelastic Properties of Physically Cross-Linked Networks. Transient Network Theory*. Macromolecules, 25:1516–1523.

[Tempel et al. 1996] Tempel, M., G. Isenberg and E. Sackmann (1996). *Temperature-induced Sol-Gel Transition and Microgel Formation in alpha-actinin Cross-linked Actin Networks: A Rheological Study*. Phys. Rev. E, 54:1802–1810.

[Tharmann] Tharmann, R. *unpublished data*.

[Tharmann 2007] Tharmann, R. (2007). *Mechanical Properties of Complex Cytoskeleton Networks*. PhD thesis, TU München.

[Tharmann et al. 2006] Tharmann, R., M. M. A. E. Claessens and A. R. Bausch (2006). *Micro- and Macrorheological Properties of Actin Networks Effectively Cross-linked by Depletion Forces*. Biophys. J., 90:2622–2627.

[Tharmann et al. 2007] Tharmann, R., M. M. A. E. Claessens and A. R. Bausch (2007). *Viscoelasticity of Isotropically Cross-Linked Actin Networks*. Phys. Rev. Lett., 98:088103.

[Trappe and Weitz 2000] Trappe, V. and D. A. Weitz (2000). *Scaling of the Viscoelasticity of Weakly Attractive Particles*. Phys. Rev. Lett., 85(2):449–452.

[Tseng et al. 2005] Tseng, Y., T. P. Kole, J. S. H. Lee, E. Fedorov, S. C. Almo, B. W. Schafer and D. Wirtz (2005). *How Actin Crosslinking and Bundling Proteins Cooperate to Generate an Enhanced Cell Mechanical Response*. Biochem. Bioph. Res. Co., 334:183–192.

[Vignjevic et al. 2006] Vignjevic, D., S. Kojima, Y. Aratyn, O. Danciu, T. Svitkina and G. Borisy (2006). *Role of Fascin in Filopodial Protrusion*. J. Cell. Biol., 174:863.

[Vignjevic et al. 2002] Vignjevic, D., D. Yarar, M. D. Welch, J. Peloquin, T. Svitkina and G. G. Borisy (2002). *Mechanism for Formation of Filopodial-like Bundles in vitro*. Mol. Biol. Cell, 13:177A–177A.

[Wagner et al. 2006] Wagner, B., R. Tharmann, I. Haase, M. Fischer and A. R. Bausch (2006). *Cytoskeletal Polymer Networks: Molecular Structure of Cross-linkers Determine Macroscopic Properties*. Proc. Natl Acad. Sci. USA, 103:13974–13978.

[Wang et al. 1975] Wang, K., J. F. Ash and S. J. Singer (1975). *Filamin, a New High-molecular-weight Protein Found in Smooth Muscle and Non-muscle Cells*. Proc. Natl Acad. Sci. USA, 72(11):4483–4486.

[Wang et al. 2002] Wang, N., I. M. Tolic-Norrelykke, J. Chen, S. M. Mijaiovich, J. Butler, J. Fredberg and D. Stamenovic (2002). *Cell Prestress. I. Stiffness and Prestress are Closely Associated in Adherent Contractile Cells*. Am. J. Physiol. Cell Physiol., 282:606–616.

[Way et al. 1995] Way, M., M. Sanders, C. Garcia, J. Sakai and P. Matsudaira (1995). *Sequence and Domain Organization of Scruin, an Actin Cross-linking Protein in the Acrosomal Process of Limulus Sperm*. J. Cell Biol., 128:51–60.

[Weitz and Oliveria 1984] Weitz, D. and M. Oliveria (1984). *Fractal Structures Formed by Kinetic Aggregation of Aqueous Gold Colloids*. Phys. Rev. Lett., 52(16):1433–1436.

[Yamashiro-Matsumura and Matsumura 1985] Yamashiro-Matsumura, S. and F. Matsumura (1985). *Purification and Characterization of an F-actin-bundling 55-Kilodalton Protein from HeLa Cells*. J. Biol. Chem., 260(8):5087–5097.

[Yamashiro-Matsumura and Matsumura 1986] Yamashiro-Matsumura, S. and F. Matsumura (1986). *Intracellular Localization of the 55-kD Actin-binding Protein in Cultured Cells: Spatial Relationships with Actin, α-actinin, Tropomyosin, and Fimbrin*. J. Cell Biol., 103:631–640.

[Ziemann et al. 1994] Ziemann, F., J. Rädler and E. Sackmann (1994). *Local Measurements of Viscoelastic Moduli of Entangled Actin Networks Using an Oscillating Magnetic Bead Micro-Rheometer*. Biophys. J., 66:2210–2216.

List of Figures

[V] picture taken from www.immediart.com

Acknowledgements

Schließlich und endlich (aber nicht zuletzt) möchte ich allen ganz herzlich danken, die zum Gelingen dieser Arbeit beigetragen haben und mich – ganz oder teilweise – auf meinem Weg durch die Promotionszeit begleitet haben:

- meinem Doktorvater **Prof. Andreas Bausch** zuallererst einmal dafür, dass er mich gegen Ende meiner Diplomarbeit von meinen Plänen, als Quereinsteiger ins Lehramt zu wechseln abgebracht hat (wenn auch auf nicht ganz subtile Weise: "Du willst Lehrer werden, spinnst du?") und mich in der Wissenschaft gehalten hat. Dann natürlich noch für die ausgezeichnete Betreuung, die wissenschaftliche Förderung und Forderung ("Man muss manche Leute überfordern damit sie auch gefordert sind.") und die manchmal chaotischen aber immer produktiven Diskussionen ("Verstehst du noch was? Ich nicht.").

- **Mireille Claessens** für die tollen Diskussionen während und außerhalb der "fruit breaks", ihre unschätzbare Hilfe beim Schreiben meiner ersten Publikationen und Rebuttals ("Better get used to it!"), ihre Gastfreundschaft bei meinem Besuch in Enschede und schliesslich für das kritische Korrekturlesen meiner Dissertation.

- **Prof. Erwin Frey** und **Claus Heussinger** (unseren "brainies") für den Theorie-Support, nicht nur in Fragen der non-affinen Biegedeformationen und floppy modes sondern auch für die anschaulichen Erläuterungen bei allen anderen Problemen und Fragen theoretischer Art ("Da habt ihr doch sicher auch so nen Exponenten gemessen, oder?")

- **Prof. Luca Cipelletti** für die Möglichkeit in seiner Arbeitsgruppe in Montpellier die Lichtstreu-Messungen vornehmen zu können

- meinen **Werkstudenten und Diplomanden** Philipp von Olshausen, Kurt Schmoller und Regina Baumgärtel für die gute Zusammenarbeit und die vielen tollen gemeinsam erzielten Ergebnisse

- allen ehemaligen und jetzigen Mitgliedern der **Cytoskelett-Arbeitsgruppe**: Marcus Bitzl, Pablo Fernandez, Simone Köhler, Yuxia Luan, Matthias Maier, Philipp von Olshausen, Kurt Schmoller, Christine Semmrich, Rainer Tharmann und Bernd Wagner für das gute Arbeitsgruppenklima und die produktiven Disskussionen im Gruppentreffen. Simone danke ich ganz herzlich für das Korrekturlesen meiner Dissertation und das Aufspüren sämtlicher Formatierungsfehler.
- allen **TAs**, also Claudia Antrecht, Gabi Chmel, Monika Rusp und Karin Vogt für die tollen Protein-Expressionen und -aufreinigungen sowie die Aufrechterhaltung des täglichen Laborbetriebs und die Bewahrung eines gewissen Ordnungsgrads in den Laboren. Monika danke ich ganz besonders für die wahrscheinlich beste Aktinpräparation der Welt und die Pflege meiner Büropflanzen während meiner Auslandsaufenthalte.
- allen anderen **Kooperationspartnern**, die gemeinsam mit mir an den verschiedenen Projekten gearbeitet haben: Jörg Auernheimer, Christian Cyron, Mónica López-García, Prof. Horst Kessler, Wolfgang Michel und Prof. Albrecht Ott
- meinen **Bürokollegen** Christina Lumme und Kurt Schmoller für die nette Bürogemeinschaft und die regelmäßigen und lebenswichtigen 15 Uhr-Kaffeepausen
- den **Sekretärinnen** Iris König-Decker, Elke Fehsenfeld, Katharina Girgensohn und Nicole Mittermüller dafür, dass sie uns Doktoranden den Rücken freihalten indem sie sich um unsere Verträge, den täglichen Papierkrieg und die diversen Dienstreiseabrechnungen kümmern
- ganz **E22/E27** für die einmalige Atmosphäre hier am Lehrstuhl, die nicht nur produktiv und wissenschaftlich inspirierend sondern auch immer entspannt und positiv wahr, nicht zuletzt in den unzähligen Kuchenpausen in der Kaffee-Ecke und – nicht zu vergessen – auf den tollen Winterschulen in Antholz
- meinem Doktorandenkolleg **CompInt** und der **bayerischen Eliteförderung** für die finanzielle Unterstützung, vor allem für die Finanzierung der diversen Konferenzbesuche
- meiner Schwester **Corinna** für das Aufspüren letzter Tippfehler in dieser Dissertation
- und schliesslich meiner **Familie** für die andauernde und langjährige Unterstützung inklusive all dem was ich bisher nicht erwähnt habe.

List of Publications

- **OL**, C.J. Cyron, K.M. Schmoller, Y. Luan, W.A. Wall and A.R. Bausch,
  Structural Polymorphism in Heterogeneous Cytoskeletal Networks,
  submitted

- W. Michel, **OL** and A. Ott,
  Microrheological Properties of Cross-linked Actin Networks as Determined by DLS Measurements,
  submitted

- **OL**, K.M. Schmoller, M.M.A.E. Claessens and A.R. Bausch,
  Cytoskeletal Polymer Networks: Viscoelastic Properties are Determined by the Microscopic Interaction Potential of Cross-links,
  submitted

- K.M. Schmoller, **OL** and A.R. Bausch,
  Internal Stress in Kinetically Trapped Actin Bundle Networks,
  Soft Matter - accepted for publication

- K.M. Schmoller, **OL** and A.R. Bausch,
  Cross-linking Molecules Modify Composite Actin Networks Independently,
  Phys. Rev. Lett. - accepted for publication

- **OL**, M.M.A.E. Claessens, Y. Luan and A.R. Bausch,
  Transient Binding and Dissipation in Cytoskeletal Networks,
  Phys. Rev. Lett. **101**, 108101 (2008)

- S. Köhler, **OL** and A. R. Bausch,
  Rheological Characterization of the Bundling Transition in F-actin Solutions Induced by Methylcellulose,
  PLoS ONE **3**(7): e2736 (2008)

- Y. Luan, **OL**, B. Wagner and A.R. Bausch,
  Micro- and Macrorheological Properties of Isotropically Cross-Linked Actin Networks,
  Biophys. J. **94**, 688-693 (2008)

- **OL** and A.R. Bausch,
  Cross-linker Unbinding and Self-Similarity in Bundled Cytoskeletal Networks,
  Phys. Rev. Lett. **99**, 158105 (2007)

- **OL**, M.M.A.E. Claessens, C. Heussinger, E. Frey and A.R. Bausch,
  Mechanics of Bundled Semiflexible Polymer Networks,
  Phys. Rev. Lett. **99**, 088102 (2007)

- **OL**, M. López-García, C. Semmrich, J. Auernheimer, H. Kessler and A. R. Bausch,
  Specific Integrin Labelling in Living Cells Using Functionalized Nanocrystals,
  Small **3**(9), 1560-1565 (2007)